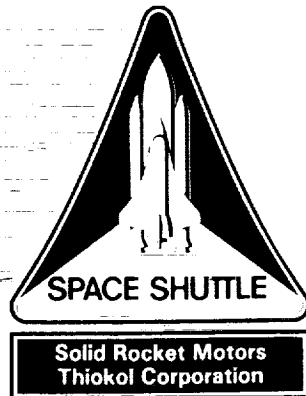


CR 184078

TWR-50068



Space Shuttle Flight Support Motor No. 1 (FSM-1) Final Test Report

13 November 1990

Prepared for

National Aeronautics and Space Administration
George C. Marshall Space Flight Center
Marshall Space Flight Center, Alabama 35812

Contract No. NAS8-30490
DR No. 5-3
WBS No. 4C204-10-01
ECS No. SS3623

Thiokol CORPORATION
SPACE OPERATIONS

P.O. Box 707, Brigham City, UT 84302-0707 (801) 863-3511

(NASA-CR-184078) SPACE SHUTTLE FLIGHT
SUPPORT MOTOR NO. 1 (FSM-1) Final Test
Report (Thiokol Corp.) 124 p CSCL 21H

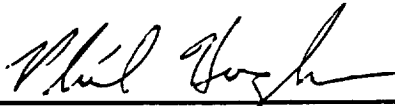
N91-16064

Unclass

G3/20 0329322

**Space Shuttle Flight Support Motor No. 1 (FSM-1)
Final Test Report**

Prepared by:

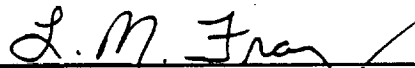


**P. D. Hughes
Test Planning and Reports
Systems Engineer**

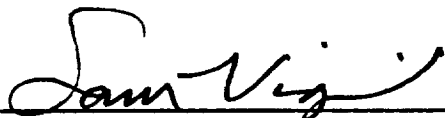
Approved by:



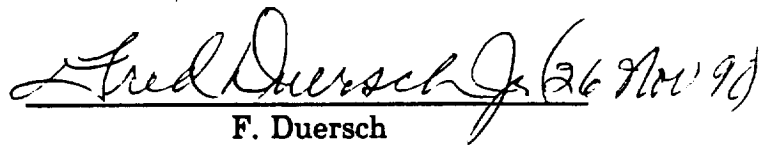
**J. R. Lavery, Manager
Requirements**



**L. M. Fray
System Integration Engineer**



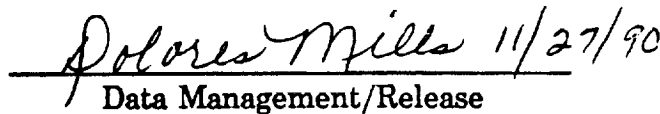
**S. Vigil
Program Manager**



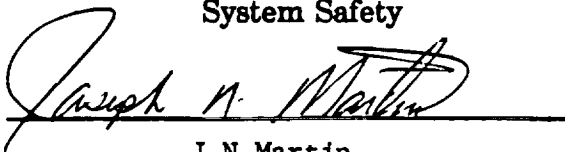
**F. Duersch
Reliability**



**K. G. Sanofsky
System Safety**



**Dolores Mills 11/27/90
Data Management/Release
ECS No. SS3623**



**J.N. Martin
Quality Assurance**

Major contributors to this report were:

Instrumentation:	D. S. Joos, W. D. South
Case/Leak Check/Seals:	T. R. Swauger, G. Abawi
Insulation:	J. A. Passman
Nozzle:	R. J. George, R. E. Lange
Joint Protection Systems:	C. L. Prokop
Ballistics/Mass Properties:	B. J. Hutchison
Aero/Thermal:	R. L. Buttars

ABSTRACT

Space Shuttle Flight Support Motor No. 1 was static test fired on 15 Aug 1990 at the Thiokol Corporation Static Test Bay T-24. FSM-1 was a full-scale, full-duration static test fire of a redesigned solid rocket motor. FSM-1 was the first of seven flight support motors which will be static test fired. The Flight Support Motor program validates components, materials, and manufacturing processes. In addition, FSM-1 was the full-scale motor for qualification of Western Electrochemical Corporation ammonium perchlorate. This motor was subjected to all controls and documentation requirements CTP-0171, Revision A.

Inspection and instrumentation data indicate that the FSM-1 static test firing was successful. The ambient temperature during the test was 87°F and the propellant mean bulk temperature was 82°F. Ballistics performance values were within the specified requirements. The overall performance of the FSM-1 components and test equipment was nominal.

CONTENTS

<u>Section</u>	<u>Page</u>
1 INTRODUCTION	1-1
1.1 TEST ARRANGEMENT AND FACILITIES	1-1
1.2 TEST ARTICLE DESCRIPTION	1-1
1.2.1 Case/Seals	1-2
1.2.2 Insulation/Liner/Inhibitor	1-6
1.2.3 Propellant	1-7
1.2.4 Nozzle/TVC	1-7
1.2.5 Ignition System	1-8
1.2.6 Joint Protection Systems	1-10
1.2.7 Nozzle Protective Plug	1-11
1.2.8 Deluge System	1-11
1.2.9 SRB Aft Skirt	1-11
1.2.10 Actuation System	1-11
2 TEST OBJECTIVES	2-1
3 EXECUTIVE SUMMARY	3-1
3.1 SUMMARY	3-1
3.1.1 Case/Seals Performance	3-1
3.1.2 Case Internal and External Insulation Performance Summary	3-1
3.1.3 Nozzle Assembly Performance	3-3
3.1.4 Ignition System Performance	3-4
3.1.5 Joint Protection Systems Performance	3-4
3.1.6 External Insulation	3-4
3.1.7 Ballistics/Mass Properties Performance	3-6
3.1.8 Static Test Support Equipment	3-6
3.1.9 Instrumentation	3-6
3.1.10 Temperature Data	3-8
3.1.11 Nozzle TVC Performance	3-8
3.2 CONCLUSIONS	3-8
3.3 RECOMMENDATIONS	3-12

CONTENTS (cont)

<u>Section</u>	<u>Page</u>
4 INSTRUMENTATION	4-1
4.1 INTRODUCTION	4-1
4.2 OBJECTIVES	4-2
4.3 CONCLUSIONS/RECOMMENDATIONS	4-2
4.3.1 Chamber Pressure Oscillations	4-2
4.3.2 Bushed Pinholes	4-2
4.3.3 Stiffener Stub Holes Outer Ligament Cracks	4-2
4.3.4 Igniter Flange Skip	4-3
4.3.5 Thermal Radiation	4-3
4.4 RESULTS/DISCUSSION	4-3
4.4.1 Forward End Chamber and Igniter Pressure	4-3
4.4.2 Forward End Chamber Pressure Oscillations	4-4
4.4.3 Nozzle Axial Extension	4-4
4.4.4 Joint Temperature Measurements	4-4
4.4.5 Case Temperature Measurements	4-4
4.4.6 Bushed Pinholes Strain	4-4
4.4.7 Stiffener Stub Holes From Outer Ligament Cracks	4-4
4.4.8 Igniter Flange Skip	4-5
4.4.9 Nose Cap Strain Gage Data	4-5
4.4.10 TVC Systems Data	4-5
4.4.11 Test Bay Instruments	4-5
5 PHOTOGRAPHY	5-1
5.1 STILL PHOTOGRAPHY	5-1
5.2 MOTION PICTURES	5-1
6 TEST RESULTS	6-1
6.1 CASE PERFORMANCE	6-1
6.1.1 Introduction	6-1
6.1.2 Objectives	6-1
6.1.3 Conclusion/Recommendations	6-1
6.1.4 Results/Discussions	6-2

CONTENTS (cont)

<u>Section</u>	<u>Page</u>
6.2 CASE INTERNAL INSULATION PERFORMANCE	6-19
6.2.1 Introduction	6-19
6.2.2 Objectives	6-19
6.2.3 Conclusions/Recommendations	6-19
6.2.4 Results/Discussion	6-20
6.3 SEALS/LEAK CHECK PERFORMANCE	6-28
6.3.1 Introduction	6-28
6.3.2 Objectives	6-28
6.3.3 Conclusions/Recommendations	6-28
6.3.4 Results/Discussions	6-30
6.4 NOZZLE PERFORMANCE	6-38
6.4.1 Introduction	6-38
6.4.2 Objectives	6-38
6.4.3 Conclusions/Recommendations	6-38
6.4.4 Results/Discussion	6-38
6.5 IGNITER PERFORMANCE	6-39
6.5.1 Introduction	6-39
6.5.2 Objectives	6-40
6.5.3 Conclusions/Recommendations	6-40
6.5.4 Results/Discussion	6-40
6.6 JOINT PROTECTION SYSTEM	6-41
6.6.1 Introduction	6-41
6.6.2 Objectives	6-42
6.6.3 Conclusions/Recommendations	6-42
6.6.4 Results/Discussion	6-42
6.7 BALLISTICS/MASS PROPERTIES	6-43
6.7.1 Introduction	6-43
6.7.2 Objectives	6-44
6.7.3 Conclusions/Recommendations	6-44
6.7.4 Results/Discussion	6-45

CONTENTS (cont)

<u>Section</u>	<u>Page</u>
6.8	STATIC TEST SUPPORT EQUIPMENT 6-71
6.8.1	Introduction 6-71
6.8.2	Objectives 6-71
6.8.3	Conclusions/Recommendations 6-71
6.8.4	Results/Discussion 6-71
7	APPLICABLE DOCUMENTS 7-1

(Appendixes are located in a separate volume)

<u>Appendix</u>	<u>Page</u>
A	DRAWING TREES A-1
B	INSTRUMENTATION LIST B-1
C	DATA PLOTS C-1
D	FLASH REPORT D-1
E	QUICKLOOK REPORT E-1
F	STRAIN VERSUS LOCATION PLOTS FOR BUSHED PINHOLE PERFORMANCE F-1
G	CRACKED STIFFENER STUB STRAIN DATA G-1
H	POSTFIRE HARDWARE EVALUATION H-1
I	THRUST VECTOR CONTROL DUTY CYCLES I-1

FIGURES

<u>Figure</u>		<u>Page</u>
1-1	FSM-1 Static Test Arrangement	1-3
1-2	FSM-1 Field Joint Configuration	1-4
1-3	FSM-1 Nozzle-to-Case Joint	1-5
1-4	Improved Nozzle Cowl Assembly Method	1-9
1-5	Plan View of Deluge System Nozzle Arrangement	1-12
1-6	Thrust Vector Actuation (TVA) System	1-13
3-1	Static Test Duty Cycle	3-9
5-1	Photography Coverage--FSM-1	5-4
6-1	Instrumentation Configuration	6-4
6-2	Strain Gage Location	6-9
6-3	Predicted Hoop Strain for Severed Outer Ligament	6-10
6-4	Predicted Hoop Strain for Intact Outer Ligament (outboard side) ...	6-12
6-5	Predicted Hoop Strain for Intact Outer Ligament (inboard side) ...	6-13
6-6	Scaled Hoop Strain Versus Measured Severed Ligament	6-16
6-7	Scaled Hoop Strain Versus Measured Intact Outer Ligament (outboard side)	6-17
6-8	Scaled Hoop Strain Versus Measured Intact Outer Ligament (inboard side)	6-18
6-9	Igniter Chamber Pressure Compared to STW-3176 Igniter Specification Limits at 80°F	6-46
6-10	Pressure Versus Time at 82°F	6-53
6-11	Vacuum Thrust Versus Time at 82°F	6-54
6-12	Vacuum Thrust to Headend Pressure Ratio	6-56
6-13	Vacuum Thrust Versus CEI Specification Limits	6-57
6-14	Ignition Transient	6-60
6-15	Data From Gage PNCA001	6-62
6-16	Axial Thrust Gage, FAPAX001	6-63
6-17	Maximum Oscillation Amplitudes--PNCAC001 1-L Acoustic Mode 2,000 sps	6-64
6-18	Maximum Oscillation Amplitudes--PNCAC001 2-L Acoustic Mode 2,000 sps	6-65
6-19	Data From Gage P000016	6-66
6-20	Maximum Static Test Motor Case Temperatures	6-72

TABLES

<u>Table</u>		<u>Page</u>
3-1	SRM Igniter Performance	3-5
3-2	S&A Test Results	3-5
3-3	Historical Data on S&A Cycle Times	3-6
3-4	FSM-1 Performance Summary	3-7
5-1	Photography and Video Coverage	5-2
5-2	Camera Control and Priority Requirements	5-3
6-1	Severed Outer Ligament	6-11
6-2	Intact Other Ligament	6-14
6-3	FSM-1 Seal Leak Testing	6-29
6-4	FSM-1 Case Factory Joint Leak Test Results	6-34
6-5	FSM-1 Nozzle Internal Joint Leak Test Results	6-35
6-6	FSM-1 Case Field Joint Leak Test Results	6-35
6-7	FSM-1 Igniter and S&A Leak Test Results	6-36
6-8	FSM-1 Nozzle-to-Case Leak Test Results	6-37
6-9	Summary of Measured Ballistic and Nozzle Performance Data	6-47
6-10	Historical 3-point Average Thrust and Pressure Rise Rate Data	6-59
6-11	Measured RSRM Ignition Performance Data at 82°F	6-58
6-12	Maximum Pressure Oscillation Amplitude Comparison	6-68
6-13	Prefire Functional Summary	6-69
6-14	Postfire Functional Summary	6-70

ABBREVIATIONS AND ACRONYMS

3-D	three-dimensional
1-L	first longitudinal
2-L	second longitudinal
ac	alternating current
ANSYS	general structural analysis (computer program)
AP	ammonium perchlorate
ASRM	advanced solid rocket motor
ATVC	ascent thrust vector control
B-B	barrier-booster
CCP	carbon-cloth phenolic
CEI	contract end item
CF/EPDM	carbon fiber-filled/ethylene-propylene-diene monomer
cg	center of gravity
CO ₂	carbon dioxide gas
COV	coefficient of variation
CP	center perforated, circular perforated
CTPB	carboxyl-terminated polybutadiene (polymer)
deg	degree
DM	development motor
DR	discrepancy report
ET	external tank
ETM	engineering test motor
FJPS	field joint protection system
FSM-1	Flight Support Motor No. 1
ft	foot
FWC	filament wound case
GEI	ground equipment instrumentation
HPM	high-performance motor
HPU	hydraulic power unit
hr	hour
Hz	hertz
ID	inside diameter
in.	inch
in. ²	square inches
ips	inches per second
I _{sp}	specific impulse
JPS	Joint Protection System
ksi	thousand square inches
lb	pound
lbf	pounds force
lbm	pounds mass

ABBREVIATIONS AND ACRONYMS (cont)

LSC	linear shaped charge
MAP	manual/automatic panel
MEOP	maximum expected operating pressure
Mlbf	million pounds force
ms	millisecond
MSFC	Marshall Space Flight Center
NA	not applicable
NASA	National Aeronautics and Space Administration
NBR	nitrile butadiene rubber
NIST	National Institute of Standards and Technology
OBR	outer boot ring
OD	outside diameter
OPT	operational pressure transducer
PBAN	polybutadiene acrylic acid acrylonitrile tempolymer
PMBT	propellant mean bulk temperature
psi	pounds per square inch
psia	pounds per square inch absolute
psig	pounds per square inch gage
PVM	production verification motor
QM	qualification motor
RSRM	redesigned solid rocket motor
RTD	resistance temperature detector
S/N	serial number
S&A	safe and arm (device)
SBRE	surface burn rate error
sccs	standard cubic centimeters per second
sec	second
sps	samples per second
SRB	solid rocket booster
SRM	solid rocket motor
TEM	technical evaluation motor
TPTA	transient pressure test article
TVA	thrust vector actuation
TVC	thrust vector control
USBI	United Space Boosters, Inc.
V	volts
WECCO	Western Electrochemical Company
°F	degree Fahrenheit

INTRODUCTION

This report documents the procedures, performance, and results from the Space Shuttle Flight Support Motor No. 1 (FSM-1) full-scale, full-duration static test fire of a redesigned solid rocket motor (RSRM). The static test fire occurred at 1330 hr on 15 Aug 1990 at the Thiokol Corporation Static Test Bay T-24. This test report includes a presentation and discussion of the FSM-1 performance, anomalies, and test result concurrence with the objectives outlined in CTP-0171 Revision A, Space Shuttle Flight Support Motor No. 1 (FSM-1) Static Fire Test Plan.

RSRMs, used in pairs, are the primary propulsive element for the space shuttle; providing impulse and thrust vector control (TVC) from SRM ignition to solid rocket booster (SRB) separation.

FSM-1 postfire inspection procedures followed TWR-60250, Volumes I through IV and TWR-60776.

1.1 TEST ARRANGEMENT AND FACILITIES

The FSM-1 static test arrangement was assembled in accordance with Drawing No. 2U65151. T-24 is equipped with a water deluge system and a CO₂ quench. The test motor included an SRB aft skirt assembly which contains the TVC subsystem and the heat shield installation. The thrust vector actuation (TVA) system is comprised of two SRB actuators and two hydraulic power units (HPU) located in the aft skirt. The HPU Ground Test Controller, HPU Manual/Automatic Panel (MAP), and the ascent thrust vector control (ATVC) units serve as the control units for the TVC subsystem.

1.2 TEST ARTICLE DESCRIPTION

The FSM-1 test assembly was in accordance with Drawing No. 7U76914. The RSRM static test motor consisted of: a lined, insulated, segmented rocket motor case loaded with solid propellant; an ignition system complete with an electromechanical safety

and arming (S&A) device, initiators, and loaded igniter; movable nozzle with flexible bearing and exit cone; and the TVC. The motor was instrumented to provide data to satisfy the test objectives. An overall view of the test article is shown in Figure 1-1. A FSM-1 drawing tree is included in Appendix A.

1.2.1 Case/Seals

The case consisted of 11 individual weld-free segments: the forward dome (Drawing No. 1U51473), six cylinder segments (Drawings No. 1U50131, 1U50717, 1U52982 and 1U52983), the external tank (ET) attach segment (Drawing No. 1U50716), two stiffener segments (Drawing No. 1U50715) and the aft dome (Drawing No. 1U50129). The 11 segments were preassembled into four subassemblies for propellant casting.

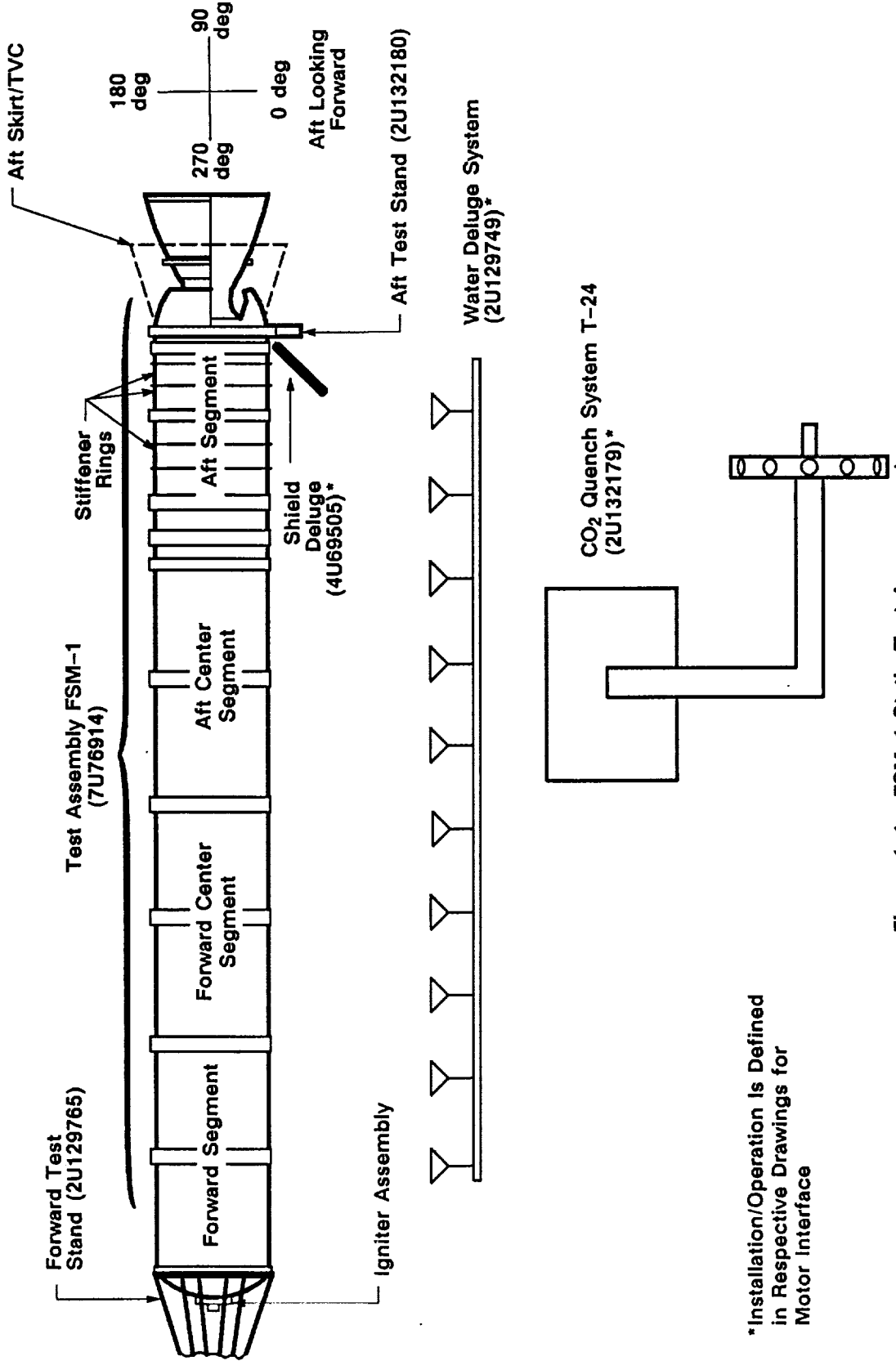
The four loaded assemblies were the forward segment assembly (Drawing No. 1U77186), the forward center segment and aft center segment assemblies (Drawing No. 1U77190), and the aft segment assembly (Drawing No. 1U76676). These individual casting segments were joined by means of capture feature tang and clevis field joints, which in turn, were held together by pins.

The nozzle-to-case joint was formed by bolting the nozzle fixed housing into the aft dome with 100 axial and 100 radial bolts which were torqued ultrasonically. The field joints had a standard RSRM insulation configuration as shown in Figure 1-2. The nozzle-to-case joint had the standard RSRM nozzle joint insulation configuration as shown in Figure 1-3.

A full set (3) of stiffener rings were installed on the aft segment. Stiffener stubs of both lightweight stiffener segments have outer ligament cracks:

- At 24 deg on aft stub of 1U50715-02, S/N 033
- At 162 deg on aft stub of 1U50715-02, S/N 017

Systems tunnels were not installed for this test.



*Installation/Operation Is Defined
in Respective Drawings for
Motor Interface

Figure 1-1. FSM-1 Static Test Arrangement

A02664a

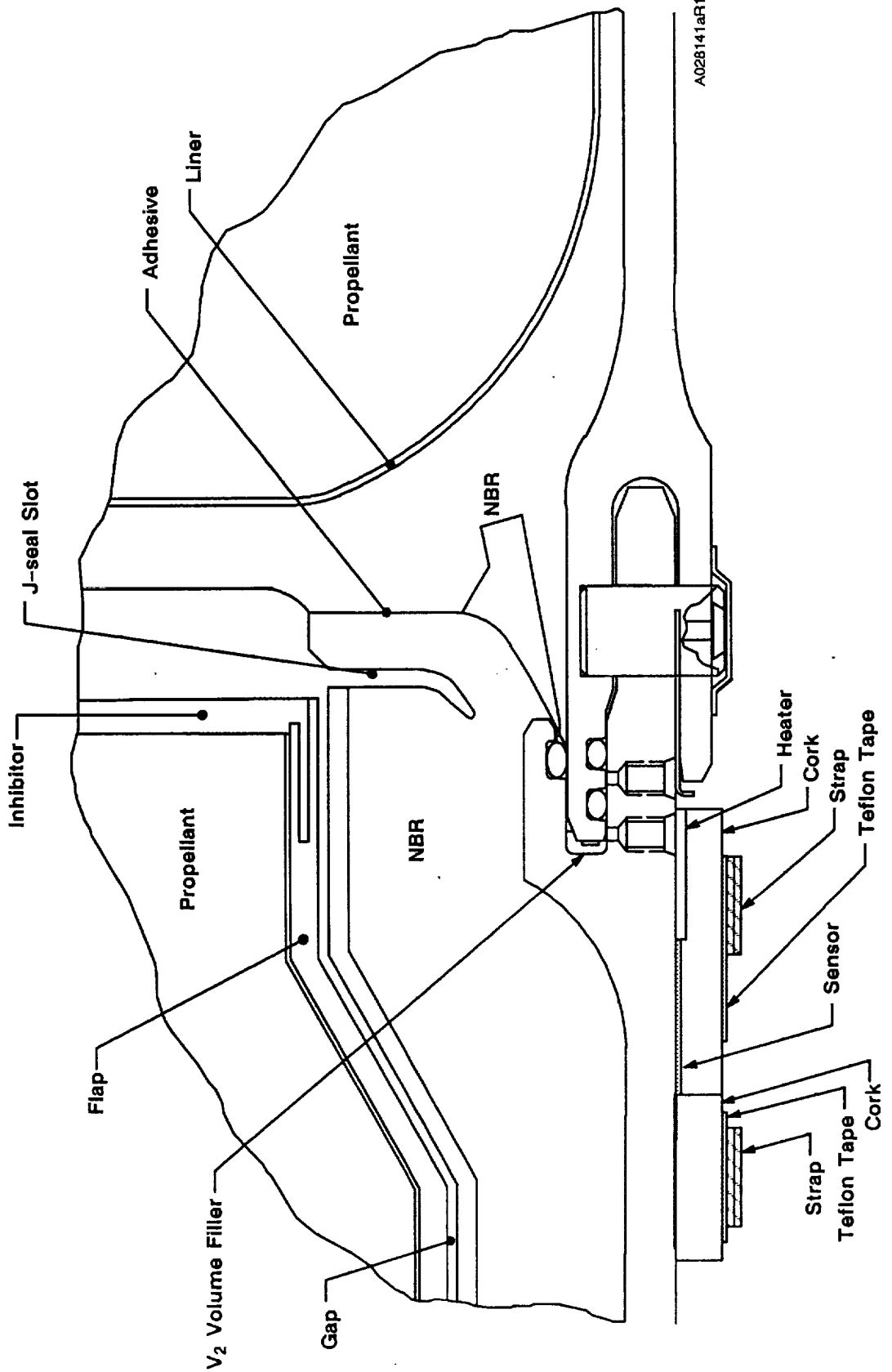


Figure 1-2. FSM-1 Field Joint Configuration

REVISION _____

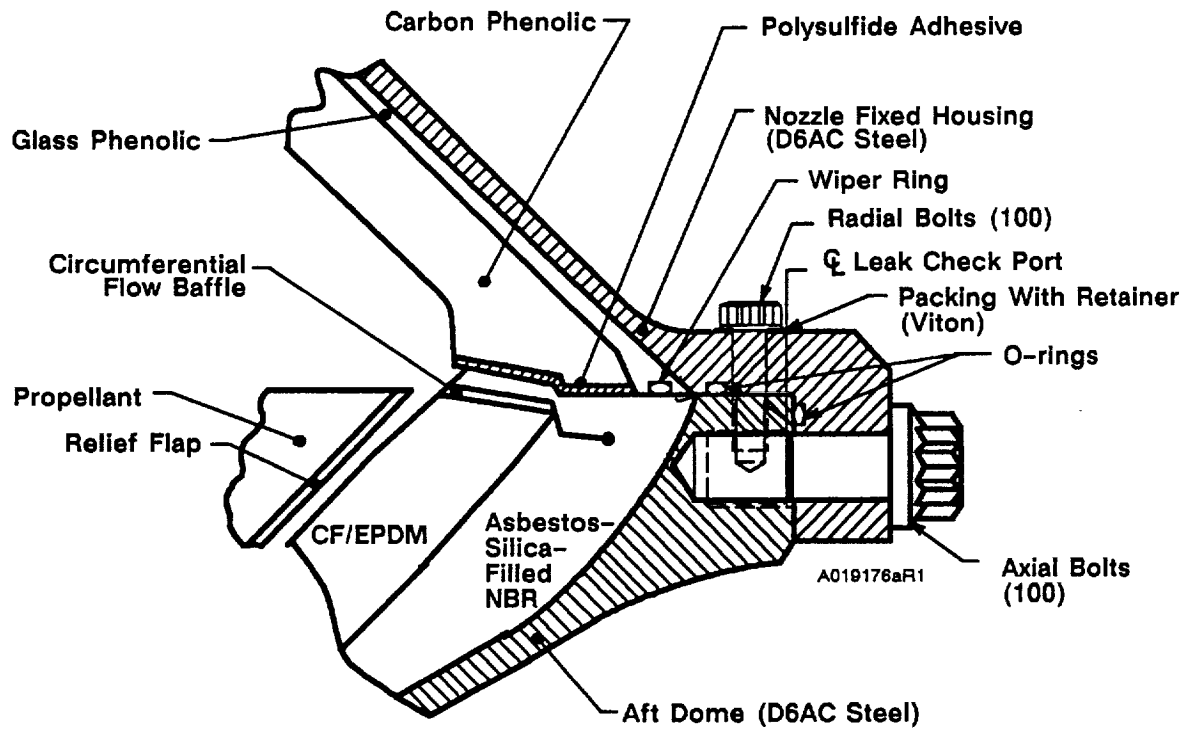


Figure 1-3. FSM-1 Nozzle-to-Case Joint

The assembly and joint configuration were full up RSRM flight configuration with the following exceptions:

- a. Standard shims, 1U51899-04, were used in the factory joints of both center segments.
- b. Bushed pinholes in clevis end of capture feature cylinders
 1. One each outer pinhole in 1U52983-02, S/N 7 and 1U52982-03, S/N 39
 2. One outer and inner pinhole in 1U52982-03, S/N 19
- c. Flight joint protection systems were not installed because of static test instrumentation. Field joint heaters closeout and in-bay seals are static test configuration.
- d. Clevis O-ring 1U75150-25 was installed in the capture feature groove of the aft field joint.
- e. MP159 bolts were installed in the igniter adapter-to-case joint.
- f. 1U51369 special washers were installed in the outer bolt row of the igniter adapter-to-case joint discrepancy report (DR No. 402566).

1.2.2 Insulation/Liner/Inhibitor

The internal insulation system included case acreage insulation, joint insulation, and propellant stress relief flaps. The insulation material used for these components is an asbestos silica-filled acrylonitrile butadiene rubber (NBR) (STW4-2621). Carbon fiber-filled ethylene-propylene-diene monomer (CF/EPDM) (STW4-2868) is bonded to the NBR in a sandwich type construction under the propellant stress relief flaps in both center segments. CF/EPDM is also used in sandwich construction in the aft dome. The CF/EPDM is installed to reduce the erosion of the insulator near the submerged nozzle in the aft dome and under the stress relief flaps in the center segments.

The liner material specified in STW5-3224 is an asbestos-filled carboxyl terminated polybutadiene (CTPB) polymer which bonds the propellant to the internal insulation in the solid rocket motor (SRM). The forward facing full web inhibitors are

made of NBR. They are located on the forward end of the center and aft segments. The aft facing partial web castable inhibitors are made of a material (STW5-3223) similar in type (CTPB polymer) to the liner. They are RSRM configuration and are located on the aft end of the forward and center segments.

All castable inhibitors (forward segment and both center segments) and the liner on both center segments and the aft segment were processed with new JAYGO mixers. These mixers will be qualified in accordance with test plan CTP-0125.

1.2.3 Propellant

The SRM propellant, TP-H1148 (STW5-3343), is a composite type solid propellant, formulated of polybutadiene acrylic acid acrylonitrile terpolymer binder (PBAN), epoxy curing agent, ammonium perchlorate (AP) oxidizer and aluminum powder fuel. Approximately 0.21 percent by weight (exact amount determined by standardization) of burning rate catalyst (iron oxide) is added to achieve the targeted propellant burning rate of 0.368 ips at 625 psia and 60°F.

The AP (STW4-2602) was from the Utah plant of Western Electrochemical Corporation (WECCO). The required laboratory and subscale qualification tests were successfully completed in accordance with test plan CTP-0112.

The propellant grain design consisted of an 11-point star with a smooth bore-to-fin cavity transition region that tapered into a center perforated (CP) configuration in the forward segment (Drawing No. 1U77186). The two center segments (Drawing No. 1U77190) were double-tapered CP configurations and the aft segment (Drawing No. 1U76676) was a triple-taper CP configuration with a cutout for the partially submerged nozzle. The aft segment nozzle cutback region was formed using a net cast molding.

1.2.4 Nozzle/TVC

The nozzle assembly (Drawing No. 1U52861) was a partially submerged convergent/divergent movable design with an aft pivot point flexible bearing (Drawing No. 1U52840).

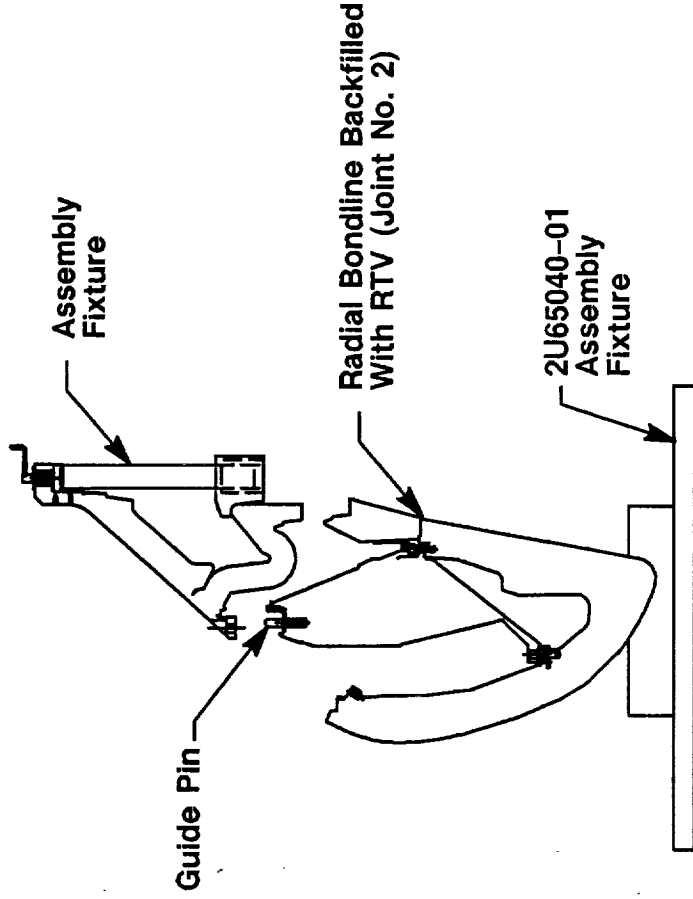
The nozzle assembly and joint configuration were RSRM flight configuration with the following exceptions:

- a. The snubber (Drawing No. 1U51063) and linear shaped charge (LSC) (Drawing No. 1U52700) were not installed for this test.
- b. The aft exit cone (Drawing No. 1U76121) contains low-density indications and was dispositioned for limited use on FSM-1.
- c. The flex bearing (Drawing No. 1U52840) was dispositioned for limited use on FSM-1.
- d. An improved Nozzle Joint No. 2 process and cowl assembly (Drawing No. 1U76586) technique (Figure 1-4) was used.
- e. A forward nose ring with triple-cured cycle on the carbon-cloth phenolic (CCP) was incorporated.
- f. No polysulfide sealant was used for external closeout of fasteners and joints.
- g. Paint scratches were protectively coated with grease instead of repaired with paint.
- h. Aft exit cone (Drawing No. 1U76121) ground equipment instrumentation GEI was not installed.
- i. Joint No. 4 glass phenolic was machined to provide acceptable O-ring squeeze.

1.2.5 Ignition System

The SRM ignition system was a modified HPM igniter assembly (Drawing No. 1U75166). It contains a single nozzle, thickened steel chamber at the nozzle end, external insulation and tapered internal insulation, and solid propellant, TP-H1178 (STW5-2833), igniter containing a case bonded 40-point star grain. The AP used in the TP-H1178 propellant was from the Utah plant of WECCO. The required laboratory and subscale qualification tests were successfully completed in accordance with test plan CTP-0112.

Improved Assembly Process



Current Assembly Process

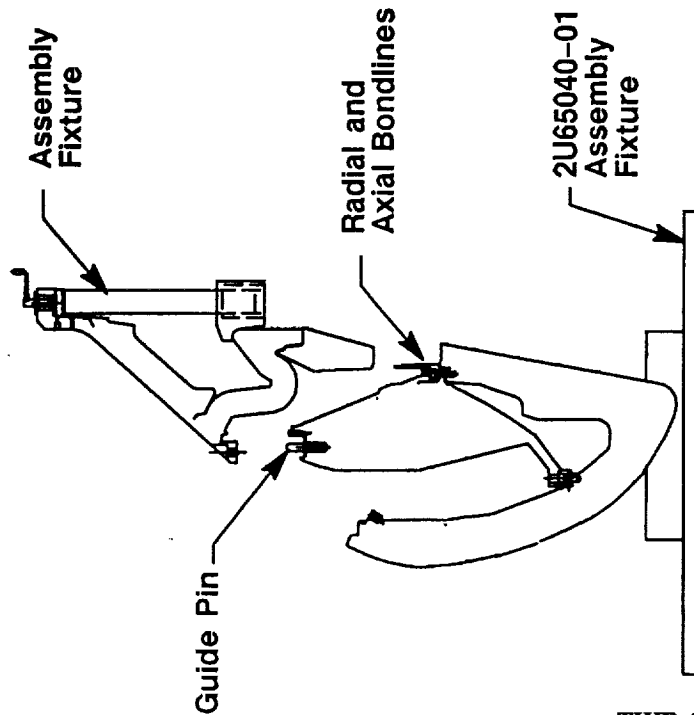


Figure 1-4. Improved Nozzle Cowl Assembly Method

REVISION _____

The forward mounted solid rocket type igniter (Drawing No. 1U75166) was modified with a CO₂ quench port. Ultrasonically torqued bolts fasten the igniter adapter to the igniter chamber. A286 bolts in the igniter adapter-to-case joint were replaced with higher strength MP159 bolts which were preloaded to a higher level.

A S&A device (1U52295-04) which uses Krytox grease to lubricate the barrier-booster (B-B) shaft O-rings was installed on the igniter.

Velostat or pink poly plastic sheets are wrapped and tightly sealed around the forward thrust adapter to simulate the thermal protection provided to the igniter and S&A by flight configuration.

1.2.6 Joint Protection Systems

Field Joint Protection Systems--Field joint heaters closeout (Drawing No. 7U77135, static test only) consists of cork strips retained with Kevlar straps. The same design was used on technical evaluation motors (TEMs) (No. 2, 3, 4 and partial 5 and 6). The external joint temperatures are sensed by two sensor assemblies mounted adjacent to the heater. Each assembly contains two resistance temperature detector (RTD) sensors.

Weatherseals were not applied to the cylinder-to-cylinder factory joint of the forward segment and the factory joint of both center segments in order to accommodate strain gages. The barrel assembly was primed and painted to protect case and 1U82840-02 hat band pin retainer was used. The in-bay seal will protect against water deluge.

Joint Heaters--Improved field joint heaters (Drawing No. 1U77252) and igniter-to-case joint heater (Drawing No. 1U77253) are installed as shown in Drawing No. 7U77135. These heaters consist of redundant, chemically etched, foil circuits which are superimposed upon one another and laminated in polyamide plastic sheets. The underside Kapton surface of the field joint heaters is coated with a pressure sensitive adhesive. This adhesive provides bonding to the case during assembly. The lead wires extend from the heaters and are terminated in electrical connectors.

An auxiliary heating system (Drawing No. 2U129410) was provided as part of the test arrangement to heat the nozzle-to-case joint if required by ambient conditions. The heating system was not needed and not used.

Heater Power Cables--RSRM joint protection system (JPS) power cables (1U76702-01, 1U76702-02, 1U76703-01, 1U76703-02, 1U76704-01, 1U76704-02, 1U76705-01, 1U76705-02, 1U76706-01 and 1U76706-02) are installed to provide 208 VAC to the RSRM field joint and igniter-to-case joint heaters.

Systems Tunnel and LSC--The systems tunnel and systems tunnel LSC were not installed.

1.2.7 Nozzle Protective Plug

A nozzle protective plug (Drawing No. 1U51711) was installed to provide an hermetic seal and protect from environmental contamination.

1.2.8 Deluge System

The deluge system and related instrumentation were similar to the configuration used on TEM motors. Deluge system nozzle arrangement is shown in Figure 1-5.

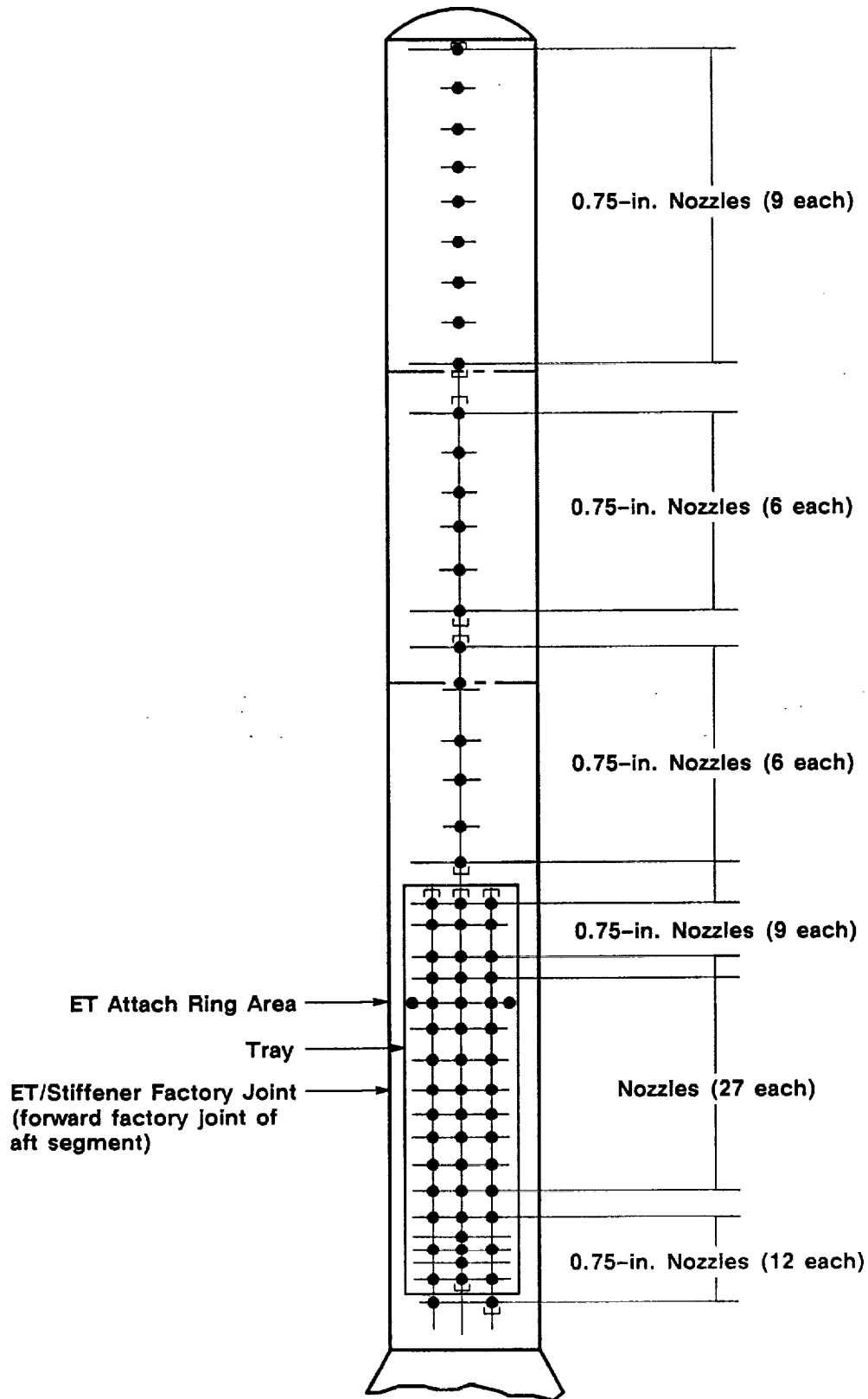
1.2.9 SRB Aft Skirt

The axial test motor includes an SRB aft skirt assembly identified on United Space Boosters Inc. (USBI) Drawing No. 14A30649-02. The aft skirt assembly contains the TVC subsystem and the heat shield installation.

1.2.10 Actuation System

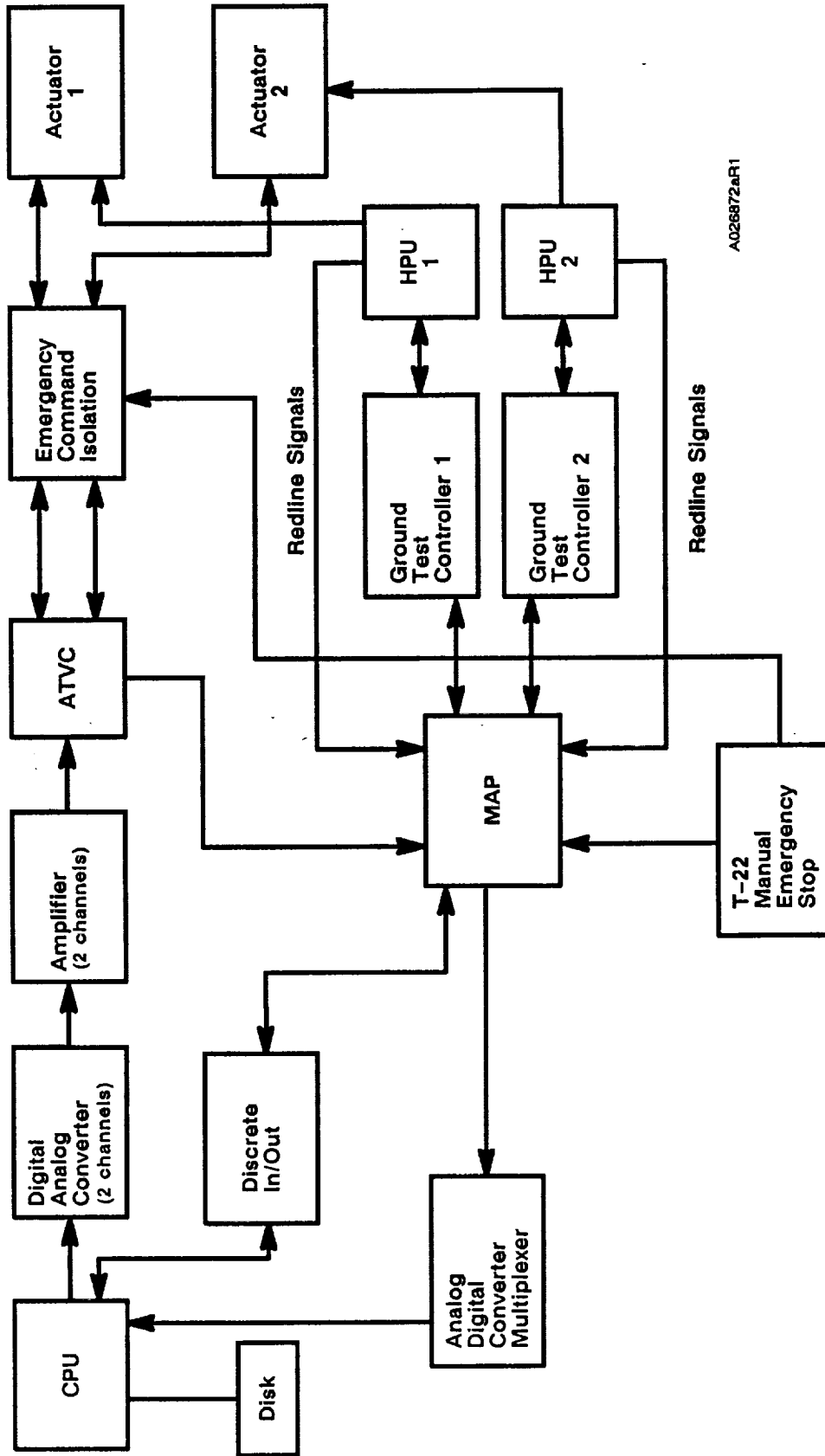
The TVA System (Figure 1-6) is comprised of two SRB actuators and two HPUs located in the aft skirt.

The HPU Ground Test Controller, HPU MAP and the ATVC units serve as the control units for the TVC subsystem.



A027440a

Figure 1-5. Plan View of Deluge System Nozzle Arrangement



A026872aR1

Figure 1-6. Thrust Vector Actuation (TVA) System

TEST OBJECTIVES

The FSM-1 test objectives of CTP-0171 were derived from the objectives of TWR-15723, Revision C, to satisfy the requirements of Contract End Item (CEI) Specification CPW1-3600A, dated 3 Aug 1987. Instrumentation was selected to provide data to satisfy the test objectives.

Qualification objectives of this test were:

- a. Certify the TP-H1148 SRM propellant manufactured using AP produced by the new WECCO Utah plant (CPW1-3600A paragraph 3.2.1.1.1.1, 3.2.1.1.1.2, 3.2.1.1.2.1, 3.2.1.1.2.2, 3.2.1.1.2.4, 3.3.1.1).
- b. Certify the TP-H1178 SRM igniter propellant manufactured using AP produced by the new WECCO Utah plant (CPW1-3600A paragraph 3.2.1.1.1.1, 3.3.1.1).

Other test objectives included:

- c. Revalidate the RSRM and its components, materials, and processes.
- d. Obtain additional data on the low-frequency chamber pressure oscillations in the motor forward end.
- e. Demonstrate the performance of triple-cured nozzle CCP components (CPW1-3600A paragraph 3.2.1.1.2.1, 3.2.1.1.2.2, 3.2.1.1.2.4, 3.2.1.4.1.1, 3.2.3, 3.2.3.1, 3.3.1.1, 3.3.6.1.1, 3.3.6.1.2.7).
- f. Demonstrate the performance of liner and castable inhibitor processed with the new JAYGO mixers (CPW1-3600A paragraph 3.3.1.1).
- g. Obtain additional data on the performance of bushed pinholes in standard weight and lightweight capture feature cylinder clevis ends.

- h. Obtain data on the performance of stiffener segments with known outer ligament cracks in the aft segment stiffener stubs.
- i. Obtain data on the effect on hardware of standard shims in the factory joint.
- j. Demonstrate assembly/disassembly of a field joint containing a primary/secondary diameter O-ring in the capture feature (CPWI-3600A paragraph 3.2.5.1).
- k. Demonstrate the performance of MP159 bolts in the igniter adapter-to-case joint.
- l. Obtain data on igniter flange skip.
- m. Obtain thermal radiation data from the nozzle plume.

EXECUTIVE SUMMARY

3.1 SUMMARY

All inspection and instrumentation data indicate that the FSM-1 static test firing was successful. Data was gathered at instrumented locations during pretest, test, and post-test operations. The information assembled from the test procedures has supplied valuable knowledge and understanding about the performance of the RSRM design components used in FSM-1.

3.1.1 Case/Seals Performance

There was no evidence of corrosion, metal damage, effects of heat or abnormal sooting to any of the case segments. There were no missing or loose pin retainer bands, fasteners, or safety wires. There was no evidence of combustion product leakage from any joint.

3.1.2 Case Internal and External Insulation Performance Summary

A summary of the FSM-1 external and internal insulation condition by component is as follows. A detailed description of the results can be found in Section 6.2.

Factory joint external EPDM weatherseals were installed only on the forward segment dome/cylinder factory joint and the three aft segment factory joints. These weatherseals were in excellent condition with no unbonds or heat effects evident. EPDM weatherseals were not installed on the forward segment, forward center segment, and aft center segment in order to accommodate instrumentation. These factory joints were covered with a plastic closeout system instead of EPDM. There was evidence of water intrusion through the plastic closeout system at each of these three factory joints.

The external EPDM insulation over the stiffener stub and rings was in excellent condition. No heat effects, discoloration, or unbonds were evident on any surface.

The nozzle-to-case joint performed well. No gas paths through the polysulfide adhesive were identified. Several small voids in the polysulfide were identified, however, no voids received gas penetration.

The internal insulation in all three of the case field joints performed as designed. No anomalous conditions were identified. J-leg tip contact was evident full circumference at each joint. All field joint insulation surfaces exhibited normal charring and erosion with no evidence of gas penetration beyond the char layer. No clevis edge separations were detected.

The condition of the igniter boss insulation was excellent with no anomalous conditions present. One blowhole through the putty was present on the igniter-to-case joint. The igniter chamber insulation was also in excellent condition.

The acreage insulation, including the internal insulation over each of the factory joints, was in good condition. No evidence of gas penetration through the insulation was identified.

The leading edge of the aft dome factory joint insulation experienced intermittent exposed voids full circumference. This condition was expected due to the large number of prefire voids detected by X-ray at this factory joint. Two areas of abnormal erosion were found on the leading edge of the aft dome factory joint insulation. The remainder of the internal acreage insulation was in excellent condition with all segments showing normal heat affects. All the NBR inhibitors and stress relief flaps exhibited normal erosion full circumference with no tears. The liner coverage of the aft and both center segments was normal, but the forward segment did exhibit a small area of unusual liner coverage. There were no gouges, separations, cuts, missing material, or other areas of excessive erosion in the internal acreage insulation.

No unacceptable conditions were found in the thermal safety factor evaluation of the nozzle-to-case joint, factory joints, and case wall acreage. Field joint thermal safety factor evaluation has not been completed to date.

The slag pool in the aft segment was small relative to previous static tests. The final slag weight was determined to be 466 lb.

3.1.3 Nozzle Assembly Performance

Post-test observations indicated no anomalous conditions. Nozzle erosion was typical.

3.1.3.1 Aft Exit Cone Assembly. The aft exit cone CCP liner exhibited typical shallow wash areas with surface ply lifting concentrated mostly along the aft 3 to 4 ft. The wash areas are located intermittently around the full circumference and measure approximately 1 to 2 ft axially, 4 in. circumferentially, and 0.2 in. deep, radially.

These wash areas are not as numerous or deep as those observed on the TEM-6 aft exit cone. This is an expected condition which is related to the ply angle of the CCP.

3.1.3.2 Forward Exit Cone. Typical dimpled erosion was exhibited on the full circumference of the forward exit cone.

3.1.3.3 Throat/Throat Inlet Rings. The throat inlet ring has a postburn impact mark (approximately 1.8 in. wide by 1.3 in. long by 0.4 in. deep). The throat ring showed typical rippled erosion on the aft 6 inches.

3.1.3.4 -503/-504 Rings. There is a postburn poppedout ply on the forward 1.5 in. of the -504 ring at 0 deg. The -503 ring had smooth erosion.

3.1.3.5 Nose Cap. There are wash areas on the forward end of the nose cap. The nose cap has a postburn wedgeout on the aft 2 in. around the full circumference.

3.1.3.6 Cowl Ring/Outer Boot Ring. The cowl ring had smooth erosion. The vent-holes appear to be plugged with slag. The outer boot ring (OBR) has typical aft end delaminations in the charred CCP. There are also intermittent wedgeouts on the aft tip adjacent to the flex boot. The forward 1 in. of the OBR has popped plies. The cowl/OBR bondline was intact.

3.1.3.7 Fixed Housing. There are typical light slag deposits on the aft 6 in. of the fixed housing.

3.1.4 Ignition System Performance

The igniter performed within the specified requirements (Table 3-1). S&A test results are summarized in Table 3-2. Historical data on S&A cycle times is shown in Table 3-3.

3.1.5 Joint Protection Systems Performance

The static test (TEM-2, -3, -4, and partial -5 and -6) joint heaters closeout for all field joints performed nominally.

Three of the factory joints were covered with clear plastic instead of EPDM weatherseals to accommodate strain gages for the bushed pinholes and referee pinholes. Water has penetrated the plastic closeout and had collected in a small pool at the bottom of the plastic at each of these joints (forward segment cylinder/cylinder, forward center segment, and aft center segment). Instrumentation was not affected by the water.

3.1.6 External Insulation

External insulation is in excellent condition. There are no unbonds, areas of damaged insulation, or other anomalous conditions on factory joint weatherseals, stiffener rings, or stub EPDM.

Three of the factory joints were covered with clear plastic instead of EPDM weatherseals to accommodate special instrumentation. Water had penetrated the plastic closeout and had collected in a small pool at the bottom of the plastic at each of these joints (forward segment cylinder/cylinder, forward center segment, and aft center segment). Instrumentation does not appear to be affected by the water.

3.1.6.3 Heater Power Cables. Operation of the new JPS heater power cables was nominal.

Refer to Section 6.6 for addition information on the FSM-1 JPS.

Table 3-1. SRM Igniter Performance

Limits at 80° ± 5°F		
Time (sec)	Pressure (psia)	
	Upper Limit	Lower Limit
0.0276	700	--
0.0315	1,250	--
0.0328	1,500	--
0.0342	1,725	--
0.0398	--	700
0.0400	1,825	--
0.0458	--	1,000
0.0500	1,960	--
0.0501	--	1,250
0.0532	--	1,500
0.0600	2,108	1,690
0.0700	2,126	1,704
0.0800	2,126	1,704
0.0900	2,115	1,695
0.1000	2,098	1,682

Table 3-2. S&A Test Results

FSM-1 S&A Test Results		
Pre-installation checkout of S&A arming voltage		
<ul style="list-style-type: none"> • Requirement 24 to 32 V • FSM-1 S&A 27.7 V 		
S&A cycle times--Requirement: 2 sec maximum		
Event	Safe to Arm (sec)	Arm to Safe (sec)
Pre-installation (off motor)	0.6	0.3
Dry Run (on motor)	0.6	0.4
Static Firing	0.6	NA

Table 3-3. Historical Data on S&A Cycle Times

Test Article	Off Motor Test Safe to Arm (sec)	On Motor Test Safe to Arm (sec)	Firing Safe to Arm (sec)	Off Motor Test Voltage to Arm (V)
QM-7	0.60			
PVM-1	0.73	0.79		
QM-8		0.90		
TEM-1	0.79	0.68		
TEM-2	0.67	0.65	0.66	
TEM-3	0.60	0.70	0.70	30.5
TEM-4	0.67	Test No. 1: 0.64 Test No. 2: 0.65	0.66	28.5
TEM-5	0.50	0.60	0.60	31.0
TEM-6	0.50	0.60	0.60	29.5

3.1.7 Ballistics/Mass Properties Performance

The ballistics performance summary (Table 3-4) shows delivered performance of all parameters within CEI specification limits and also within the narrower nominal 2.5σ limit for evaluation of ballistics performance.

3.1.8 Static Test Support Equipment

The water deluge system, CO₂ quench, and other test support equipment performed as expected during all required test operations.

3.1.9 Instrumentation

FSM-1 test article instrumentation measurements consisted of: forward end chamber pressure; forward end chamber pressure oscillation; igniter pressure; joint temperatures; case temperature for deluge control; case acreage and propellant grain temperatures/PMBT; nozzle throat temperatures; nozzle flex bearing temperatures; aft end free air temperatures; case vibration; nozzle position; igniter adapter flange skip; case pinhole strain; case stiffener stub strain; nozzle inlet housing strain; case acreage and joint radial growth; and nozzle growth. Off motor instrumentation measurements

Table 3-4. FSM-1 Performance Summary

	CEI Spec Limits at Vacuum and 60°F	Nominal 2.5σ Acceptance Limits at Vacuum and 60°F	Predicted at 60°F	Delivered at 60°F
Web Time (sec)	105.5 to 116.7	109.6 to 113.1	110.5	110.7
Action Time	115.2 to 131.2	121.1 to 125.9	122.4	121.1
Web time Average Headend Pressure (psia)	629.6 to 700.0	653.7 to 671.5	668.8	670.1
Maximum Headend Pressure (psia)	854.8 to 973.6	896.4 to 928.2	924.6	923.4
Maximum Sea Level Thrust (Mlbf)	2.88 to 3.26	3.02 to 3.11	3.09	3.09
Web Time Average Vacuum Thrust (Mlbf)	2.46 to 2.74	2.56 to 2.63	2.62	2.61
I _{sp} Average Delivered (lbf*sec/lbm)	266.5 to 270.3	266.5 to 269.9	268.4	267.7
Web Time Vacuum Total Impulse (Mlbf*sec)	286.3 to 292.1	286.5 to 291.5	289.2	289.1
Action Time Vacuum Total Impulse (Mlbf*sec)	293.9 to 299.9	294.3 to 298.8	296.7	295.9
Ignition Interval (sec), Time to 563.5 psia*	0.202 to 0.262	0.213 to 0.250	0.232	0.228
Maximum Pressure Rise Rate (psi/10 ms)*	70.9 to 115.9	72.9 to 107.3	91.0	97.1
Burn Rate (ips), at 60°F and 625 psi	NA	NA	0.370	0.370
Igniter Maximum Pressure*	NA	NA	2,004	1,898

*Values listed are at delivered temperature of 82°F

FSM-1 loaded propellant weight = 1,106,109 lbm

consisted of: thrust; thrust vector control systems; test stand water deluge pressure; timing; and nozzle plume thermal radiation.

3.1.10 Temperature Data

Temperature data were nominal. The ambient temperature during the test was 87°F and the propellant mean bulk temperature (PMBT) was 82°F.

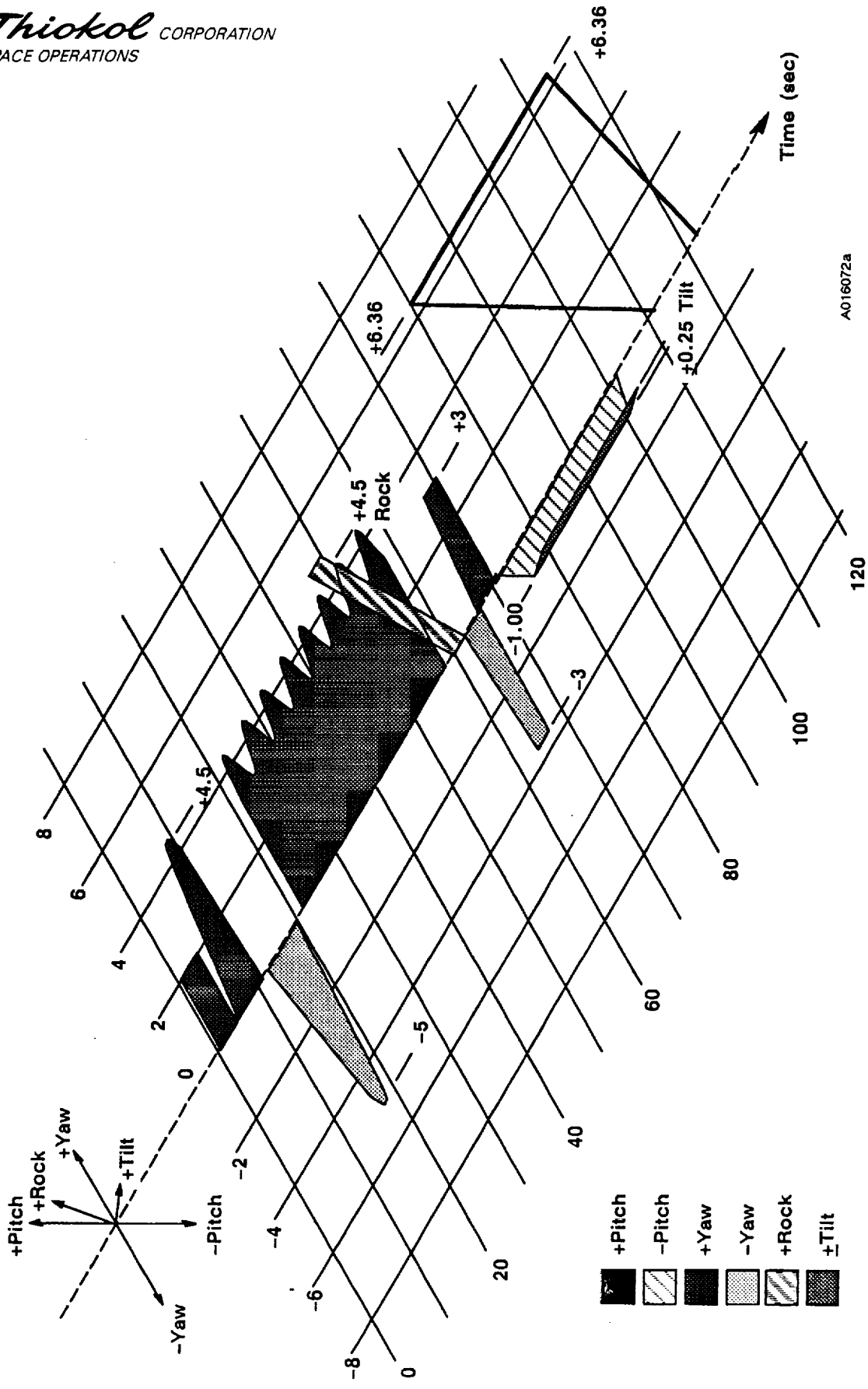
3.1.11 Nozzle TVC Performance

The TVC system performed as planned and followed the specified duty cycle (Figure 3-1).

3.2 CONCLUSIONS

The following listing is the conclusions as they relate specifically to the objectives and the applicable CEI specification (CPW1-3600) paragraphs. Additional information about each conclusion can be found in the applicable referenced section.

<u>Objective</u>	<u>CEI Paragraphs</u>	<u>Conclusions</u>
A. Certify the TP-H1148 SRM propellant manufactured using AP produced by the new WECCO Utah plant.	3.2.1.1.1.1, Ignition Interval; 3.2.1.1.1.2, Pressure Rise Rate; 3.2.1.1.2.1, Nominal Thrust Time Curve; 3.2.1.1.2.2, Performance Tolerances and Limits; 3.2.1.1.2.4, Impulse Gates; 3.3.1.1, Selection of Materials, Parts, and Processes	The FSM-1 ballistic performance was very close to predicted. All values were within the CEI specification limits as well as the more stringent 2.5σ limits (Table 3-4; Figure 6-13; and Section 6.7).
B. Certify the TP-H1178 SRM igniter propellant manufactured using AP produced by the new WECCO Utah plant.	3.2.1.1.1.1, Ignition Interval; 3.3.1.1, Selection of Materials, Parts, and Processes	Igniter ballistic performance met CEI specification and STW3-3176 requirements although delivered performance was lower than predicted (Figure 6-9).



A016072a

Figure 3-1. Static Test Duty Cycle

REVISION _____

- | | | |
|--|---|--|
| C. Revalidate the RSRM and its components, materials, and processes. | None | Successful firing of FSM-1 revalidated the RSRM, its components, materials, and processes. |
| D. Obtain additional data on the low-frequency chamber pressure oscillations in the motor forward end. | None | FSM-1 exhibited chamber pressure oscillations similar to previously tested RSRMs. The first longitudinal (1-L) mode oscillations were typical for an RSRM. RSRM 1-L mode amplitudes were lower than for high performance motors (HPMs) (Figures 6-15 through 6-19). |
| E. Demonstrate the performance of triple-cured nozzle CCP components 3.2.1.1.2.1, Nominal Thrust Time Curve; | 3.2.1.1.2.2, Performance Tolerances and Limits;
3.2.1.1.2.4, Impulse Gates;
3.2.1.4.1.1, Actuator Stall Force;
3.2.3, Reliability;
3.2.3.1, Primary Structure, Thermal Protection, Pressure Vessels;
3.3.1.1, Selection of Materials, Parts and Processes;
3.3.6.1.1, Structural Safety Factors;
3.3.6.1.2.8, Nozzle Performance Margins of Safety | Initial inspection indicate that the additional carbon-wrap cure cycle did not have any adverse effects on the liner performance or ballistic performance. Performance was estimated to be similar to that of a forward nose ring with the standard two cure cycles (Section 6.4). |
| F. Demonstrate the performance of liner and castable inhibitor processed with the new JAYGO mixers. | 3.3.1.1, Selection of Materials, Parts, and Processes | The liner process with the new JAYGO mixers was normal and typical of past RSRM motors (Section 6.2). |

- | | | |
|---|--|---|
| <p>G. Obtain additional data on the performance of bushed pinholes in standard weight and lightweight capture feature cylinder clevis ends.</p> | <p>None</p> | <p>The bushed pinholes at Stations 691.5, 1011.5 and 1331.5 were visually examined for gross deformation of the bushing or parent material and none was detected (Section 6.1.4.7). Useful data was obtained and is included in Appendix F.</p> |
| <p>H. Obtain data on the performance of stiffener segments with known outer ligament cracks in the aft segment stiffener stubs.</p> | <p>None</p> | <p>The previously cracked holes in the aft stiffener stubs were inspected and no further elongation of cracks was noted (Section 6.1.4.8). Useful data was obtained and is included in Appendix G.</p> |
| <p>I. Obtain data on the effect on hardware of standard shims in the factory joint.</p> | <p>None</p> | <p>All factory joints were in excellent condition sustaining no damage during the firing or disassembly operations proving that the standard shims have no adverse effect on the factory joint hardware (Section 6.1.4.6).</p> |
| <p>J. Demonstrate assembly/disassembly of a field joint containing a primary/secondary diameter O-ring in the capture feature.</p> | <p>3.2.5.1, Assembly/Disassembly of Segments</p> | <p>No damage occurred to the O-ring or aft field joint hardware from use of the single size O-ring in the capture feature (Appendix H, Section 6.3).</p> |
| <p>K. Demonstrate the performance of MP159 bolts in the igniter adapter-to-case joint.</p> | <p>None</p> | <p>Post-test inspection of the bolts revealed no signs of yielding or structural deformation (Section 6.5.4).</p> |

L. Obtain data on igniter flange skip. None

Data on igniter flange skip were collected and documented in TWR-61213. Measured data correlated closely to predicted even though some contact may have occurred between the bolts and adapter through holes at about 750 psi (Section 6.5.4).

M. Obtain thermal radiation data from the nozzle plume. None

Eight channels of nozzle plume data were successfully recorded from radiometers installed off motor. These data were supplied to NASA for use in the ASRM program.

3.3 RECOMMENDATIONS

Based on the results of this test, the following recommendations have been made:

It is recommended that AP from WECCO be fully qualified for use in future flight motors pending final test results from the Qualification Plan for Ammonium Perchlorate from Western Electrochemical Corporation's new Utah Plant for TP-H1148 and TP-H1178 Propellant, CTP-0112, Rev A.

The additional CCP cure cycle (three total) may be needed on future RSRM nozzle components to prevent scrapping of acceptable CCP parts.

It is recommended that a new, single size O-ring be created with properties which satisfy current requirements for both capture feature and primary/secondary O-rings.

INSTRUMENTATION

4.1 INTRODUCTION

FSM-1 test article instrumentation measurements consisted of: forward end chamber pressure; forward end chamber pressure oscillation; igniter pressure; joint temperatures; case temperature for deluge control; case acreage and propellant grain temperatures/PMBT; nozzle throat temperatures; nozzle flex bearing temperatures; aft end free air temperatures; case vibration; nozzle position; igniter adapter flange skip; case pinhole strain; case stiffener stub strain; nozzle inlet housing strain; case acreage and joint radial growth; and nozzle growth. Off motor instrumentation measurements consisted of: thrust; thrust vector control systems; test stand water deluge pressure; timing; and nozzle plume thermal radiation. Four hundred and thirty-two data channels were recorded during the motor firing, of which 359 were attached and indexed to the motor.

Strain was measured around bushed pinholes and outer ligament cracked stiffener stub holes for the first time on a full-scale static test. These data channels constituted the majority (206) of measurements on FSM-1.

Appendix B contains the instrumentation list. The new instrumentation channel numbering system that began on TEM-5 was used on FSM-1. The instrumentation list presents both the old and new instrumentation channel numbers. This text of this report will refer only to the new instrumentation identification numbers.

Appendix C contains the plots of the instrumentation channels. Refer to the instrumentation list (Appendix B) for a description of the data channel plots. The plots in Appendix C are presented in the order that they are listed in the instrumentation list.

4.2 OBJECTIVES

The motor was instrumented to support the objectives of the FSM-1 test. Several objectives which were specifically for gathering data by instrumentation were:

- D. Obtain additional data on the low-frequency chamber pressure oscillations in the motor forward end.
- G. Obtain additional data on the performance of bushed pinholes in standard weight and lightweight capture feature cylinder clevis ends.
- H. Obtain data on the performance of stiffener segments with known outer ligament cracks in the aft segment stiffener stubs.
- L. Obtain data on igniter flange skip.
- M. Obtain thermal radiation data from the nozzle plume.

4.3 CONCLUSIONS/RECOMMENDATIONS

4.3.1 Chamber Pressure Oscillations

Operational pressure transducer (OPT) headend pressure oscillation measurements compared well with the baseline Minuteman (used on all static test motors through TEM-4) and OPT (used on TEM-5 and TEM-6). It is recommended that instrumentation continue to be used on future TEMs to expand the database on pressure oscillation and joint performance.

4.3.2 Bushed Pinholes

All strain gage data (180 channels) were usable. Axial strain predictions were somewhat inaccurate because the pretest analysis did not use line loads induced by bending. For a detailed discussion of data, see Section 6.1.4.7. Strain versus time plots for all bushed pinhole data are in Appendix F.

4.3.3 Stiffener Stub Holes Outer Ligament Cracks

Specified instrumentation ranges were incorrect for 11 of 26 channels of the stiffener stub holes resulting in unusable data. Outer ligament cracked stiffener stub holes will

be instrumented on TEM-7 and critical reviews and analyses are being conducted to assure recovery of usable data.

4.3.4 Igniter Flange Skip

Data on igniter flange skip was collected and is documented in TWR-61213, which correlates analysis with test data from the FSM-1 motor. Some contact probably occurred between the igniter bolts and adapter through holes at about 750 psi. This contact may have hindered the unrestrained skip a few mils. Igniter flange skip will again be measured on a future full-scale static test. This data will be collected for the igniter redesign program. The instrumentation design and arrangement will be modified to avoid interference with other hardware.

4.3.5 Thermal Radiation

Eight channels of thermal radiation data was collected at MSFC's requested and provided as directed. Twenty-two channels will be collected for the TEM-7 static test at MSFC's request.

4.4 RESULTS/DISCUSSION

Overall, the FSM-1 instrumentation performed very well. No problems were encountered during the installation of the instrumentation. The instrumentation calibrations conformed to the systems requirements of MIL-STD-45662. All calibrations were performed to the standards of the National Institute of Standards and Technology (NIST).

4.4.1 Forward End Chamber and Igniter Pressure

Four pressure transducers were installed to measure motor chamber and igniter pressure (Data Channels PNCAC001 through PNCAC004). Three gages measured chamber pressure and one gage measured igniter pressure. The performance of each gage was nominal.

4.4.2 Forward End Chamber Pressure Oscillations

The forward end OPT data channel was alternating current (ac)-coupled and processed through special signal conditioning systems for headend chamber mean pressure (Data Channel PNCAC001) and headend chamber pressure oscillation measurements. The oscillation measurements were satisfactory. Refer to Section 6.7 for additional information on chamber pressure oscillation.

4.4.3 Nozzle Axial Extension

Twelve extensometers were installed to measure nozzle position. Nozzle position was successfully determined as measured by the extensometers during motor pressurization and tailoff. Performance of each extensometer was nominal. Section 6.4.4.9 has additional nozzle extensometer information.

4.4.4 Joint Temperature Measurements

RTDs were successfully used to control the temperatures of the field joint and igniter-to-case joint heaters. The RTDs are inherent to the configuration of the field joint heaters. The RTDs for the igniter-to-case joint are bonded to the igniter adapter surface. Refer to Section 6.7 for additional RTD information.

4.4.5 Case Temperature Measurements

Twenty thermocouples were bonded on the bottom of the case to measure case temperature during motor cooldown and deluge water spray control. Case temperature was successfully monitored and recorded for 60 hr after ignition. Refer to Section 6.8 for additional case temperature information.

4.4.6 Bushed Pinholes Strain

Section 6.1.4.7 contains detailed results and discussion of bushed pinholes strain.

4.4.7 Stiffener Stub Holes Strain From Outer Ligament Cracks

Detailed results and discussion of stiffener stub holes strain from outer ligament cracks is contained in Section 6.1.4.8.

4.4.8 Igniter Flange Skip

Detailed results and discussion of igniter flange skip is contained in TWR-61213.

4.4.9 Nose Cap Strain Gage Data

Detailed results and discussion of nose cap strain gage data is contained in TWR-61407.

4.4.10 TVC Systems Data

All data from operation of the TVC system was nominal.

4.4.11 Test Bay Instruments

Thrust stand force gages and deluge system pressure gages provided satisfactory data.

PHOTOGRAPHY

Photographic coverage was required to document the test, test configuration, instrumentation, and any anomalous conditions which may have occurred. The FSM-1 photographs and video tapes are available from the Thiokol Corporation Photographic Services department.

5.1 STILL PHOTOGRAPHY

Still color photographs of the test configuration were taken before, during, and after the test. Photographs were taken of joints each 45 deg minimum and at anomalous conditions.

5.2 MOTION PICTURES

Cameras were located and positioned in accordance with test plan CTP-0171 Revision A plus one additional high-speed camera to cover instrumentation posts on which the eight radiometers were mounted.

Color motion pictures of the test were taken with five video, two real-time documentary, ten high-speed cameras, and two still-sequence cameras. All cameras functioned properly for the test. Documentary motion pictures are recorded on Roll No. 8267, high-speed motion pictures on Roll No. 8268, and videotape on No. V0614. Cameras are listed in Table 5-1. Camera start and stop times are listed in Table 5-2. The camera setup is shown in Figure 5-1.

Table 5-1. Photography and Video Coverage

Camera	Station	Location	Type	Coverage
1	3	North Wall	HS	Igniter Port
2	3	North Wall	HS	Center Forward and Center Joint
3	2	North Road	Video	Overall Motor
4	6	North Field	HS	Center Aft and Nozzle-to-Case Joints
5	6	North Field	Doc	Aft Case, Nozzle and Plume
6	6	North Field	HS	Nozzle, 200 ft Plume
7	9	South Field	Doc	Overall Motor and Plume
8	8	South Field	HS	Nozzle, 200 ft Plume
9	8	South Field	HS	Center Aft and Nozzle-to-Case Joints
10	8	South Field	Video	Aft Case, Nozzle and Plume, and Deluge
11	4	South Wall	Video	Aft Joint--Nozzle and Plume
12	4	South Wall	HS	Center Forward and Center Joints
13	4	South Wall	HS	Igniter Port
13a	4	South Wall	Video	Igniter and CO ₂ Quench System
14	11	Thrust Block	Video	Top of Case, Nozzle and Plume
15	11	Thrust Block	HS	Top of Case, Nozzle and Plume
Add	6	North Field	HS	Radiometers
CODE: HS - 10 each 300 pps Doc - 2 each 24 pps Video - 5 each Real-time				

Table 5-2. Camera Control and Priority Requirements

Camera	Controller	Station	Start Time	Stop Time	Priority
1	5	3	T-5 sec	T+ 150 sec	M
2	6	3	T-5 sec	T+ 150 sec	M
3	NA	2	Manual	Manual	R
4	9	6	T-5 sec	T+ 150 sec	M
5	10	6	T-15 sec	T+ 180 sec	R
6	9	6	T-5 sec	T+ 150 sec	M
7	15	9	T-15 sec	T+ 180 sec	M
8	16	8	T-5 sec	T+ 150 sec	M
9	16	8	T-5 sec	T+ 150 sec	M
10	NA	8	Manual	Manual	R
11	NA	4	Manual	Manual	R
12	8	4	T-5 sec	T+ 150 sec	M
13	8	4	T-5 sec	T+ 150 sec	M
13a	NA	4	Manual	Manual	R
14	NA	11	Manual	Manual	R
15	20	11	T-5 sec	T+ 150 sec	M
Add	9	6	T-5 sec	T+ 150 sec	R
Station	Location		Station	Location	
2	Northwest of Bay		6	North of Nozzle	
3	North of Bay		8	South of Nozzle	
4	South Wall		9	South and Aft of Nozzle	
			11	Top of Thrust Block	

M = mandatory R = required

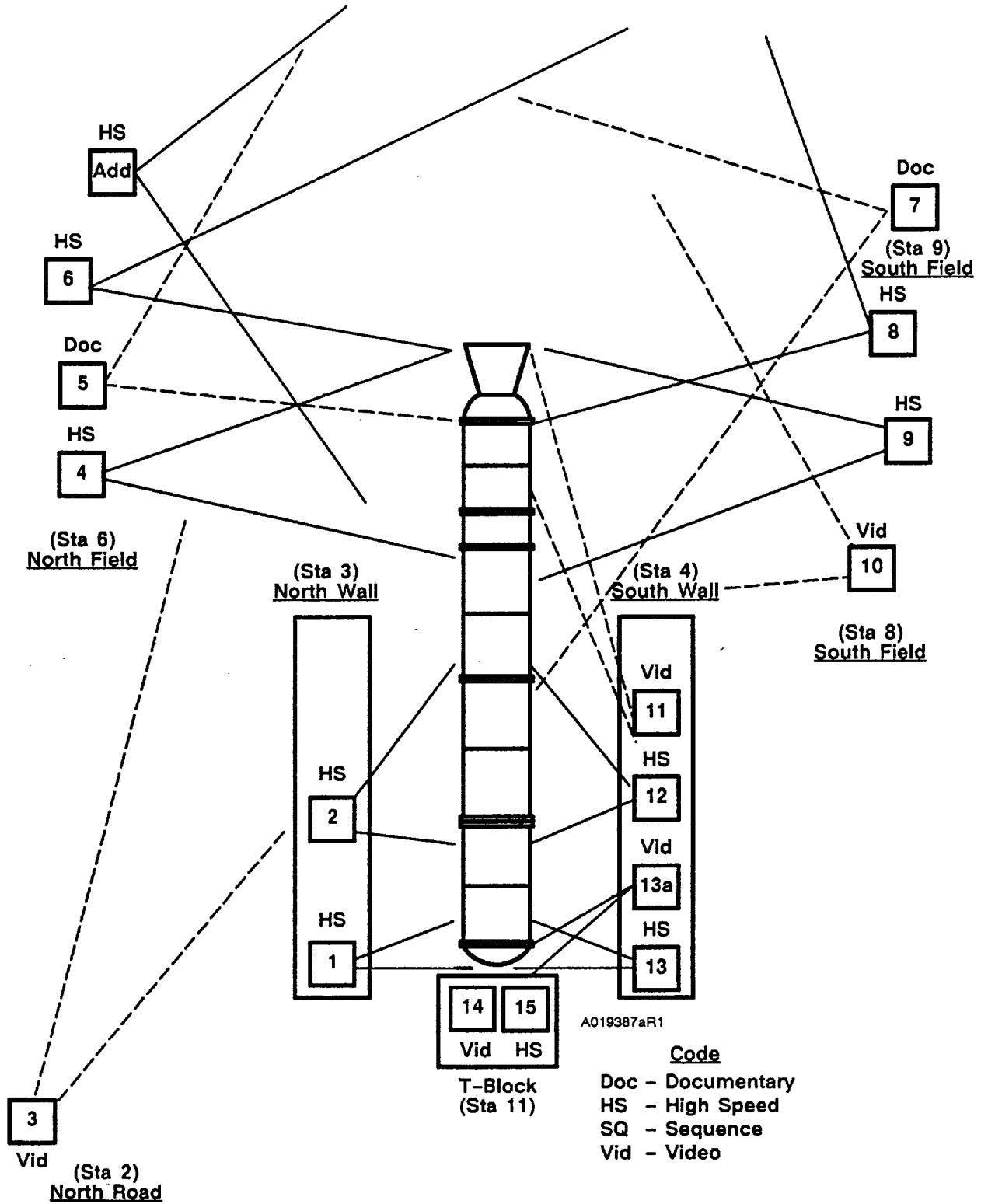


Figure 5-1. Photography Coverage—FSM-1

TEST RESULTS

6.1 CASE PERFORMANCE

6.1.1 Introduction

The external case hardware and joints were in excellent condition with no visible damage or heat effect. No anomalies associated with case or joint hardware occurred in the FSM-1 static test. Assembly procedures proved adequate, and chamber pressure was contained.

6.1.2 Objectives

The objectives from Section 2 regarding case performance are:

- g. Obtain additional data on the performance of bushed pinholes in standard weight and lightweight capture feature cylinder clevis ends.
- h. Obtain data on the performance of stiffener segments with known outer ligament cracks in the aft segment stiffener stubs.
- i. Obtain data on the effect on hardware of standard shims in the factory joint.

6.1.3 Conclusion/Recommendations

All sealing surfaces were visually inspected and found to be in good condition with no evidence of damage, corrosion, or excess grease coverage, with the exception of the forward field joint outer clevis leg outside diameter (OD). Medium corrosion was observed from 100 to 250 deg and between the hat band and clevis tip. It appeared that the grease coating had been removed to accommodate instrumentation installation, resulting in corrosion of the exposed metal. No apparent metal damage was found during the joint inspections, although each field joint had typical scattered pinhole metal slivers.

The hat bands were removed and the bushed pinholes at Stations 691.5, 1011.5, and 1331.5 were visually examined (without pulling the joint pin out) for gross

deformation of the bushing or parent material. None was detected. Bushing positional measurements were taken and no movement of the bushings was detected. The bushings performed as expected with no detrimental effects noted.

The previously cracked holes in the aft stiffener stubs at 24 deg and 162 deg were inspected and no further elongation was noted. Adjacent pinholes were also inspected and no damage was noted.

6.1.4 Results/Discussion

6.1.4.1 Forward Field Joint. There was no corrosion found on either the tang or clevis and no apparent metal damage was found during the inspection, except the corrosion and typical scattered pinhole slivers documented in Section 6.1.3.

6.1.4.2 Center Field Joint. There was no corrosion found on either the tang or clevis. No apparent metal damage was found during the inspection, except for typical scattered pinhole metal slivers.

6.1.4.3 Aft Field Joint. The condition of the joint was nominal. There was no corrosion found on either the tang or clevis. Typical scattered pinhole metal slivers were observed. Otherwise, no apparent metal damage was found during the inspection.

6.1.4.4 Nozzle-to-Case Joint. The sealing surfaces were visually inspected and found to be in good condition with no evidence of damaged or heat effected metal surfaces. Five of the radial bolt plugs had minor disassembly damage.

6.1.4.5 Internal Nozzle Joints. The sealing surfaces were visually inspected and found to be in good condition with no evidence of damage or corrosion. Excessive grease coverage was noted on Joints No. 4 and 5. The grease prevented complete backfill of the room temperature vulcanization (RTV) at 0 to 135 deg and 237 to 260 deg on Joint No. 4. Joint No. 5 had excessive grease around the full circumference.

6.1.4.6 Factory Joints. Each of the factory joints proved to be in excellent condition. The sealing surfaces sustained no damage during the firing or disassembly operations. The standard shims had no adverse effect on the factory joint hardware.

6.1.4.7 Bushed Pinhole Performance. The repair of RSRM joint pinholes through bushing installation is viewed as a practical alternative to scrapping case hardware with oversized or damaged holes. Vendor machining problems as well as elongation and wear due to multiple usage have resulted in a number of segments with these problems.

Three case segments with bushings installed as a result of machining difficulties were included on FSM-1. In an effort to further characterize bushing performance, FSM-1 was instrumented to gather data concerning the use of bushings in the clevis pinholes. To accomplish this, both bushed and nonbushed holes were instrumented with strain gages at strategic locations to characterize the stress field around the hole. The gages selected were strip type to better characterize the rapidly changing stress gradient. As one would expect the stress concentration at the hole leads to higher stresses near the hole tapering off with distance. Also, provisions were made to visually inspect the bushing and surrounding area for damage, as well as, to inspect the bushings inside diameters for elongation.

The intent of this test was to demonstrate the minimal effect the bushing repair has on the stresses in the part. Also, this was the first time the pinhole region was instrumented during a motor firing. Therefore, it provides the opportunity to verify analytical predictions of the region near the pinholes.

Figure 6-1 illustrates the gage configuration and shows the pinhole locations for both the bushed and nonbushed instrumented holes.

The horizontal orientation of the motor in the test stand induces a large bending moment in the steel case. In an effort to minimize differences between the bushed hole and its nonbushed counterpart (due to the bending effect), the non-bushed hole location was determined by mirroring the bushed hole location about the motor vertical centerline.

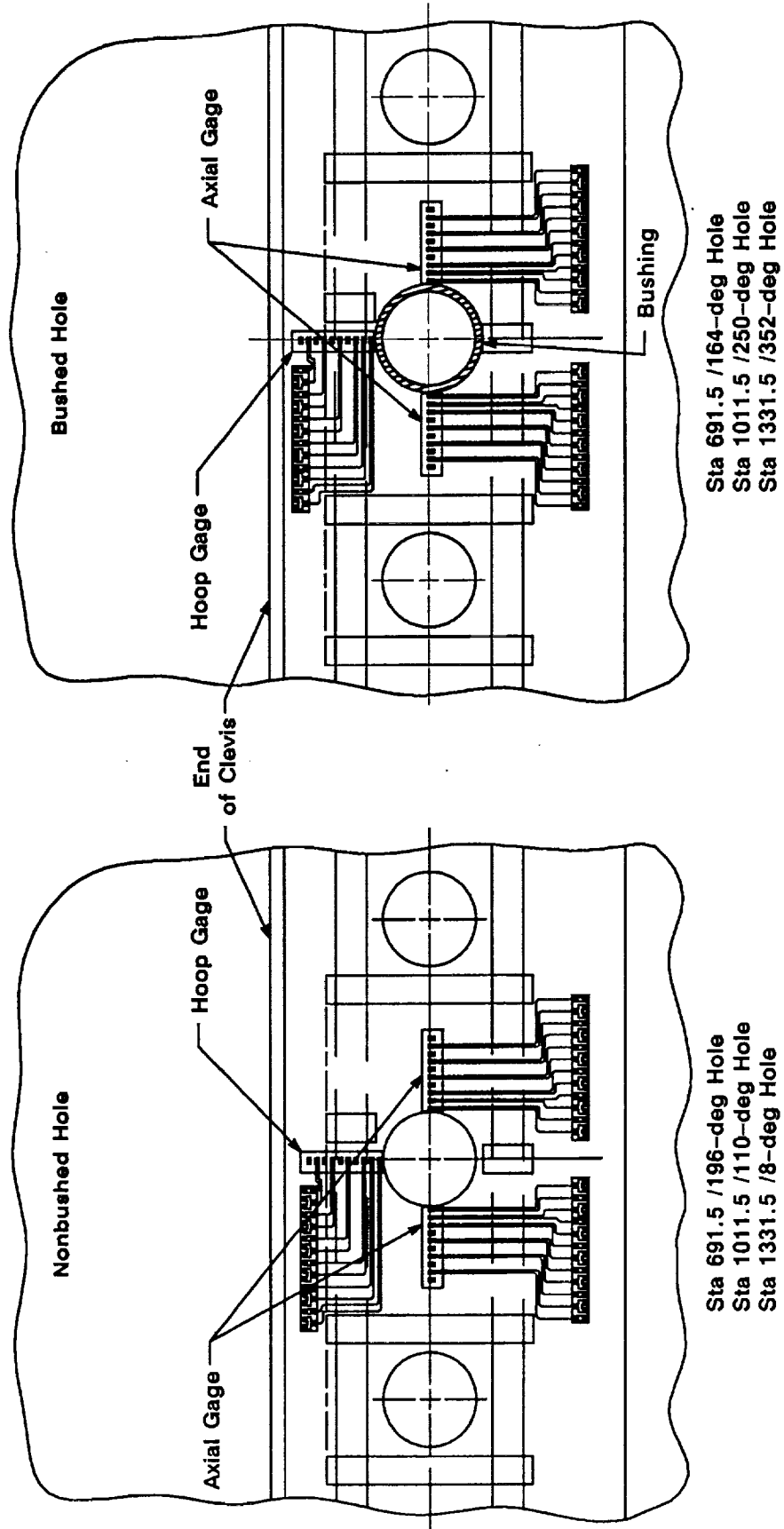


Figure 6-1. Instrumentation Configuration

A030404a

A finite element analysis (ANSYS code, plastic analysis) was used to predict the strains at the pinhole region. The predictions were based on the maximum expected operating pressure (MEOP) of 1,004 psig and axial line loads from the flight load case. The analysis did not use line loads induced by bending, for the test configuration load case. This deficiency makes the axial strain predictions somewhat inaccurate. To compensate for the higher pressure used in the analysis the predicted strain values have been "knocked down" (linear interpolation) to match the actual motor pressure of 933 psig. This resulted in a knock down factor of 0.93. The bending effect did not enter into bushed versus nonbushed comparisons since steps were taken to minimize the effect, as mentioned earlier. However, it does lead to several interesting results in the axial strain data, as is described later. In all the comparison charts, the maximum strain induced by internal pressure loading was used as the compared value. Figures 1A through 6A in Appendix F show comparisons of the bushed versus nonbushed hole strains, Figures 1A and 4A also provide a comparison with analytical prediction for the nonbushed hole at Sta 691.5. The figures are divided up into hoop and axial data for each of the motor joint stations which were instrumented. The horizontal axis on the graphs represent the distance from the edge of the hole. The distance from the hole edge to the first gage on the strip was measured before the test to minimize errors associated with gage positioning. However, given the difficulty associated with this task, the tolerance on that measurement is approximately +0.010 in. which is still a source of possible error in the results. The maximum measured strains were always at the gage nearest the hole edge, reflecting the stress riser associated with the hole. The strain versus time plots for all the gages have been included in Appendix F. Drawing 7U76913 provides a cross reference for gage number versus gage location.

The hoop strain measurements (see Figures 1A through 3A in Appendix F) showed excellent correlation between bushed and nonbushed holes with very little difference noted. In fact, for one of the three joint stations instrumented, the bushed hole actually resulted in a lower hoop strain measurements than its counterpart nonbushed hole. This is evidence that the difference in the strain between the

bushed and nonbushed holes is within the level of accuracy of the test parameters and are very minimal as was predicted in TWR-60094. Also, the analytical predictions for Sta 691.5 were very accurate, giving added confidence in the overall analysis of the RSRM joints.

The axial gages, however, were much less obvious at first glance. Several variable parameters lead to the initial confusion:

- a. The presence of a moderate compressive strain spike at the 691.5 motor station.
- b. The presence of a small amplitude cyclic vibration (approxiamtely 1.8 Hz) in the strain data.
- c. The axial strain measurements at the 691.5 station also appeared to be quite low in comparison with others.
- d. The peak axial strain did not always occur at peak motor pressure.

Upon further research, all these factors appear to be tied together.

Briefly, the Dynamics section has determined that the fundamental (bending) frequency for the assembled motor in the test stand is approximately 1.8 Hz. This matches the cyclic data from the test very well. The 691.5 station instrumented holes were very near the top of the motor (extreme compressive fiber in bending). This causes the pin to bear against the opposite side of the pinhole more than during the pressurized case. For reasons outside the scope of this report, compressive loads reacted through the pins may induce tensile stresses at the locations of the axial gages. The gages which are zeroed out just prior to the test actually have an induced stress at the zero point. When the motor is pressurized, the stress is relieved (as the pin begins to want to bear against the opposite side of the hole) before it again begins picking up load. This relieving action is sensed by the strain gage as compressive strain. This would explain the compressive spike. To correlate with the predicted data, which did not include test configuration bending effects, we must consider the maximum strain at the 691.5 station to be from the compressive peak to tensile peak strain. This value is used in the comparison figures. The other instrumented holes

were either near the neutral axis of the motor, or the bending action already caused the hole to be bearing against the same side as the pressure loads would induce. Therefore, the same effect would not be noted for those holes, as was the case. Lastly, the burning away of the propellant in the motor during the test gradually reduces the bending effect throughout the test. Again, due to the relative positions of the instrumented holes with respect to the neutral axis of the motor, each gage was zeroed out with either a tensile or compressive stress induced. Thus, as the propellant burns away, the reducing bending moment either appears to feed the strain magnitude or detracts from it. This factor caused two observable phenomena: 1) the axial strains at the 691.5 station appear to be higher at lower motor pressures, well into the firing; and 2) the gages do not come back to zero at zero motor pressure. More work is required to verify that our logic in explaining these phenomena is accurate.

With all this information in mind, the axial data is presented in Figures 4A through 6A of Appendix F. The two strip gages measuring axial strains on each hole were included for redundancy. The strip chosen to provide comparison in the graphs was selected on the basis of how much data they supplied. Bushed versus nonbushed comparisons are shown, as well as the predicted strains for the hole at Sta 691.5. As can be seen, there is little difference between the bushed and nonbushed results as was predicted. Also, analytical predictions, while based on different line loads, are on the same order of magnitude as would be expected. The axial strains are very low in comparison with hoop strains and do not dictate the acceptability of the bushing repair.

Post-test visual observations indicated that the bushings performed very well. This was further substantiated by bushing elongation measurements which indicated that the bushing only elongated approximately 0.002 in., which resulted in post-test diameters well below our refurbishment requirement. As a last point, there was earlier speculation that the bushing might move inside the parent hole. The bushings were inspected at strategic times throughout motor processing, both pre- and post-test and it was demonstrated that the bushings do not move.

In conclusion, the test was very successful. The bushings performed as expected with no detrimental effects noted. More work is desirable to help characterize the oddities concerned with the axial data, however, since the oddities represent no particular structural concern this work should not be looked upon as a constraint against the further testing of bushings in the joint pinholes. Finally, it is recommended that we consider the condition of the pinholes in the region of the bushed hole when determining the inside diameter of the bushing. By making the diameters of the bushed hole the same or similar to the adjacent holes, we would ensure that the bushed hole would carry no more or less than its fair share of the load.

6.1.4.8 Cracked Stiffener Stub Performance. All the results from the FSM-1 stiffener stub hoop strain predictions and comparisons are shown in Tables 6-1 and 6-2. The data set of strain versus time is found in Appendix G. Specified instrumentation ranges were incorrect for 11 of 26 channels of the stiffener stub holes resulting in unusable data. Outer ligament cracked stiffener stub holes will be instrumented on TEM-7 and critical reviews and analyses are being conducted to assure recovery of usable data. The tables contain the actual test data as well as the predicted values for the hoop strain at the strain gauge locations. All strains in Tables 6-1 and 6-2 are microstrain values. The headend pressure during the test was measured at 933 psig. Since the predicted values were calculated from an analysis that assumed a head end pressure of 1,004 psi, scaling was necessary to establish a relevant comparison. The scaled value is notes as " ϵ adjusted." Table 6-1 lists the data for the stiffener stubs that had severed outer ligaments.

From the information in Table 6-1 it is evident that the strain increases close to the hole. Figure 6-2 shows the strain gage locations. This would seem to indicate that the highest strain would occur directly at the edge of the pinhole. However, by examining a finer resolution of calculated strains (Figure 6-3.) it can be seen that the maximum strain is 28500 and it occurs 0.020 in. away from the edge of the hole. This is due to the bolt bearing against the sidewall of the hole during pressurization. Since

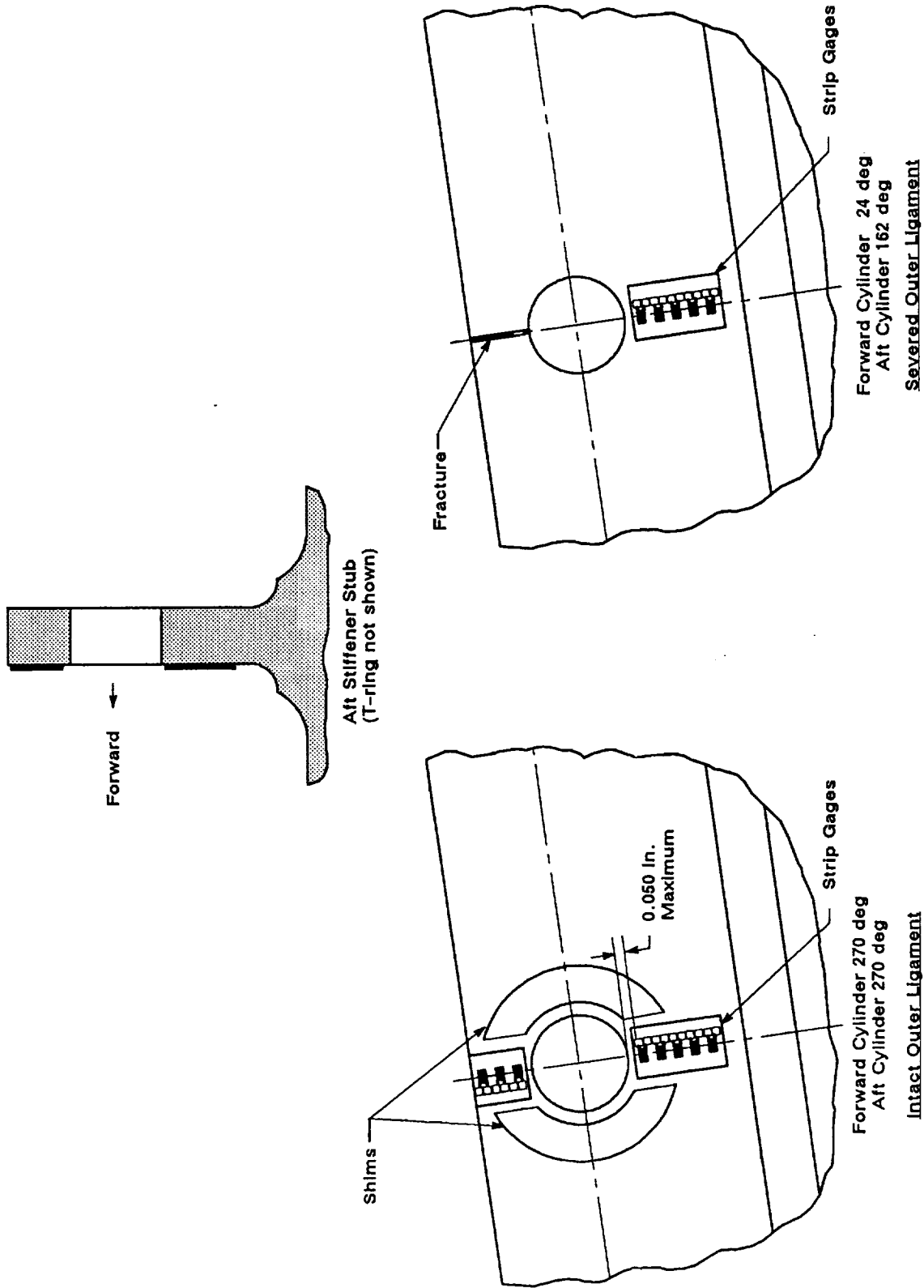
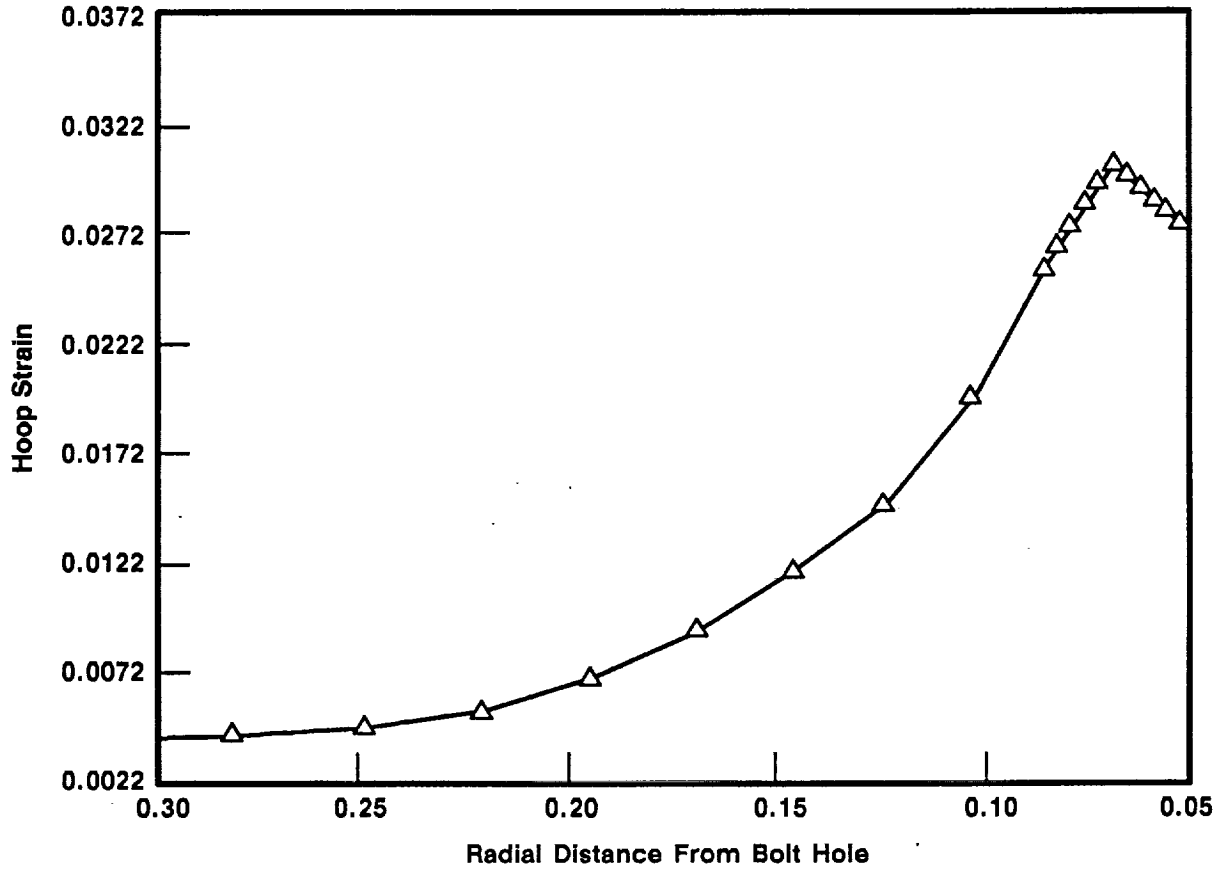


Figure 6-2. Strain Gage Location

A030403a

Strain for Severed Outer Ligament With Ring



A030408a

Figure 6-3. Predicted Hoop Strain for Severed Outer Ligament

the actual strain gage data was collected only every 0.010 in., this effect was not detected.

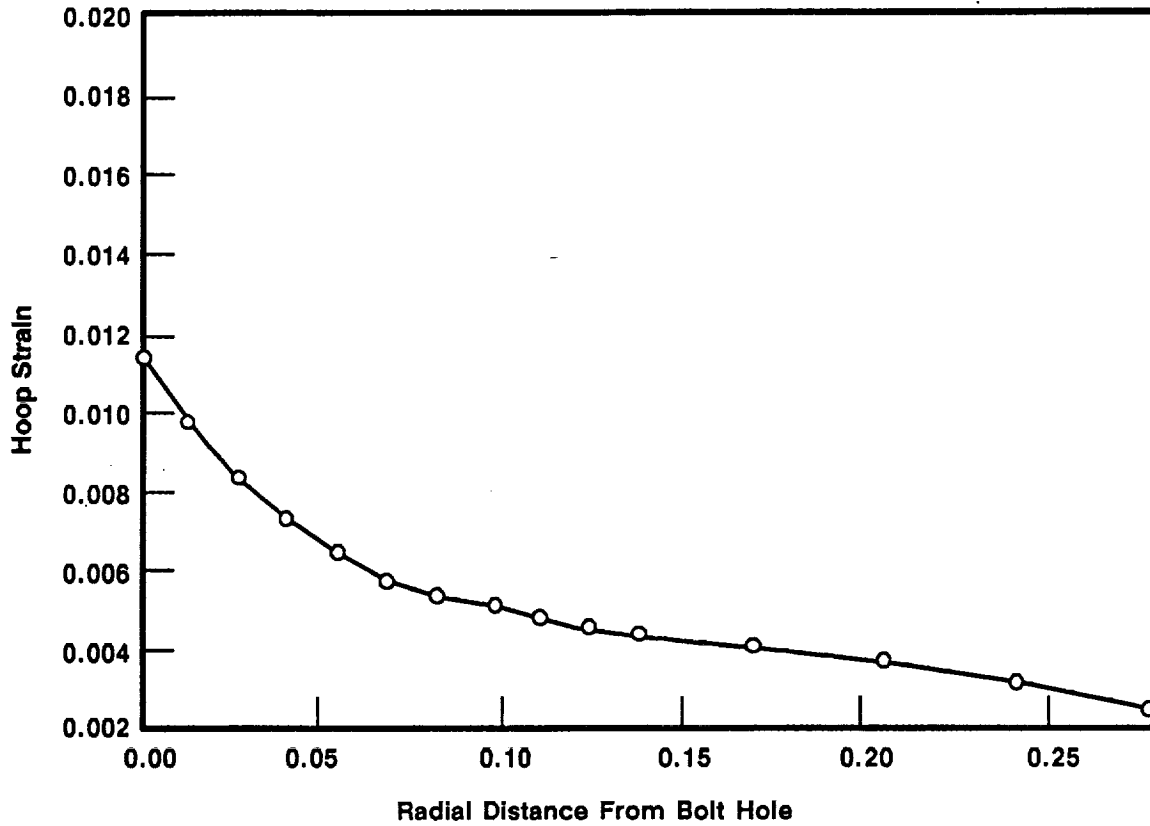
Table 6-1. Severed Outer Ligament

Gage	Location (± 0.010)	ε Measured (933 psig)	ε Predicted (1,004 psi)	ε Adjusted (93%)	Error (%)
K24	0.025	NA	29,426	27,345	NA
L24	0.050	NA	27,175	25,253	NA
K23	0.100	NA	15,436	14,344	NA
L23	0.160	NA	8,759	8,140	NA
K22	0.200	NA	6,428	5,973	NA
L22	0.240	4,250	5,095	4,735	11.4
K21	0.275	4,200	4,529	4,209	0.2
L21	0.330	3,750	4,054	3,767	0.5
K20	0.350	3,900	3,937	3,659	6.2
L20	0.400	3,200	3,732	3,468	8.4

Table 6-2 contains all the information on the intact stiffener stub holes. As expected the intact stub holes have strains much lower than the holes with a severed outer ligament.

Figures 6-4 and 6-5 show a continuous approximation of the predicted hoop strain for the outer and inner ligaments of the intact stiffener stub respectively. By examining Figure 6-5, it can be seen that like the case with the severed outer ligament, the hoop strain in the stub with the intact outer ligament increases as you move close to the hole and then drops at the edge of the hole. Based on the predicted values, the highest hoop strain for the inner ligament of the intact stub is 15,500 at 0.026 in. off the edge of the hole. The maximum hoop strain for the outer ligament of the intact stub is 10,330 and is located at the edge of the hole. All the calculated data for both the severed and intact outer ligament stubs are found in

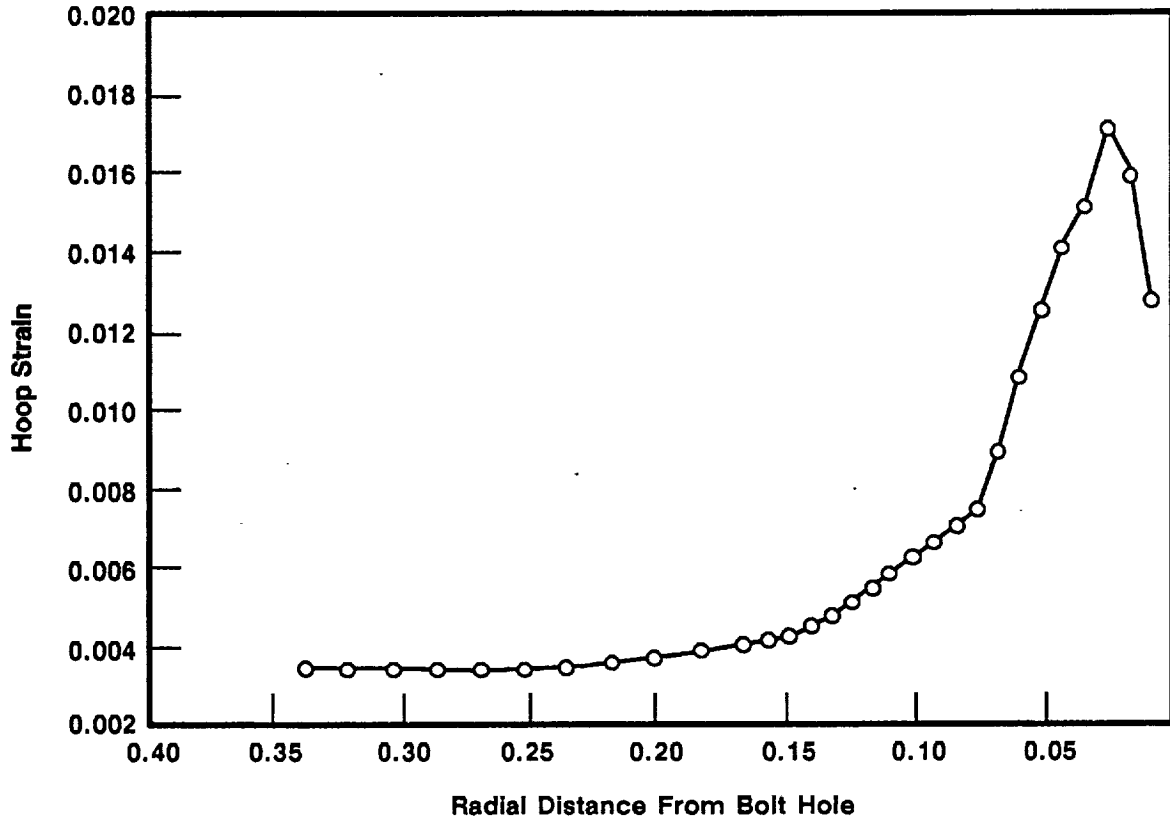
Strain for Intact Outer Ligament With Ring
Outer Ligament



A030409a

Figure 6-4. Predicted Hoop Strain for Intact Outer Ligament (outboard side)

Strain for Intact Outer Ligament With Ring
Inner Ligament



A030410a

Figure 6-5. Predicted Hoop Strain for Intact Outer Ligament (inboard side)

- b. Nominal Geometry
- c. Headend pressure = 1,004
- d. For the severed ligament case - A cracked stiffener stub was located at every other hole.

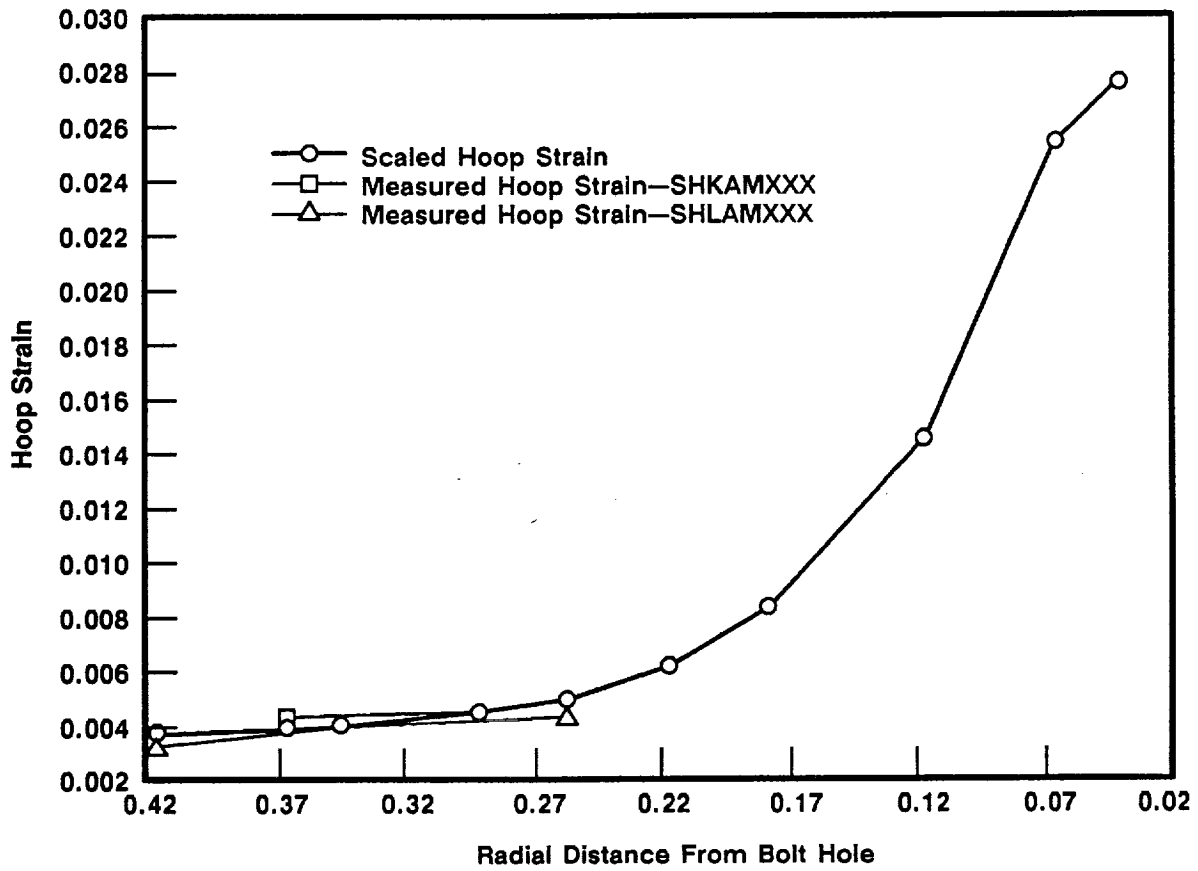
A comparison to the actual and predicted strain values for each gage location is listed in the "Error (%)" column. The differences range from 0.2 to 17.8 percent. This difference in actual and predicted values is explainable if all the inaccuracies and errors are examined. There are four areas that were considered to be the largest contributors to the difference between the actual and calculated values:

- a. Difference in material properties
- b. Inaccuracy in strain gage location measurement
- c. Difference in headend pressure
- d. Gage inaccuracy

The difference in material properties is the largest single contributor to the error associated with areas of large strain. A yield strength of 180 ksi was used in the finite element representation of the stiffener. The actual yield strength of this stiffener is 194.4 ksi. Since a lower strength material was used for the finite element model, it would predict larger strains, particularly in the areas of greatest strain (i.e. close to the pinholes.) This is evident in Figures 6-6, 6-7, and 6-8, where it can be seen that the actual and predicted values are quite close away from the pinhole and start to deviate as you move closer to the hole. This supports the argument that the model is predicting more plastic deformation than the real hardware experiences, resulting in a larger predicted strain.

Another area of concern is the inaccuracy of the measurements (± 0.010 in.) that were used to determine the strain gage location. Figures 6-3 and 6-4 show that a 0.010 in. difference in location could result in a 2,140 microstrain difference for the intact ligament and a 2,300 microstrain difference for the severed ligament. This location error coupled with the 2 percent accuracy limit of the gage could result in a significant deviation, making it difficult to accurately predict the hoop strain.

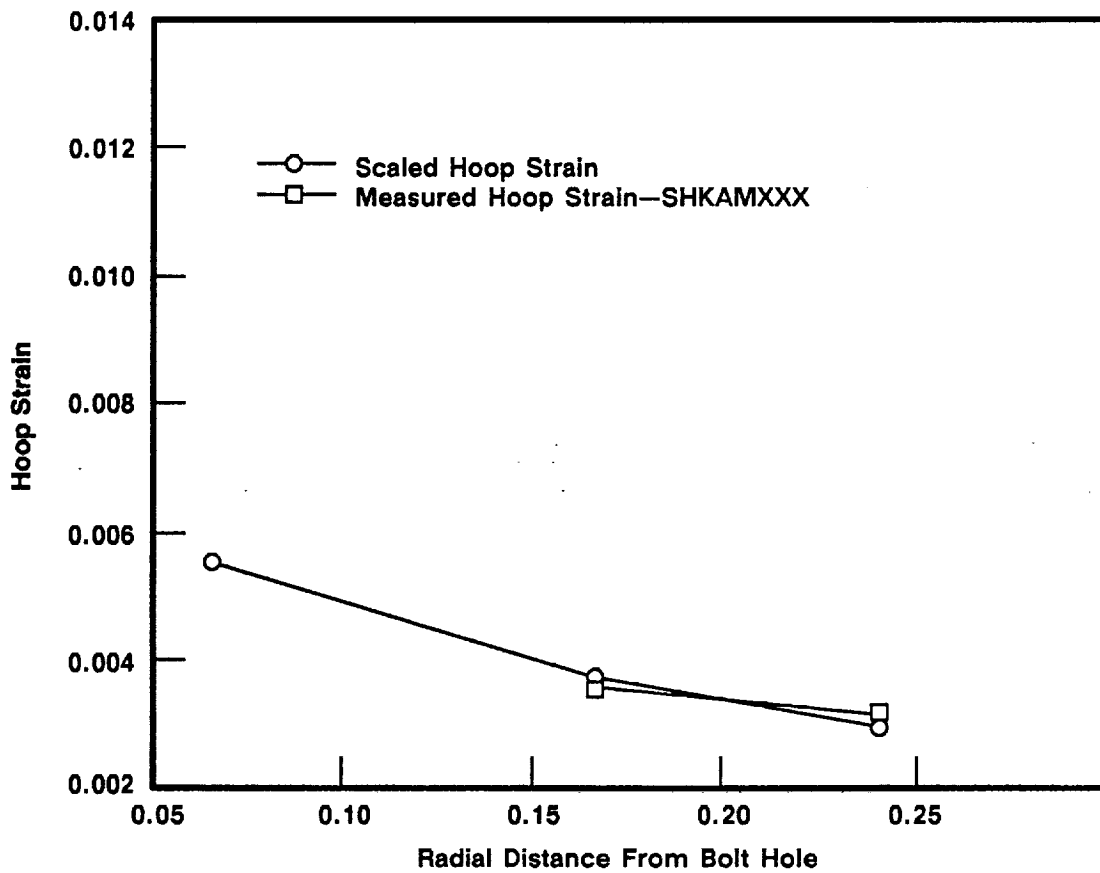
**Strain for Severed Outer Ligament With Ring
Inner Ligament at Gage Locations**



A030406a

Figure 6-6. Scaled Hoop Strain Versus Measured Severed Ligament

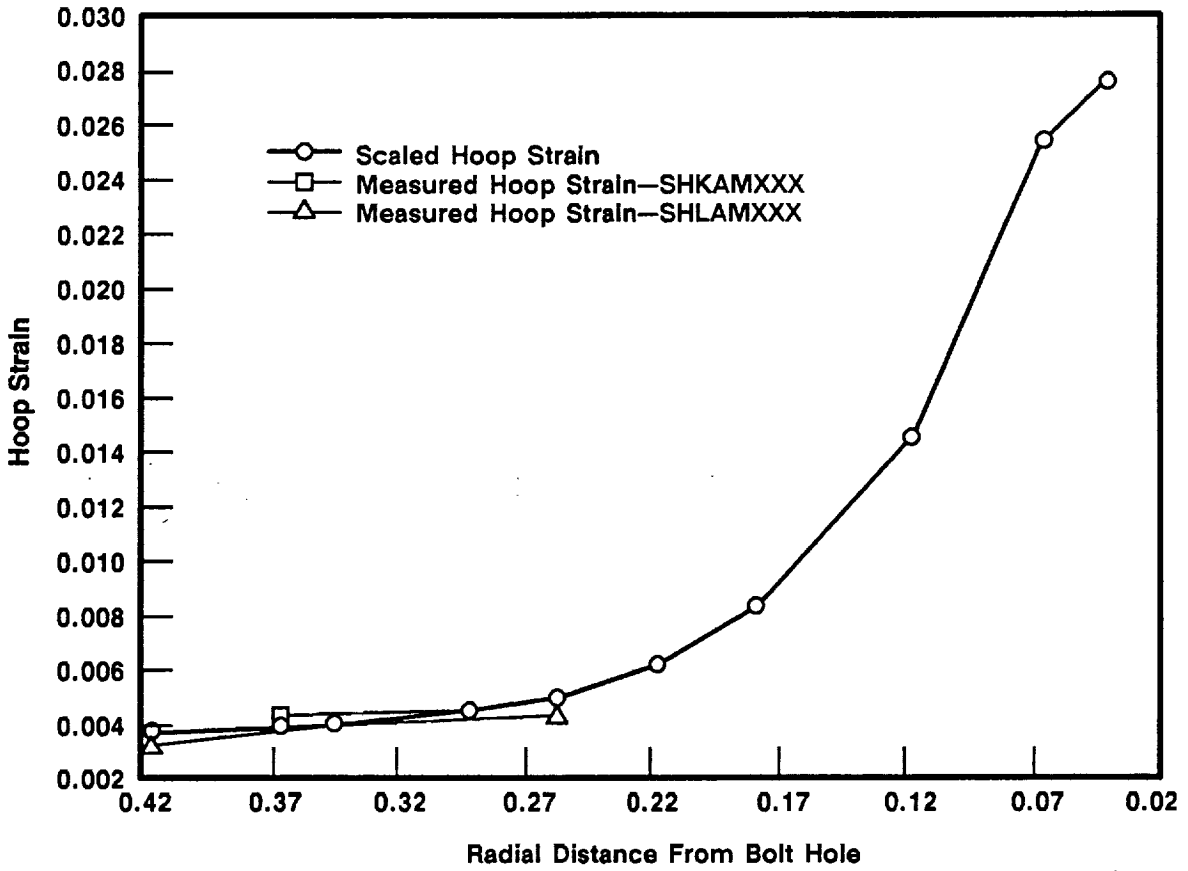
Strain for Intact Outer Ligament With Ring
Outer Ligament



A030405a

Figure 6-7. Scaled Hoop Strain Versus Measured Intact Outer Ligament (outboard side)

**Strain for Severed Outer Ligament With Ring
Inner Ligament at Gage Locations**



A030407a

Figure 6-8. Scaled Hoop Strain Versus Measured Intact outer Ligament (inboard side)

The headend pressure was also a contributor to the inconsistency between actual and predicted values. As stated previously, the analysis was performed using a headend pressure of 1,004 psi. The actual test pressure only reached 933 psig. A simple linear relationship between pressure and strain was assumed and the strains were scaled accordingly. The values used in Figures 6-6, 6-7 and 6-8 have been adjusted by this scale factor (93 percent). The values listed in the ϵ adjusted column on Tables 6-1 and 6-2 also used the 93 percent scale factor.

Based on the data and information presented here, it can be concluded that the finite element method of determining hoop strain in the metal case hardware is sufficient. While the accuracy may be less than desired, it is quite good when considering all the error that is introduced by the various parameters.

6.2 CASE INTERNAL INSULATION PERFORMANCE

6.2.1 Introduction

The internal insulation system included case acreage insulation, joint insulation, and propellant stress relief flaps. See Section 1.2.2 for additional insulation configuration details.

6.2.2 Objectives

The test objective from Section 2 regarding insulation performance was:

- F. Demonstrate the performance of the liner and castable inhibitor processed with the new JAYGO mixers.

6.2.3 Conclusions/Recommendations

The internal and external insulation performed as expected, with the exception of the abnormal erosion patterns on the internal insulation at the aft dome factory joint. The exposed insulation plies on the aft dome were expected, due to prefire insulation voids found during X-ray.

6.2.4 Results/Discussion

6.2.4.1 FSM-1 Visual Evaluations of Case Internal Insulation Performance. During the postfire evaluation, Insulation Design documented the condition of the external factory joint weatherseals, stiffener rings, stiffener stub, nozzle-to-case joint, case field joints, igniter joints, igniter insulation, segment acreage insulation, NBR inhibitors, and stress relief flap regions. The condition of the FSM-1 insulation components is discussed in the following subsections.

6.2.4.2 Factory Joint External Weatherseals. Factory joint external weatherseals were installed only on the forward segment dome/cylinder factory joint and the three aft segment factory joints. The weatherseals installed were in excellent condition. There were no heat affects, unbonds, damaged insulation, or other anomalous conditions. EPDM weatherseal was not installed on the other factory joints.

The three remaining factory joints; forward segment cylinder/cylinder, forward center segment cylinder/cylinder, and aft center segment cylinder/cylinder were covered with plastic vacuum bag material instead of EPDM in order to accommodate instrumentation. Water penetrated the plastic closeout and collected in a small pool at the 0-deg location in the plastic. This was most evident in the forward center and aft center segments. The forward segment had minor water intrusion through the plastic closeout system. The instrumentation did not appear to be affected by the water.

6.2.4.3 Stiffener Stub and Rings. The insulation over the forward stiffener stub and the stiffener rings was in excellent condition with no heat effects discoloration, or unbonds noted on any surface.

6.2.4.4 Nozzle-to-Case Joint. The nozzle-to-case joint performed as expected with no polysulfide blowholes identified across the bondline. Several small voids were identified in the polysulfide located forward of the step intermittently around the circumference. The largest measured approximately 1.0 in. circumferentially by 0.3 in. longitudinally. There was one void aft of step at 338.4 deg located 0.25 in. aft

of step. This void measured 0.3 in. circumferentially by 0.35 in. longitudinally. No voids received gas penetration. Several small pieces of polysulfide were found on the wiper ring. These pieces were loose and located at vent slot locations indicating that this was caused by disassembly and does not represent a problem in the design or function of the joint. Polysulfide porosity was evident in the step region full circumference.

The failure mode of the polysulfide bondline at disassembly was disassembly 70 percent cohesive within the polysulfide, 10 percent adhesive at the NBR to polysulfide interface, and 20 percent adhesive at the phenolic to polysulfide interface. The vent slots showed an average polysulfide fill of 62 percent with values ranging from 0 to 100 percent fill.

The bondline around the circumference demonstrated erosion similar to that observed on previous RSRM motors. The polysulfide was decomposed further into the joint than the flap erosion. For approximately 0.47 in. aft of the erosion, the polysulfide was partially decomposed and bubbled. Although the material was partially decomposed, no gas flow occurred in the adhesive bondline decomposed region.

The insulation erosion in the joint region was similar to the condition of previous RSRM flight motors. The NBR flap and baffle appeared to be bonded in place and in excellent shape with normal heat effects and erosion.

6.2.4.5 Aft Field Joint. The joint insulation configuration performed as designed. The joint insulation surfaces exhibited normal charring and erosion.

The general appearance of the pressure sensitive adhesive was noted. Contact within the joint was based on the flat appearance and matted texture of the adhesive, and noncontact was based on the glossy appearance of the adhesive. The joint appeared to have made excellent bondline contact full circumference at the tip of the J-leg. The bondline contact was measured at 0, 90, 180, and 270 deg. The average contact was 1.09 in. outboard from the tip of the remaining J-leg insulation.

No evidence of motor chamber gas leakage to the O-rings or past the J-joint insulation was identified.

Sooting into the joint bondline was seen in the lower quadrant. This sooting was normal and caused by disassembly. A small dark colored area was found in the pressure sensitive adhesive at 240 deg. This appears to be foreign material that was present prefire. There was no evidence of gas penetration or noncontract in the area and the function of the joint was not affected.

Cracks and crazing were noted on the clevis insulation in the radius region intermittently full circumference. The worst condition occurred at 2 deg and measured 0.025 in. deep by 0.80 in. circumferential by 0.005 in. wide. None of the cracks had any effect on the function of the joint.

No recordable (over 0.10 in. deep) clevis edge separations were detected.

6.2.4.6 Center Field Joint. The joint insulation configuration performed as designed. The joint insulation surfaces exhibited normal charring and erosion.

The joint appeared to have made contact full circumference at the tip of the J-leg. There were intermittent areas of glossy adhesive near the tip of the J-leg on the tang indicating minimal contact with heat soak. Minimum contact was obvious at 202 deg, with glossy adhesive starting 0.15 in. outboard of the remaining material. Some of these shiny areas appeared to have thicker adhesive than normal. The bondline contact was measured at 0, 90, 180, and 270 deg. The average contact was 1.23 inches.

No evidence of motor chamber gas leakage to the O-rings or past the J-joint insulation was identified.

A small strip of orange colored material was found near the capture feature O-ring groove on the tang insulation at about 213 deg. This appears to be tape adhesive residue and had no effect on the joint insulation. Dark colored spots in the adhesive were found on the tang insulation at 236, 238, and 240 deg. These were located in an area approximately 0.80 in. outboard of the remaining material and

typically measured 0.30 in. radially by 1.0 in. circumferentially. The same dark spots were seen in the clevis adhesive intermittently full circumference. There was no evidence of gas penetration or noncontact in any of these areas and the function of the joint was not affected. This condition is very similar to the spot seen on the aft field joint and appears to be foreign material that was present prefire. Normal sooting from disassembly was present in the lower quadrant.

Minor crazing was seen on the clevis insulation in the radius region intermittently full circumference. No actual cracks were found.

No recordable (over 0.10 in. deep) clevis edge separations were detected.

6.2.4.7 Forward Field Joint. The joint insulation configuration performed as designed. The joint insulation surfaces exhibited normal charring and erosion.

The joint appeared to have made contact full circumference at the tip of J-leg. An area of minimal contact was seen at 182 deg measuring 0.3 in. outboard of the remaining material. There was evidence of J-leg tip contact at this location. The bondline contact was measured at 0, 90, 180, and 270 deg. The average contact was 1.07 inches.

No evidence of motor chamber gas leakage to the O-rings or past the J-joint insulation was identified.

A crack with no measurable depth was noted from 262-270-274 deg in the radius region of the clevis insulation along with very minor crazing at 266 deg. The crazing also had no measurable depth.

Normal sooting from disassembly was present in the lower quadrant.

No recordable (over 0.10 in. deep) clevis edge separations were detected.

6.2.4.8 Igniter Joints and Insulation. The igniter-to-case joint insulation and igniter boss insulation were both in excellent condition. An evaluation of the insulation to case interface revealed no edge separations. The boss molded insulation surface was in good condition with normal erosion on the inboard surface.

The overall condition of the putty in the igniter-to-case joint was good. The color of the putty was a consistent light olive green. The putty exhibited 100 percent cohesive failure and nominal tack for the full circumference. There was one blowhole present through the putty at 230 deg. The blowhole measured 1.5 in. circumferentially at the aft edge and 0.25 in. circumferentially at the forward edge with a axial length of 2.3 inches. The blowhole resulted in soot on the metal surface forward of the putty intermittent full circumference.

The condition of the putty and joint insulation in the adapter-to-chamber joint has not been evaluated to this date.

The igniter internal and external insulation was in normal condition. No areas of blistering or abnormal erosion were present.

6.2.4.9 Aft Segment Acreage Insulation. The aft segment internal insulation was in good condition.

The forward facing NBR inhibitor stub exhibited normal erosion around the circumference. Measurements of the inhibitor stub were taken every 30 deg and recorded. The inhibitor height ranged from 4.5 to 9.0 in. which is within the expected range. There were no inhibitor tears greater than 3.0 in. in length noted on this inhibitor.

The segment had light spotty liner remaining extending approximately 3.0 in. aft of the clevis end full circumference. This condition has been seen before on static tests.

The erosion in the aft dome was similar to past flight motors. NBR under the CF/EPDM was exposed from 90-0-200 deg in the area roughly 23.0 in. forward of the nozzle boss to 4.0 in. forward of the nozzle boss. This is a common condition in the aft dome.

The aft dome factory joint experienced abnormal erosion on the leading edge of the factory joint insulation buildup from 60-90-180 deg and 225-270-320 deg. The forward edge buildup was eroded approximately 2.0 in. further than the surrounding

(normal) erosion profile resulting in a step-like insulation profile 0.30 to 0.50 in. deep. This condition had been seen on a previous static motor but its cause has not been determined as of yet.

The leading edge of the aft dome factory joint insulation buildup also experienced intermittent exposed insulation voids (blister like appearance) full circumference. The largest exposed void was found on top of the aft dome factory joint at 264 deg and measured 2.0 in. circumferential by 1.0 in. longitudinal. Several linear shaped exposed voids were also found intermittently full circumference. These were located at approximately 70 in. forward of the dome boss. The largest was located at 15 deg and measured 1.4 in. circumferential by 1.4 in. longitudinal by 0.15 in. radial. This condition was noted as a ply separation on the original PFOR because of its shape and location. After further evaluation the noted ply separation was determined to be an exposed insulation void (ref DR No. 401315) detected by prefire X-rays. The exposed insulation voids found were expected due to the large number of prefire voids (78) noted in the referenced DR at this factory joint.

The slag pool in the aft segment was small compared to previous static tests. The slag pool measured approximately 188.0 in. axial length by 41.0 in. circumferential width as the forward end. Its weight was determined to be 466 lb.

The remainder of the aft segment acreage insulation was in normal condition. There were no gouges, separations, cuts, missing material, or other areas of blisters or excessive erosion.

6.2.4.10 Aft Center Segment Acreage Insulation. The aft center segment internal insulation was in excellent condition. The forward facing NBR inhibitor stub exhibited uniform erosion full circumference. Measurements of the remaining NBR inhibitor stub were taken every 30 deg and recorded. The inhibitor stub heights ranged from 10.5 to 14.5 in. for this segment, which is within the expected tolerance bond. There were no inhibitor tears greater than 3 in. in length noted on this segment.

The liner coverage on the aft center segment was normal compared with previous static tests. Liner coverage was heavy near the clevis end and generally missing aft of the factory joint.

The cartable inhibitor was completely missing full circumference, and the stress relief flap was eroded back to the flap bulb full circumference. Both of these conditions are typical of an aft center segment. The CF/EPDM under the flap was eroded to the flap bulb full circumference except at two areas, 320-0-20 deg and 40-50-60 deg where a maximum of 6.0 in. of CF/EPDM was remaining. The exposed NBR under the flap was heat affected.

No evidence of blisters, separations, gouges, cuts, missing material, or excessive erosion was identified in the aft center segment.

6.2.4.11 Forward Center Segment Acreage Insulation. The forward center segment internal insulation was in excellent condition.

The forward facing NBR inhibitor stub exhibited uniform erosion full circumference. Measurements of the remaining NBR inhibitor stub were taken every 30 deg and recorded. The inhibitor stub heights ranged from 22.5 to 27.5 in., which is common for a forward center segment. There were no inhibitor tears greater than 3 in. in length noted on this segment.

The liner coverage on the forward center segment was normal compared with previous static tests. Liner coverage was heavy near the clevis end and generally missing aft of the factory joint.

The cartable inhibitor was completely missing full circumference, and the stress relief flap was eroded back approximately 10.5 to 13.5 in. from the tang end full circumference. Both of these conditions are typical of a forward center segment. The CF/EPDM under the flap exhibited normal erosion with slight blistering (less than 1.5 in. diameter) evident intermittent full circumferences. NBR was exposed under the flap from 90-180-230 deg. This NBR was heat affected.

No evidence of separations, gouges, cuts, missing material, or excessive erosion was identified in the forward center segment.

6.2.4.12 Forward Segment Acreage Insulation. The forward segment internal insulation was in good condition.

The liner coverage on the forward segment was normal with the exception of an area at 270 deg located approximately 135 in. forward of the tang end. This area measured about 58.0 in. circumferentially by 26.0 in. radially and contained only light (spotty) liner coverage. Other similar but smaller areas of light liner coverage were seen adjacent to this larger area. This entire area aft of the star pattern to the flap bulb usually was heavy liner coverage full circumference, however, no unusual erosion was seen at this location and all thermal safety factor requirements were met. The 11-point star pattern in the liner was easily distinguishable, and the star and nonstar liner termination points were typical of past static motors.

The cartable inhibitor was completely missing full circumference. The stress relief flap showed erosion typical of a forward segment. The CF/EPDM under the flap also exhibited normal erosion.

No evidence of blisters, separations, gouges, cuts, missing material, or excessive erosion was identified in the forward center segment.

6.2.4.13 Insulation Thermal Performance. No unacceptable conditions were found in the thermal safety factor evaluation of the nozzle-to-case joint, factory joints, and case wall acreage. There was only one location, the 161.4 in. station 0 deg plane in the aft center segment, that apparently violated the compliance thermal safety factor requirement. This station is located over the factory joint in a region of insulation ply buildup. An analysis of the insulation surface condition, surrounding prefire and postfire data, and visual inspection of this location indicated that the prefire and postfire measurements were not taken at the same location. Insulation Design has determined that the apparent safety factor violation is due to erroneous data and is not an actual safety factor violation.

6.3 SEALS/LEAK CHECK PERFORMANCE

6.3.1 Introduction

6.3.1.1 Seals. All seals were current RSRM flight configuration except for a clevis O-ring 1U75150-25 which was installed in the capture feature groove of the aft field joint.

6.3.1.2 Leak Test. After each pressure vessel joint was assembled, a leak test was performed to determine the integrity of the seals. The leak tests usually consisted of a joint volume determination and a pressure decay test. The volume and pressure information was combined with temperature and time data, collected during the test, and used in the calculation of a leak rate, expressed in terms of standard cubic centimeters per second (sccs). Each leak test has a maximum allowable leak rate. Some specifications require only a maximum pressure decay over time. This method is sufficient based on the small, constant volumes, and the equivalent leak rates, which are conservative when using all worst-case variables.

Table 6-3 lists each joint which was leak tested on FSM-1, the corresponding leak test specification, and the equipment used.

6.3.2 Objectives

6.3.2.1 Seals. The test objective from Section 2 regarding seals was:

J. Demonstrate assembly/disassembly of a field joint containing a primary/secondary diameter O-ring in the capture feature.

6.3.2.2 Leak Tests. The leak tests on FSM-1 were performed to verify that the joints were properly assembled and the O-rings would perform properly. Leak test results were nominal and within allowable limits.

6.3.3 Conclusions/Recommendations

6.3.3.1 Seals. No damage occurred to the O-ring or aft field joint hardware from use of the single size O-ring in the capture feature (Appendix H). It is recommended that a new single size O-ring be created with critical properties which satisfy current

requirements for both capture feature and primary/secondary O-rings. Recommended O-ring dimensions are:

"W" diameter = 0.290 ± 0.004 in.

"A" diameter = 141.300 + 0.100 / - 0.720

Table 6-3. FSM-1 Seal Leak Testing

Joint	Specification	Equipment
Case Factory Joints	STW7-2747	2U129714
Nozzle Joint No. 1	STW7-3475	8U76248
Nozzle Joint No. 2	STW7-3476	2U129714
Nozzle Joint No. 3	STW7-3477	2U129714
Nozzle Joint No. 4	STW7-3478	2U129714
Nozzle Joint No. 5	STW7-3320	2U129714
Case Field Joints	STW7-3447	8U76902
Nozzle-to-Case Joint	STW7-3448	2U129714
Ignition System Inner Gasket	STW7-3632	2U126714
Outer Gasket	STW7-3632	2U126714
Special Bolt		
Installation	STW7-3632	2U129714
S&A Joint	STW7-3633	8U76500
Transducer Assembly	STW7-2853	2U65686
B-B	STW7-2913	2U65848

6.3.3.2 Leak Tests. Seals were acceptable for the FSM-1 joints as determined by leak testing including the procedures and equipment used to obtain the results.

6.3.4 Results/Discussion

6.3.4.1 Seals. Postfire inspection showed that the overall condition of seals was slightly better than previous test motors (Appendix H).

A single-size O-ring was investigated for use in the capture feature and the clevis O-ring grooves. The use of a single-size O-ring eliminates the possibility of switching the O-rings during assembly and could provide some cost savings to the RSRM program.

Testing was conducted on transient pressure test article (TPTA) hardware at MSFC (TWR-60752) and on the FSM-1 aft field joint. The objective of the single size O-ring testing was to determine if the same size O-ring which is installed in the primary and secondary O-ring grooves can also be installed in the capture feature O-ring groove without damaging the O-ring. This supports the requirement in Specification CPW1-3600A paragraph 3.2.5.1 which states that the RSRM shall be capable of assembly/disassembly in both the vertical and horizontal position.

Three dry fit tests were conducted in the vertical test stand at MSFC. A clevis O-ring was installed in the capture feature groove for each of the dry fit tests. No damage occurred to the capture feature O-rings on any of the three dry fit tests.

The FSM-1 dry fit test was conducted in a horizontal test stand. No damage occurred to the capture feature O-ring during assembly or disassembly.

The O-rings chosen for the tests had a large cross sectional diameter and a large "A" diameter (hoop). O-ring squeeze and volume fill were increased which produced a worst-case condition for the tests.

It is recommended that a new size O-ring be created with a squeeze no less than 10 percent (capture feature requirement) and squeeze no less than 16.5 percent (primary/secondary requirement).

6.3.4.1.1 Forward Field Joint. The FSM-1 forward field joint was disassembled on 10 Sep 1990. The condition of the joint was nominal. No hot gas or soot was observed past the O-rings. There was no evidence of damage to the O-rings while in

the groove. Light corrosion was found intermittently over the full circumference between the hat band paint strip and the end of the clevis leg, worst case being 100 to 200-deg arc. This is the area that normally covered by the weatherseal on flight hardware and is not greased at the time of assembly. The grease on the O-rings and sealing areas was very light and did not meet STW7-2999 requirements. Pinhole slivers were found in the clevis pinholes located at 214, 272, 330, 336, and 342 deg. This is caused by installation of the pins at assembly. Otherwise, no apparent metal damage was found during the inspection. The leak check port plug and port were in nominal condition.

6.3.4.1.2 Center Field Joint. The FSM-1 center field joint was disassembled on 5 Sep 1990. The condition of the joint was nominal. No hot gas or soot was observed past the O-rings. There was no evidence of damage to the O-rings while in the groove. Typical light corrosion was found intermittently around the outer clevis leg outer diameter. The grease on the O-rings and sealing areas was as prescribed in STW7-2999. Pinhole slivers were found in the clevis pinholes located between 0 and 90 deg. This is caused by installation of the pins at assembly. There were six small radial scratches at 140 deg on the tang inside diameter (ID). The scratches are less than 0.010 in. in depth and not on the seal surface. The leak check plug and port were in nominal condition.

6.3.4.1.3 Aft Field Joint. The FSM-1 aft field joint was disassembled on 4 Sep 1990. The condition of the joint was nominal. No hot gas or soot reached the primary O-ring. No damage was found on the primary or secondary O-rings while in the groove. No corrosion was observed on the tang or the clevis joints. Typical pinhole metal slivers were found intermittently around the circumference of the clevis joint. This is caused by installation of the pins at assembly. Otherwise, no apparent metal damage was found during the inspection. The grease on the O-rings and sealing areas was as prescribed in STW7-2999. No damage was observed to the leak check port plug or any of the seal surfaces.

The capture feature O-ring installed in the aft field joint was a larger O-ring than the current flight configuration. The capture feature O-ring was the same size as the primary and secondary O-rings. A single size O-ring is being investigated to eliminate the possibility of switching the O-rings during assembly. Inspection revealed no damage to the capture feature O-ring during assembly or disassembly.

The clevis of the aft field joint was previously used on a flight motor and fretting was documented at 180-deg location. Post-fire evaluation found no new fretting.

6.3.4.1.4 Nozzle-to-Case Joint. The FSM-1 nozzle-to-case joint was disassembled on 6 Sep 1990. The condition of the joint was nominal. No hot gas or soot was observed past the O-rings. There was no evidence of damage to the O-rings while in the groove. The polysulfide was past the wiper ring at the vent slot locations. A new type of radial bolt hole plug was used and while several of the plugs were damaged, the wiper ring was protected much better than with previous plugs. The grease on the O-rings and sealing areas was as prescribed in STW7-2999. No corrosion was observed on any of the joint areas and no metal damage was found on the sealing surfaces.

6.3.4.1.5 Internal Nozzle Joints. Forward Exit Cone-to-Aft Exit Cone (Joint No. 1)--The post-fire evaluation of the FSM-1 aft exit cone-to-forward exit cone joint was conducted on 27 Aug 1990. The sealing surfaces were visually inspected and found to be in good condition with no evidence of damage, corrosion, or excess grease coverage. In groove evaluation found no erosion, heat effects, or damage on the O-rings.

RTV was in contact with the primary O-ring inner surface approximately 95 percent of the circumference. No pressure path was found through the RTV rubber. No RTV was found past or on the sealing crown of the primary O-ring. The sealing surfaces were in nominal condition.

Forward End Ring-to-Nose Inlet Housing (Joint No. 2)--The postfire evaluation of the forward end ring-to-nose inlet housing was conducted on 13 Sep 1990. The

sealing surfaces were visually inspected and found to be in good condition with no evidence of damage, corrosion, or excess grease coverage. The primary O-ring was damaged at 135 deg during disassembly.

Nose Inlet Housing-to-Throat Support Housing (Joint No. 3)--The postfire evaluation of the nose inlet housing-to-throat was conducted on 13 Sep 1990. The sealing surfaces were visually inspected and found to be in good condition with no evidence of damage, corrosion, or excess grease coverage. There was no damage to the O-rings; however, there was soot to the primary O-ring at 188 to 191 deg and a blowhole in the RTV at 183 deg.

Forward Exit Cone-to-Throat Support Housing (Joint No. 4)--The postfire evaluation of the forward exit cone-to-throat support housing was conducted on 13 Sep 1990. The sealing surfaces were visually inspected and found to be in good condition with no evidence of damage or corrosion. Excess grease inhibited the RTV-backfill from 0 to 135 deg and from 237 to 260 deg. There was no damage to the O-rings.

Fixed Housing-to-Aft End Ring (Joint No. 5)--The postfire evaluation of the fixed housing-to-aft end ring was conducted on 13 Sep 1990. The sealing surfaces were visually inspected and found to be in good condition with no evidence of damage or corrosion. There was excess grease the full circumference of the joint, particularly in the leak check groove. There was no damage to the O-rings.

6.3.4.1.6 Igniter. S&A-to-Igniter Adapter--Inspection of the S&A-to-igniter adapter joint and gasket revealed no anomalous conditions; however, typical sooting was noted on the ID and both faces of the gasket but not past the primary seal. No damage to the gasket seals or the S&A sealing surfaces was found. Refer to Section 6.5.4 for information about the S&A disassembly.

Igniter Outer Joint

The FSM-1 igniter outer joint was disassembled on 13 Sep 1990. The condition of the joint was nominal. New ultrasonically torqued MP159 attach bolts were used in the

outer joint. No damage to the threads of the forward dome boss was found. There was a blowhole through the outer joint putty at 230 deg. The blowhole was approximately 1.5 in. wide at the entrance and 0.25 in. wide at the exit. No pressure or soot was found to or past the primary seal. No soot found on either side of the gasket retainer. There was no indication of heat effects on the gasket, chamber, or forward dome. There was no evidence of missing cadmium plating on the gasket. No seal damage was found. The leak check port plug and port were in nominal condition.

Igniter Inner Joint

6.3.4.2 Leak Tests. The sets of equipment used to test the FSM-1 joints are shown in Table 6-3. The test specifications are listed in this table as well. The specific joint results are discussed below.

The case field joint leak test results are shown in Table 6-4. The results of the leak tests for the factory joints were nominal.

Table 6-4. FSM-1 Case Factory Joint Leak Test Results

Pressure (psig)	Allowable Leak Rate (sccs)	Actual Leak Rates (sccs)						
		Forward		Center Forward	Center Aft	Aft		
		DM-CY	CY-CY			ET-ST	ST-ST	DM-ST
185 P-S	0.072	0.0075	0.0048	0.0069	0.0098	0.0091	0.0097	0.0059
30 P-S	0.0082	0.0011	0.0012	0.0007	0.0006	0.0009	0.0009	0.0025

P-S = primary-to-secondary cavity DM = dome
 ET = external tank attachment CY = cylinder
 ST = stiffener

The nozzle internal joint leak test results are shown in Table 6-5. The results of the leak tests for the nozzle internal joints were nominal.

Table 6-5. FSM-1 Nozzle Internal Joint Leak Test Results

Joint No.	Maximum Test Pressure	Allowable Leak Rate, High/Low (sccs)*	Actual Leak Rate High/Low (sccs)
1	83	0.029/0.0082	0.0027/0.009
2	920	0.084/0.0082	0.0146/-0.0005
3	740	0.070/0.0082	0.0054/-0.0001
4	144	0.053/0.0082	0.0026/0.0002
5	920	0.084/0.0082	0.0037/0.0014

*High/Low = 1,000 psig/30 psig

The case field joint leak test results are shown in Table 6-6. These joints were tested with the assembly stands in place. The tests were not repeated after the assembly stands were removed because on previous RSRM test motors there was no degradation or change in performance of the field joints after the stands were removed. The results of the leak tests for the field joints were nominal.

Table 6-6. FSM-1 Case Field Joint Leak Test Results

Pressure (psig)	Maximum Leak Rate (sccs)	Actual Leak Rate (sccs)		
		Forward	Center	Aft
1,000 P-S	0.10	0.0193	0.0038	0.0245
30 P-S	0.0082	0.0004	-0.0006	-0.0003
100 P-C	0.037	0.0159	0.0327	0.0317
0 P-S*	0.037	0.0002	0.0007	0.0007
30 P-C	0.0082	-0.0002	0.0003	0.0009
0 P-S*	0.0082	0.0001	0.0004	0.0002

P-S = primary-to-secondary cavity

P-C = primary seal-to-capture feature cavity

*Monitor pressure rise P-S cavity

The ignition system leak test results are shown in Table 6-7. The equipment was identical to that used to test most of the RSRM flight joints. All results were within the limits.

Table 6-7. FSM-1 Igniter and S&A Leak Test Results

Joint Seal	Allowable Leak Rate (sccs), High/Low*	Actual Leak Rate (sccs), High/Low
Igniter Inner	0.10/0.0082	0.0042/-0.0003
Outer	0.10/0.0082	0.0056/-0.005
Igniter OPT	0.10/0.0082	0.0032/-0.0004
S&A	0.10/0.0082	0.0025/0.0001
OPT** (4 bolts)	10 psi/10 min 1 psi/10 min	3.0/0.0 3.0/0.0 2.0/0.0 4.0/0.0
B-B	1 psi/10 min	0.0

*High/Low = 1,000 psig/30 psig

**OPTs tested at 1,024 and 30 psig

Table 6-8 lists the results of the FSM-1 nozzle-to-case joint leak test. The 2U129714 equipment was used to test the FSM-1 nozzle-to-case joint. All leak test results were within the allowable limits.

Table 6-8. FSM-1 Nozzle-to-Case Leak Test Results

Pressure (psig)	Allowable Leak Rate (sccs)	Actual Leak Rate (sccs)
920 P-S	0.0840	0.0047
30 P-S	0.0082	-0.0007
25 P-W	5 psi/5 min	0.169 psi
0 P-S*	0.0082	-0.0001
Stat-O-Seal	0 bubble/sec	No leak

P-S = primary-to-secondary cavity
P-W = primary-to-wiper cavity

6.4 NOZZLE PERFORMANCE

6.4.1 Introduction

The FSM-1 nozzle was a standard RSRM (Drawing No. 1U52861) nozzle assembly which incorporated several modifications. Modifications consisted of reducing the primary O-ring groove depth in Joint No. 4, the forward nose ring carbon cloth was cured three times and an improved cowl assembly bonding method with Joint No. 2 back-filled with RTV silicone rubber (similar to PVM-1, QM-8, and TEM-6). A complete description of the FSM-1 nozzle configuration, with emphasis on configuration and assembly process changes, is presented in Section 1.

6.4.2 Objectives

- E. Demonstrate the performance of triple-cured nozzle CCP components.
- M. Obtain thermal radiation data from the nozzle plume.

6.4.3 Conclusions/Recommendations

Inspections indicate that each configuration change incorporated on the FSM-1 nozzle met the performance margins of safety and that each change will be recommended for incorporation on future RSRM nozzles.

Improved Nozzle Cowl Assembly Process. The improved cowl bonding process was used on TEM-6. EA 913NA adhesive did not squeeze out and mix with the RTV in Joint No. 2 as is typically seen. The RTV penetrated into the joint uniformly as intended. Depth exceeded engineering requirements and it is recommended that this assembly process be used on future static and flight motor nozzles.

6.4.4 Results/Discussion

Overall, the postburn condition of the nozzle liners were as expected. This section focuses on design/process changes and results that were unique to FSM-1; the performance of all additional nozzle components not mentioned were successful. Design configuration/modification are specified within parentheses.

6.4.4.1 Nose Inlet Assembly (RSRM/One Additional Cure Cycle on the Forward Nose Ring CCP (Triple Cure)). The forward nose ring liner erosion was smooth and uniform and appeared typical of previous post-test and postflight RSRM rings. Initial inspection indicates that the additional CCP cure cycle did not have any adverse effect on the liner performance. Performance was estimated to be similar to that of a forward nose ring with the standard two cure cycles. The forward nose ring performance margin of safety was verified after the ring had been sectioned and inspected, and found to be positive (0.17 minimum at Sta 28, 270 deg).

6.4.4.2 Nozzle Internal Joint No. 2 (Nose Cap, Bearing, Cowl, No Configuration Changes, Improved Cowl Assembly Bonding Method and RTV Backfill). The Joint No. 2 gap appeared normal (0.10 in.) with the gap being equal all the way around. The RTV was visible at the char line 360 deg.

Because of the improved cowl bonding process, the EA 913NA adhesive did not squeeze out and mix with the RTV in Joint No. 2 as typically seen in the flight configuration joint.

6.4.4.3 Nozzle Internal Joint No. 4 (Throat/Forward Exit Cone, Modified Primary O-ring, Groove Depth). The primary O-ring groove was modified to provide an acceptable O-ring squeeze using hardware that would not normally meet the squeeze requirement. Modified hardware passed the required leak check tests.

6.5 IGNITER PERFORMANCE

6.5.1 Introduction

The SRM ignition system was a modified HPM igniter assembly containing a single nozzle, thickened steel chamber at the nozzle end, external insulation, tapered internal insulation, and solid propellant (TP-H1178) igniter containing a case bonded 40-point star grain. The AP used in the TP-H1178 propellant is from WECCO's Utah plant. The required laboratory and subscale qualification tests were successfully completed in accordance with test plan CTP-0112. The ignition system was modified with a CO₂ quench port. Ultrasonically torqued bolts

fastened the igniter adapter to the igniter chamber. A286 bolts in the igniter adapter-to-case joint were replaced with higher strength MP159 bolts which were preloaded to a higher level.

A S&A device using Krytox grease to lubricate the B-B shaft O-rings was installed on the igniter. Velostat or pink poly plastic sheets were wrapped and tightly sealed around the forward thrust adapter to simulate the thermal protection provided to the igniter and S&A by flight configuration. All indications are that operation was within specification limits. Postfire disassembly showed no anomalies.

6.5.2 Objectives

The objectives from Section 2 regarding the igniter are:

- A Certify the TP-H1148 SRM igniter propellant manufactured using AP produced by the new WECCO Utah plant.
- K Demonstrate the performance of MP159 bolts in the igniter adapter-to-case joint.
- L Obtain data on igniter flange skip.

6.5.3 Conclusions/Recommendations

Igniter. Postfire inspection revealed no anomalous conditions. One outer joint putty blowhole was observed.

6.5.4 Results/Discussion

Igniter/S&A. Igniter ballistic performance was as expected. Igniter chamber insulation, adapter insulation, and igniter joint insulation had normal erosion. Both the inner and outer joints had consistent putty color and tack and 100 percent cohesive failure.

The outer joint had a putty blowhole at 230 deg and measured 1.5 in. circumferentially at the beginning and necked down to 0.25 in. at the adapter.

There was intermittent soot from the blowhole around the full circumference of the seal, but no soot past the primary seal.

The S&A device performed as expected, with the safe to arm cycle time being 0.6 sec.

FSM-1 used MP159 bolts on the igniter adapter-to-case joint. Inspection of the bolts showed no signs of yielding or structural deformation.

Data on igniter flange skip was collected and is documented in TWR-61213, which correlates analysis with test data from the FSM-1 motor. The actual measured FSM-1 outer joint skip when corrected for gage placement is 0.045 in. with an apparent coefficient of friction at the joint interface of 0.175 in. The worst-case skip is 0.050 in. when corrected for MEOP.

6.6 JOINT PROTECTION SYSTEM

6.6.1 Introduction

Field joint heater closeout consisted of cork strips retained with Kevlar straps. The external joint temperatures were sensed by two sensor assemblies mounted adjacent to the heater. Weatherseals were not applied to the cylinder to cylinder factory joint of the forward segment and the factory joint of both center segments in order to accommodate strain gages. Improved field joint heaters and igniter-to-case joint heater were installed in accordance with Drawing No. 7U77135. The heaters consisted of redundant, chemically etched foil circuits which were superimposed on one another and laminated in polyamide plastic sheets. The underside Kapton surface of the field joint heaters was coated with a pressure sensitive adhesive, which provided bonding to the case during assembly. The lead wires extending from the heaters were terminated in electrical connectors. The nozzle-to-case joint was not required to be temperature conditioned, as dictated by ambient conditions.

6.6.2 Objectives

There are no objectives from Section 2 concerning the JPS.

6.6.3 Conclusions/Recommendations

There was no damage or heat effect to any of the field joint protection systems (FJPS).

6.6.4 Results/Discussion

6.6.4.1 Field Joint Heater Control System. The field joint heater temperature control system operated as predicted and maintained the temperatures at the controlling RTD at $97.5^{\circ} \pm 1^{\circ}\text{F}$.

The four temperature sensors at each field joint were continuously monitored and the coldest sensor was manually selected for temperature control. Plots of the RTD temperature for each joint are included in Appendix C.

6.6.4.2 Nozzle Heater Control System. No nozzle temperature conditioning was necessary, as dictated by ambient conditions. The nozzle-to-case joint, internal nozzle joints, flex bearing, and TVC system were within the required thermal operating range.

6.6.4.3 Igniter Heater Control System. The igniter temperature control system maintained the igniter temperature within the specified temperature range of $95^{\circ} \pm 1^{\circ}\text{F}$. Plots of the RTD temperatures for the igniter joint are included in Appendix C.

6.6.4.4 Post-Test Inspection

6.6.4.4.1 FJPS. Post-test inspection was conducted with the FJPS still on the motor and no evidence of damage was observed.

6.7 BALLISTICS/MASS PROPERTIES

6.7.1 Introduction

The SRM propellant, TP-H1148, was a composite type solid propellant, formulated of PBAN, epoxy curing agent, AP oxidizer and aluminum powder fuel. A small amount of burning rate catalyst (iron oxide) was added to achieve the desired propellant burn rate. The AP was produced at the new WECCO plant in Cedar City, Utah. Since AP has significant effects on the ballistics of a motor, it became necessary to fire a full scale motor static test motor to qualify the new WECCO AP plant.

Since only one static test was performed, more stringent ballistic limits were used to evaluate the success of the test motor. The purpose of these limits was to determine if a change from the current population occurred with the new AP source. These limits were developed from historical RSRM data.

The propellant grain design consists of a forward segment with an 11-point star that transitions into a tapered circular perforated (CP) configuration, two center segment double-tapered CP configurations, and an aft segment triple-taper CP configuration with a cutout for the partially submerged nozzle.

In addition to the ballistic analysis, this section contains the predicted/ measured prefire and postfired mass properties data for the total FSM-1 motor. This section also shows compliance to:

- a. Part I of the "Prime Equipment Contract End Item Detail" Specification, CPW1-3600A paragraph 3.2.2.2 and Addendum E of CPW1-3600A, paragraphs 3.2.2.2.1 and 3.2.2.2.3.
- b. Thiokol Corporation imposed requirements (established in TWR-16877 Revision C, "Redesigned Solid Rocket Motor Mass Properties Uncertainty Analysis", Table XIX, page 18, 14 Dec 1988).

6.7.2 Objectives

The primary test objectives from Section 2 regarding ballistics/mass properties are:

- a. Certify the TP-H1148 SRM propellant manufactured using AP produced by the new WECCO Utah plant (CPW1-3600A paragraph 3.2.1.1.1.1, 3.2.1.1.1.2, 3.2.1.1.2.1, 3.2.1.1.2.2, 3.2.1.1.2.4, and 3.3.1.1).
- b. Certify the TP-H1178 SRM propellant manufactured using AP produced by the new WECCO Utah plant (CPW1-3600A paragraph 3.2.1.1.1.1, 3.3.1.1).

6.7.3 Conclusions/Recommendations

The FSM-1 ballistic performance was very close to predicted. The actual burn rate matched the predicted burn rate at 0.370 ips at 625 psia and 60°F. All values were within the CEI specification limits as well as the more stringent 2.5 σ limits (see Table 3-4). The ignition characteristics of the motor and the ballistic performance compared well with previous RSRM performance. All performance values indicate that the WECCO AP does not change any of the motor's ballistic characteristics. It is recommended that AP produced from WECCO be fully qualified for use in future flight motors.

FSM-1 inert weight of 147,785 lb is 1,175 lb below the specified CEI maximum of 148,960 lb (CPW1-3600A Addendum E, paragraph 3.2.2.2.1). All inert, loaded, and burnout centers of gravity (cg) are within CEI limits (CPW1-3600A Addendum E, paragraph 3.2.2.2.3). The measured propellant weight of 1,106,109 lb is 1,969 lb above the specified minimum CEI limit of 1,104,140 lb (CPW1-3600A, Addendum E, paragraph 3.2.2.2.2). The measured slag for FSM-1 amounts to 466 lb.

The actual expended inert weight of 7,978 lb is derived from the postfire measured data. The RSRM FSM-1 measured mass properties are within recommended CEI CPW1-3600A Addendum E requirements.

The igniter, which also had propellant containing WECCO AP, also fired successfully. Although the delivered performance was lower than predicted, it met the specification requirements listed in STW3-3176 (Figure 6-9). It is recommended that WECCO AP be accepted for use in RSRM igniters.

The FSM-1 motor exhibited chamber pressure oscillations similar to previously tested Space Shuttle RSRMs. The 1-L mode oscillations were typical for an RSRM. In general, RSRM 1-L mode amplitudes are larger than those for HPMs.

6.7.4 Results/Discussion

A comparison of FSM-1 performance with predicted values and with the nominal RSRM performance revealed few differences. The predicted burn rate for FSM-1 was 0.370 ips at 625 psia and 60°F, the target burn rate was 0.368 ips and the delivered burn rate was 0.370 ips. The 5-in. CP motor burn rate was 0.364 ips, which was slightly higher than the target 5-in. CP burn rate of 0.362 ips. A scale factor of 1.0175 was applied to the 5-in. CP data to establish a full-scale predicted motor burn rate. The actual scale factor was 1.0165. The slightly high predicted and delivered burn rate is well within normal variation and approximately one sigma from the target burn rate.

Table 6-9 is a summary of the measured ballistic and nozzle performance data as provided by Test area personnel. This table lists pre- and postfire nozzle geometry, calculated efficiencies, measured ballistic data at the firing PMBT of 82°F, and ballistic data corrected to 40°, 60°, and 90°F. Table 3-4 shows a complete comparison of the CEI Specification limits, the 2.5 σ acceptance limits, the predicted values, and the delivered values all referenced to 60°F. The acceptance limits were established because the qualification plan of the WECCO AP consisted of only one full scale static test. The 2.5 σ limits were calculated to ensure that no change from the current population of RSRMs occurred. The results of the test in fact show that no change has occurred.

Figure 6-10 is a comparison of measured and predicted pressure-time histories and Figure 6-11 is a comparison of measured and predicted vacuum

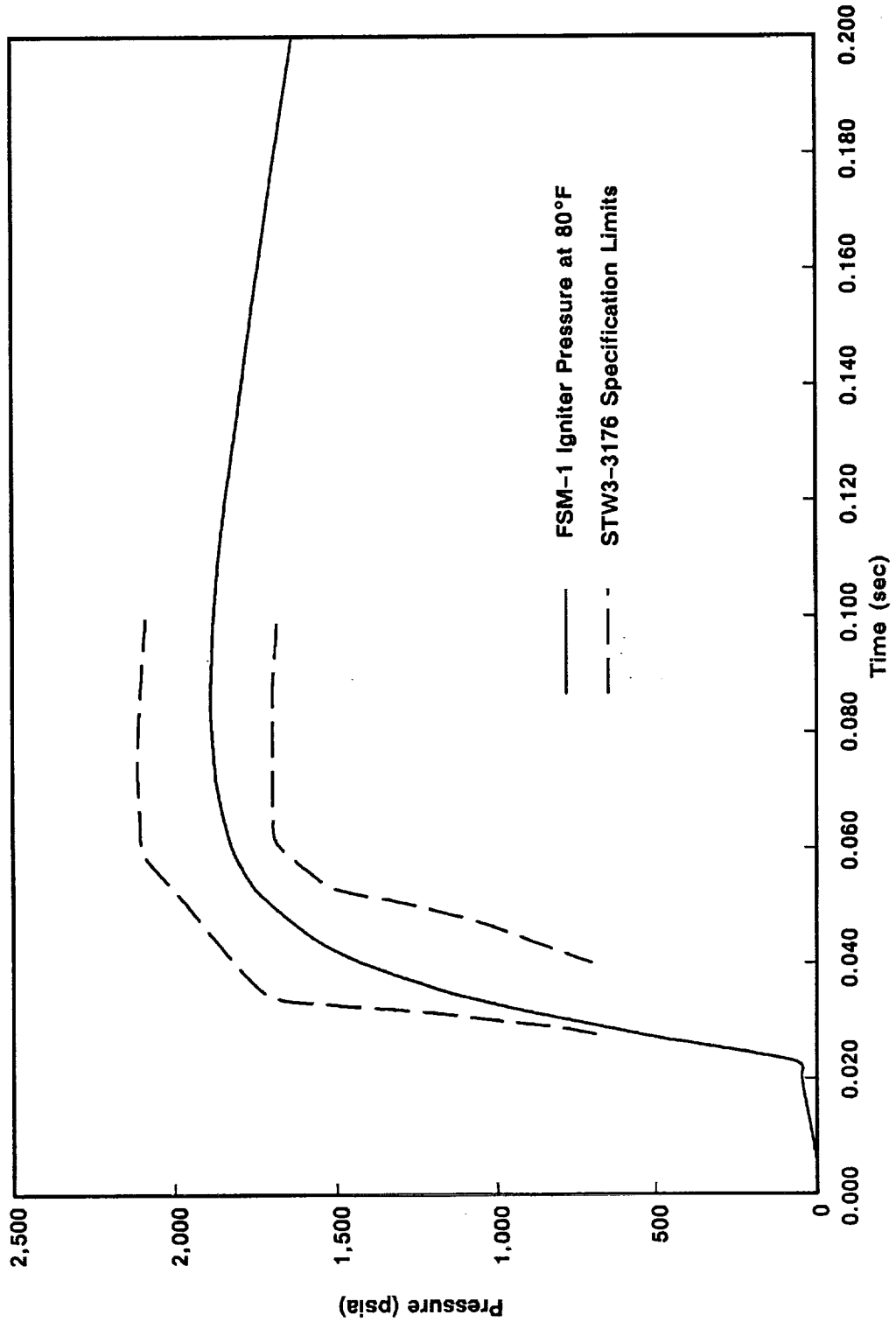


Figure 6-9. Igniter Chamber Pressure Compared to STW3-3176 Igniter Specification Limits at 80°F

A030421a

Table 6-9. Summary of Measured Ballistic and Nozzle Performance Data

A. Ambient Conditions

Date and time at fire pulse (hr) (15 Aug 1990)	13.5
Ambient temperature (°F)	85.00
Measured mean bulk temperature (°F)	82.00
Measured ambient pressure (psia)	12.27

B. Weight Data

Total loaded propellant weight (lbf)	1,106,109.0
Total expended weight (lbf)	1,111,722.0
Unexpended propellant residue (slag) (lbf)	500.0
Expended inert weight	
1. Forward segment (lbf)	683.0
2. Forward center segment (lbf)	641.0
3. Aft center segment (lbf)	989.0
4. Aft segment (including nozzle from field joint forward) (lbf)	3,800.0
5. Total expended inerts (lbf)	6,113.0
Total expended propellant weight (lbf)	1,105,609.0

C. Nozzle Data

Initial throat area (in. ²)	2,276.9
Final throat area (in. ²)	2,460.9
Web time average throat area (in. ²)	2,373.0
Action time average throat area (in. ²)	2,380.6
Total time average throat area (in. ²)	2,380.8
Initial exit area (in. ²)	17,596.1
Final exit area (in. ²)	17,637.1
Total time average exit area (in. ²)	17,616.6
Web time average throat radial erosion rate (ips)	0.00959
Action time average throat radial erosion rate (ips)	0.00901
Total time average throat radial erosion rate (ips)	0.00897
Initial expansion ratio	7.7280
Web time average expansion ratio	7.4237
Action time average expansion ratio	7.3999
Action time average nozzle efficiency	0.97587
Total time average nozzle efficiency	0.97624

Table 6-9. Summary of Measured Ballistic and Nozzle Performance Data (cont)

D. Time and Ballistic Data

Time at first indication of headend pressure (sec)	0.032
Ignition delay time (sec)	-0.018
Time at 90 percent maximum igniter pressure (sec)	0.050
Ignition interval time (sec)	0.228
Ignition rise time (sec)	0.196
Time when headend chamber pressure achieves 563.5 psia during ignition (sec)	0.228
Time at last indication of headend pressure (sec)	118.927
Time at web bisector (sec)	107.942
Web time (sec)	107.714
Action time (sec)	118.214
Total time (sec)	118.895
Tailoff thrust decay time (sec)	0.485
Maximum change in thrust over 10 ms during ignition (lb)	237,256
Maximum igniter pressure (psia)	1,895
Maximum measured headend pressure (psia)	943.70
Time at maximum headend pressure (sec)	0.620
Maximum thrust (lb)	3,229,377
Time at maximum thrust (sec)	17.356
Maximum thrust corrected to vacuum (lb)	3,445,354
Maximum thrust corrected to sea level (lb)	3,186,603
Maximum stagnation pressure (psia)	879.6
Web time average headend chamber pressure (psia)	686.87
Action time average headend chamber pressure (psia)	641.32
Web time average nozzle stagnation pressure (psia)	671.18
Action time average nozzle stagnation pressure (psia)	626.94
Initial thrust (lb)	3,020,518
Initial thrust corrected to vacuum (lb)	3,236,426
Initial thrust corrected to sea level (lb)	2,977,758
Web time average thrust (lb)	2,466,183
Web time average thrust corrected to vacuum (lb)	2,682,316
Action time average thrust (lb)	2,294,569
Action time average thrust corrected to vacuum (lb)	2,506,335
Characteristic exhaust velocity (ft/sec)	5,075.66

Table 6-9. Summary of Measured Ballistic and Nozzle Performance Data (cont)

E. Impulse Data

Measured total impulse (Mlbf-sec)	271.374
Total impulse corrected to vacuum (Mlbf-sec)	296.469
Measured impulse at 20 sec (Mlbf-sec)	62.438
20-sec impulse corrected to vacuum (Mlbf-sec)	66.740
Measured impulse at 60 sec (Mlbf-sec)	164.466
60-sec impulse corrected to vacuum (Mlbf-sec)	177.411
Web time impulse (Mlbf-sec)	265.642
Web time impulse corrected to vacuum (Mlbf-sec)	288.922
Action time impulse (Mlbf-sec)	271.249
Action time impulse corrected to vacuum (Mlbf-sec)	296.283
I_p (sec)	244.102
I_p corrected to vacuum (sec)	266.676
Web time specific impulse (sec)	245.344
Web time specific impulse corrected to vacuum (sec)	266.846
Action time I_p (sec)	244.140
Action time I_p corrected to vacuum (sec)	266.672
Propellant I_{sp} (sec)	245.452
Propellant I_{sp} corrected to vacuum (sec)	268.150

F. Pressure Integral Data

Total time pressure integral (lb/in. ² -sec)	75,864.0
Web time pressure integral (lb/in. ² -sec)	73,985.9
Action time pressure integral (lb/in. ² -sec)	75,822.3

Table 6-9. Summary of Measured Ballistic and Nozzle Performance Data (cont)

Corrected to 40°F

G. Time and Ballistic Data

Time and first indication of headend pressure (sec)	0.036
Time when headend chamber pressure achieves 563.5 psia during ignition (sec)	0.246
Time at last indication of headend pressure (sec)	124.580
Time at web bisector (sec)	113.200
Web time (sec)	112.954
Action time (sec)	123.821
Maximum measured headend pressure (psia)	898.10
Time at maximum headend pressure (sec)	0.650
Maximum thrust corrected to vacuum (lbf)	3,278,632
Maximum nozzle stagnation pressure (psia)	837.1
Web time average headend chamber pressure (psia)	653.45
Action time average headend chamber pressure (psia)	610.67
Web time average nozzle stagnation pressure (psia)	638.53
Action time average nozzle stagnation pressure (psia)	596.98
Web time average thrust corrected to vacuum (lbf)	2,551,851
Action time average thrust corrected to vacuum (lbf)	2,386,553

H. Impulse Data

Total impulse corrected to vacuum (Mlbf-sec)	295.704
20-sec impulse corrected to vacuum (Mlbf-sec)	63.422
60-sec impulse corrected to vacuum (Mlbf-sec)	169.959
Web time impulse corrected to vacuum (Mlbf-sec)	288.241
Action time impulse corrected to vacuum (Mlbf-sec)	295.505
I_{sp} corrected to vacuum (sec)	265.988
Web time I_{sp} corrected to vacuum (sec)	266.158
Action time I_{sp} corrected to vacuum (sec)	265.983
Propellant I_{sp} corrected to vacuum (sec)	267.458

C-2

Table 6-9. Summary of Measured Ballistic and Nozzle Performance Data (cont)

Corrected to 60°F

I. Time and Ballistic Data

Time and first indication of headend pressure (sec)	0.034
Time when headend chamber pressure achieves 563.5 psia during ignition (sec)	0.237
Time at last indication of headend pressure (sec)	121.855
Time at web bisector (sec)	110.643
Web time (sec)	110.405
Action time (sec)	121.122
Maximum measured headend pressure (psia)	919.54
Time at maximum headend pressure (sec)	0.635
Maximum thrust corrected to vacuum (lbf)	3,356,999
Maximum nozzle stagnation pressure (psia)	857.1
Web time average headend chamber pressure (psia)	669.22
Action time average headend chamber pressure (psia)	625.06
Web time average nozzle stagnation pressure (psia)	653.93
Action time average nozzle stagnation pressure (psia)	611.05
Web time average thrust corrected to vacuum (lbf)	2,613,386
Action time average thrust corrected to vacuum (lbf)	2,442,791

J. Impulse Data

Total impulse corrected to vacuum (Mlbf-sec)	296.068
20-sec impulse corrected to vacuum (Mlbf-sec)	64.981
60-sec impulse corrected to vacuum (Mlbf-sec)	173.454
Web time impulse corrected to vacuum (Mlbf-sec)	288.531
Action time impulse corrected to vacuum (Mlbf-sec)	295.876
I_p corrected to vacuum (sec)	266.314
Web time I_p corrected to vacuum (sec)	266.485
Action time I_p corrected to vacuum (sec)	266.311
Propellant I_p corrected to vacuum (sec)	267.787

Table 6-9. Summary of Measured Ballistic and Nozzle Performance Data (cont)

Corrected to 90°F

K. Time and Ballistic Data

Time and first indication of headend pressure (sec)	0.031
Time when headend chamber pressure achieves 563.5 psia during ignition (sec)	0.225
Time at last indication of headend pressure (sec)	117.890
Time at web bisector (sec)	107.017
Web time (sec)	106.792
Action time (sec)	117.169
Maximum measured headend pressure (psia)	952.65
Time at maximum headend pressure (sec)	0.614
Maximum thrust corrected to vacuum (lbf)	3,478,054
Maximum nozzle stagnation pressure (psia)	888.0
Web time average headend chamber pressure (psia)	693.30
Action time average headend chamber pressure (psia)	647.36
Web time average nozzle stagnation pressure (psia)	677.46
Action time average nozzle stagnation pressure (psia)	632.85
Web time average thrust corrected to vacuum (lbf)	2,707,416
Action time average thrust corrected to vacuum (lbf)	2,529,939

L. Impulse Data

Total impulse corrected to vacuum (Mlbf-sec)	296.613
20-sec impulse corrected to vacuum (Mlbf-sec)	67.389
60-sec impulse corrected to vacuum (Mlbf-sec)	178.885
Web time impulse corrected to vacuum (Mlbf-sec)	289.130
Action time impulse corrected to vacuum (Mlbf-sec)	296.431
I_{sp} corrected to vacuum (sec)	266.805
Web time I_{sp} corrected to vacuum (sec)	266.974
Action time I_{sp} corrected to vacuum (sec)	266.802
Propellant I_{sp} corrected to vacuum (sec)	268.281

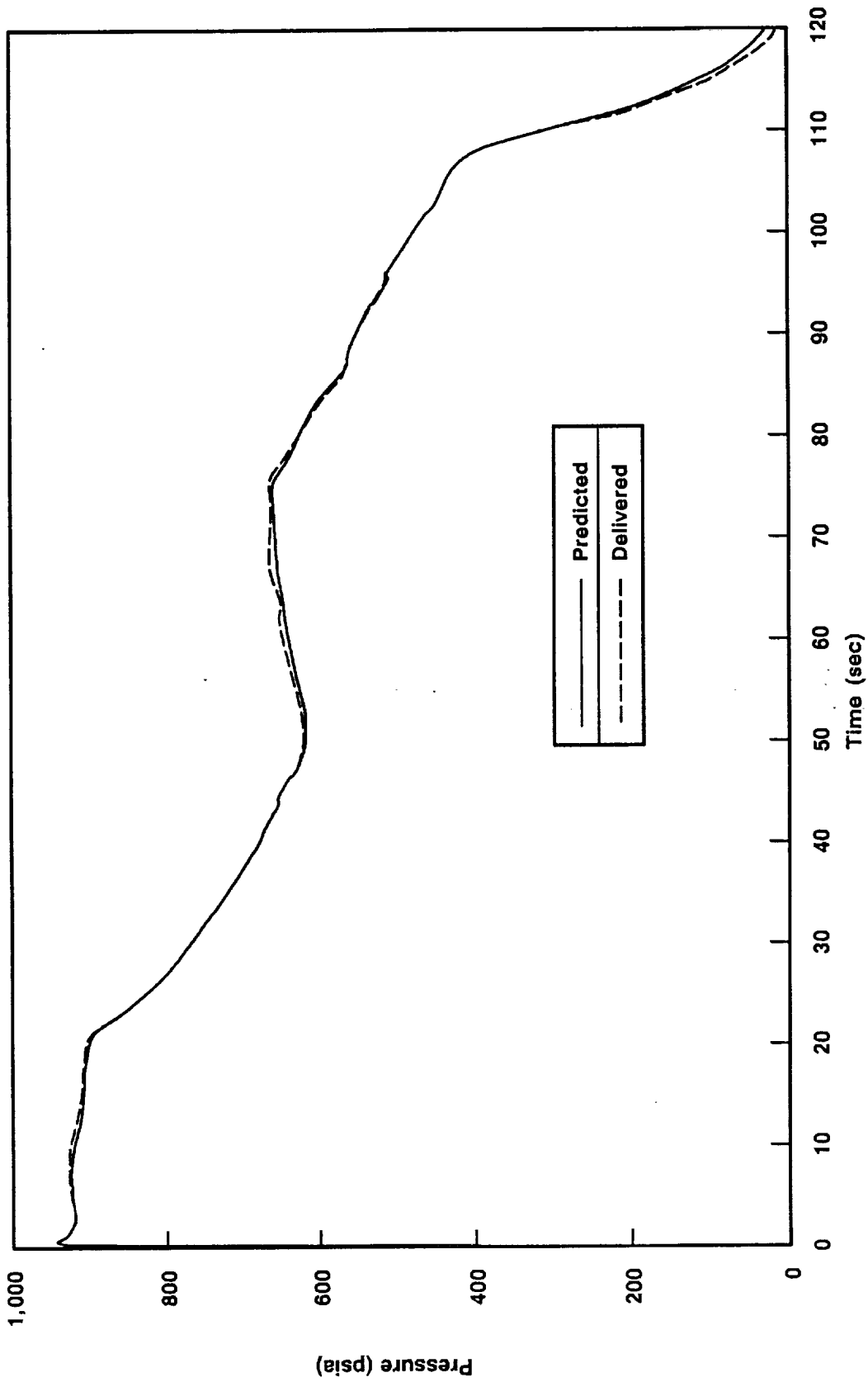
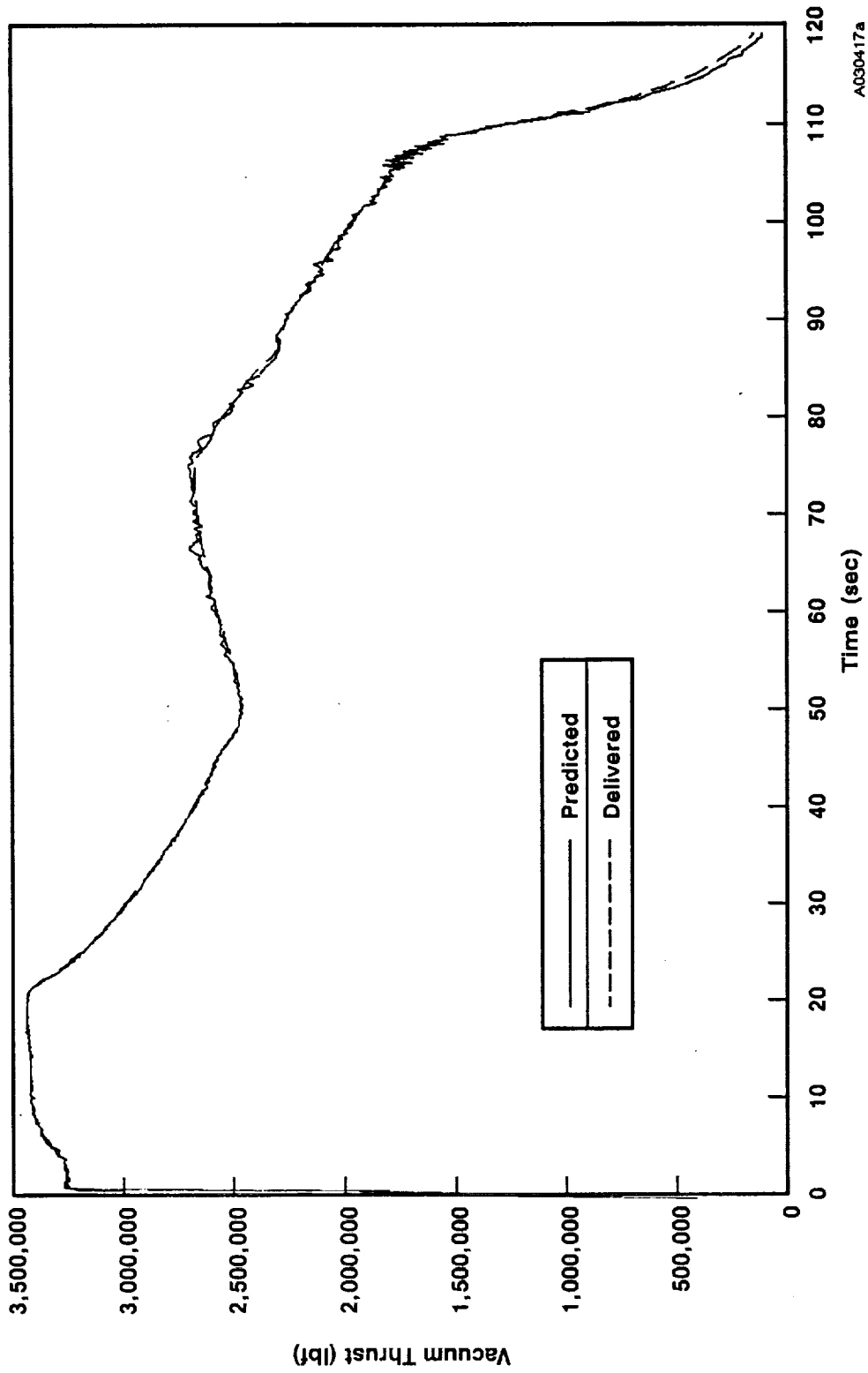


Figure 6-10. Pressure Versus Time at 82°F

A030416a



A030417a

Figure 6-11. Vacuum Thrust Versus Time at 82°F

thrust-time histories. The measured and predicted performance compared well for this motor. The close match between the predicted and actual performance traces show the predicted burn rate was accurate and the surface burn rate error (SBRE) factor did not change. SBRE is the factor that accounts for model geometry error and directional burn rate differences. A comparison of the thrust-to-headend chamber pressure ratios for all the RSRM static tests with measured thrust data is shown in Figure 6-12. The traces are all similar including FSM-1.

There are a few performance items that should be noted. The tailoff of the motor (time between web and action time) dropped off a little sharper than predicted. The tailoff period was predicted to be about 12 sec. The delivered time was a second shorter than predicted. This can be seen in both the pressure and the thrust plots. This phenomenon had a slight effect on several ballistic values. The I_{sp} was 0.7 sec lower than predicted. None of the effects are outside the RSRM experience base and they cannot be attributed to the use of the WECCO AP.

A comparison of FSM-1 thrust data at 60°F and a burn rate of 0.368 ips at 625 psia and 60°F with the CEI Specification CPW1-3600A, thrust-time limits at 0.368 ips is shown on Figure 6-13. The FSM-1 performance was within average population limits. Note that the limits are for the average of the historical SRM population not an individual motor. The historical motor population is well within the limits. None of the individual motor performance tolerances and limit parameters were exceeded.

The impulse gates at 20 sec, 60 sec, and action time from FSM-1 data adjusted to 0.368 ips and 60°F were within the CEI specification nominal limits. The nominal limits only apply to the population average. The FSM-1 20-sec impulse was 64.5 lbf-sec and the limit is 63.5 lbf-sec minimum. The 60-sec impulse was 172.4 lbf-sec and the limits were 171.5 lbf-sec minimum and

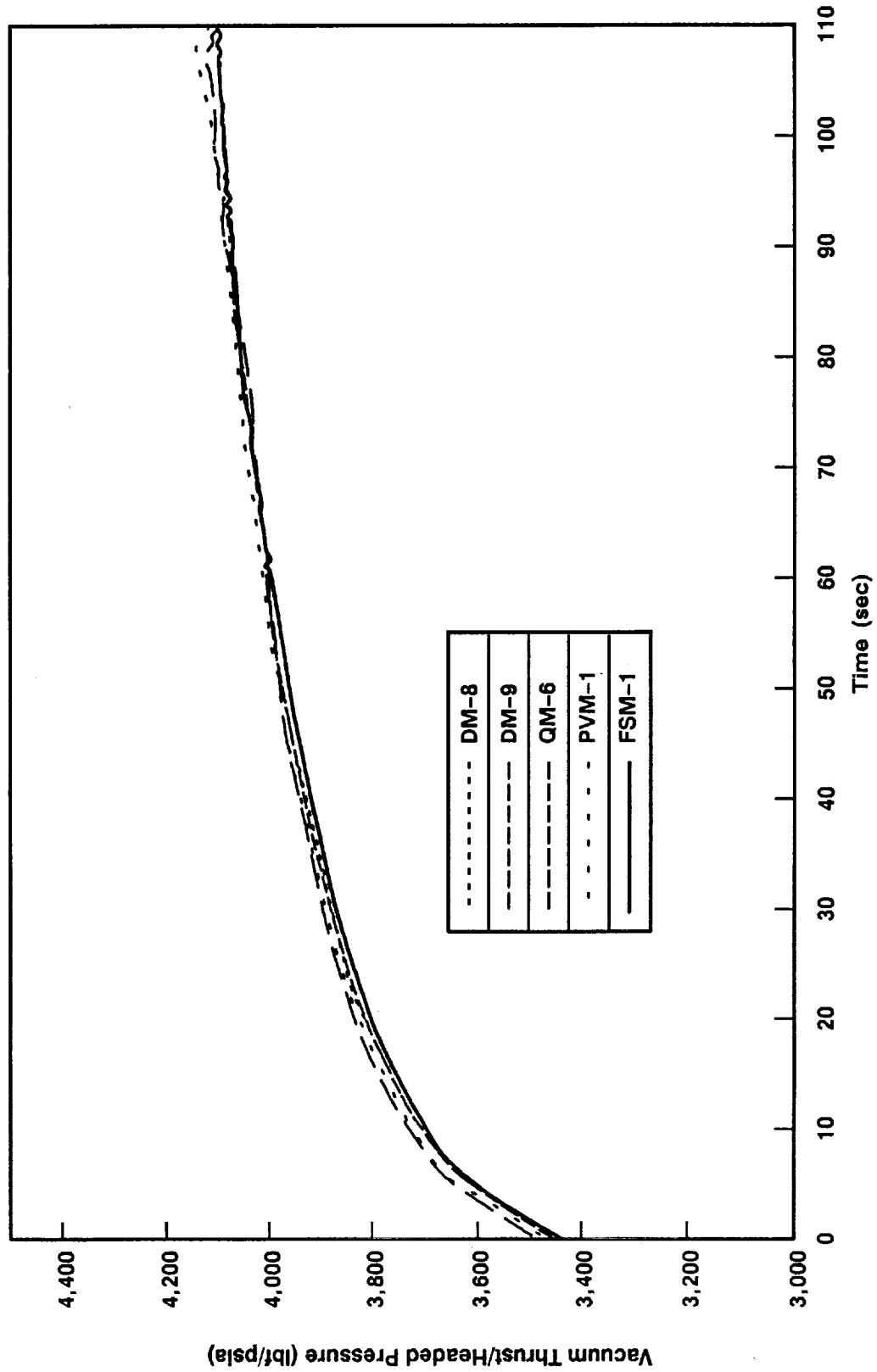


Figure 6-12. Vacuum Thrust-to-Headed Pressure Ratio

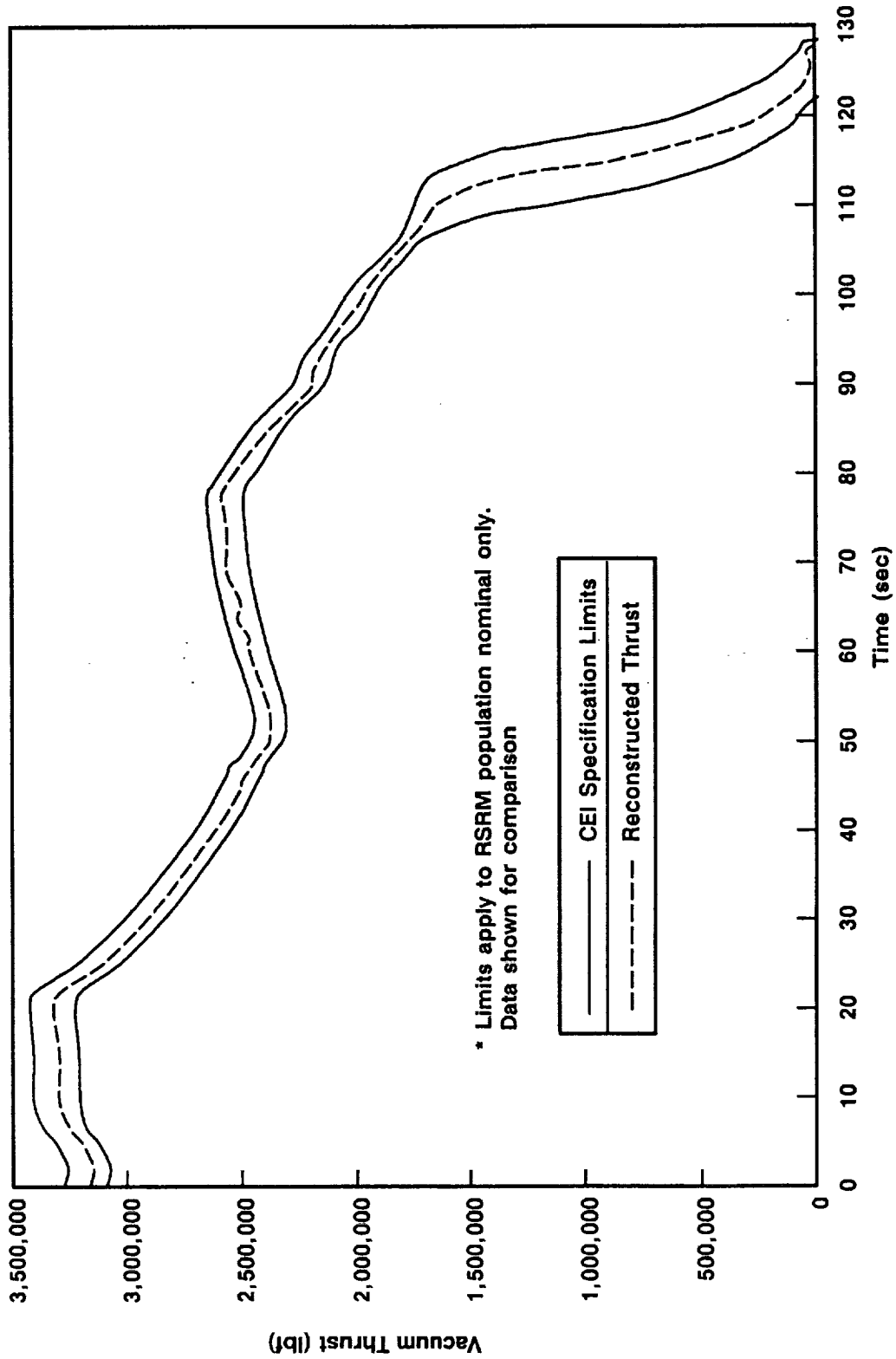


Figure 6-13. Vacuum Thrust Versus CEI Specification Limits*

178.4 lbf-sec maximum. The action time impulse was 296.1 lbf-sec and the limit is 294.1 minimum.

The FSM-1 ignition performance satisfied the ignition interval and the maximum pressure rise rate requirements as shown in Table 6-10. A plot of the measured data comparing the ignition transients of the RSRM static tests is shown in Figure 6-14. The FSM-1 transient was very similar to previously measured motor ignition performance. The FSM-1 maximum pressure rise rate was 97.1 psi /10 ms. The historical three point average pressure rise rate is 90.07 psi/10 ms with a variation of 6.80 psi/10 ms. FSM-1 was consistent with the nominal rise rates for the population. A summary table showing the historical pressure rise rates, thrust rise rates and ignition intervals is shown in Table 6-10. A summary of the FSM-1 ignition events is shown in Table 6-11.

Table 6-11. Measured RSRM Ignition Performance Data at 82°F

Parameter	FSM-1	CEI Specification Requirement
Maximum Igniter Mass Flow Rate (lbm/sec) (80°F)	337.6	NA
Ignition Transient (sec) (0 to 563.5 psia)	0.228	0.202 - 0.262
Maximum Pressure Rise Rate (psi/10 ms)	97.1	70.9 - 115.9
Pressure Level at Start of Maximum Rise Rate (psia)	231	NA
Time Span of Maximum Pressure Rise (ms)	152 to 162	NA
Equilibrium Pressure 0.6 sec (ignition end) (psia)	944	NA
Time to First Ignition (sec) (begin pressure rise)	0.027	NA

The FSM-1 igniter grain configuration was identical to the RSRM flight and static test igniter design. The igniter was cast from propellant batch number G720001 out of Lot 43 using TP-H1178 propellant. The igniter propellant also contained the WECCO AP. FSM-1 was the last step in qualifying the WECCO AP igniters. The delivered maximum mass flow rate was 337.6 lbm/sec at 80°F for

Table 6-10. Historical 3-point Average Thrust and Pressure Rise Rate Data

Motor	Occurrence Time	Pressure Rise Rate	Occurrence Time	Thrust Rise Rate	Ignition Interval
<u>Static Test</u>					
DM-2	0.1480	85.30	0.1480	245,380	0.2330
QM-1	0.1560	86.38	0.1560	246,128	0.2362
QM-2	0.1640	93.58	0.1720	234,960	0.2391
QM-3	0.1560	94.45	0.1520	245,615	0.2287
QM-4	0.1505	91.96	0.2225	234,438	0.2192
ETM-1A	0.1520	86.72	0.1560	230,023	0.2279
TEM-1	0.1520	85.13	0.1520	238,583	0.2255
TEM-2	0.1520	94.40	0.1520	288,772	0.2280
TEM-3	0.1520	88.51	NA	NA	0.2272
TEM-4	0.1480	81.52	0.1520	279,764	0.2283
TEM-5	0.1560	87.12	NA	NA	0.2299
TEM-6	0.1600	84.49	0.1520	273,946	0.2342
DM-8	0.1680	77.00	0.1760	257,272	0.2424
DM-9	0.1640	81.00	0.1720	275,525	0.2436
QM-6	0.1480	87.40	0.1520	211,476	0.2321
QM-7	0.1480	99.60	NA	NA	0.2230
PVM-1	0.1520	92.80	0.1520	294,664	0.2338
QM-8	0.1720	72.30	NA	NA	0.2517
FSM-1	0.1520	97.06	0.1440	250,453	0.2278
<u>Flight Motors</u>					
SRM-1A	0.1530	87.58			0.2373
SRM-1B	0.1500	91.57			0.2358
SRM-2A	0.1530	90.74			0.2348
SRM-2B	0.1660	90.27			0.2345
SRM-3A	0.1500	91.05			0.2308
SRM-3B	0.1500	89.68			0.2271
SRM-5A	0.1530	95.10			0.2361
SRM-5B	0.1660	84.43			0.2380
SRM-6A	0.1530	92.72			0.2342
SRM-6B	0.1470	88.22			0.2329
SRM-7A	0.1500	99.90			0.2282
SRM-7B	0.1500	99.32			0.2276
SRM-8A	0.1530	106.29			0.2224
SRM-8B	0.1500	91.06			0.2196
SRM-9A	0.1530	92.31			0.2303
SRM-10A	0.1530	92.89			0.2373
SRM-10B	0.1500	84.56			0.2342
SRM-13B	0.1410	98.85			0.2115
RSRM-1A	0.1501	99.0			0.2296
RSRM-1B	0.1596	80.5			0.2310
RSRM-2A	0.1564	87.3			0.2390
RSRM-2B	0.1501	100.2			0.2342
RSRM-3A	0.1560	82.70			0.2414
RSRM-3B	0.1529	89.90			0.2408
	Number	43		15	43
	Average	90.07		255,799	0.2321
	Standard Deviation	6.80		23,880	0.0072
	COV (%)	7.55		9.34	3.12

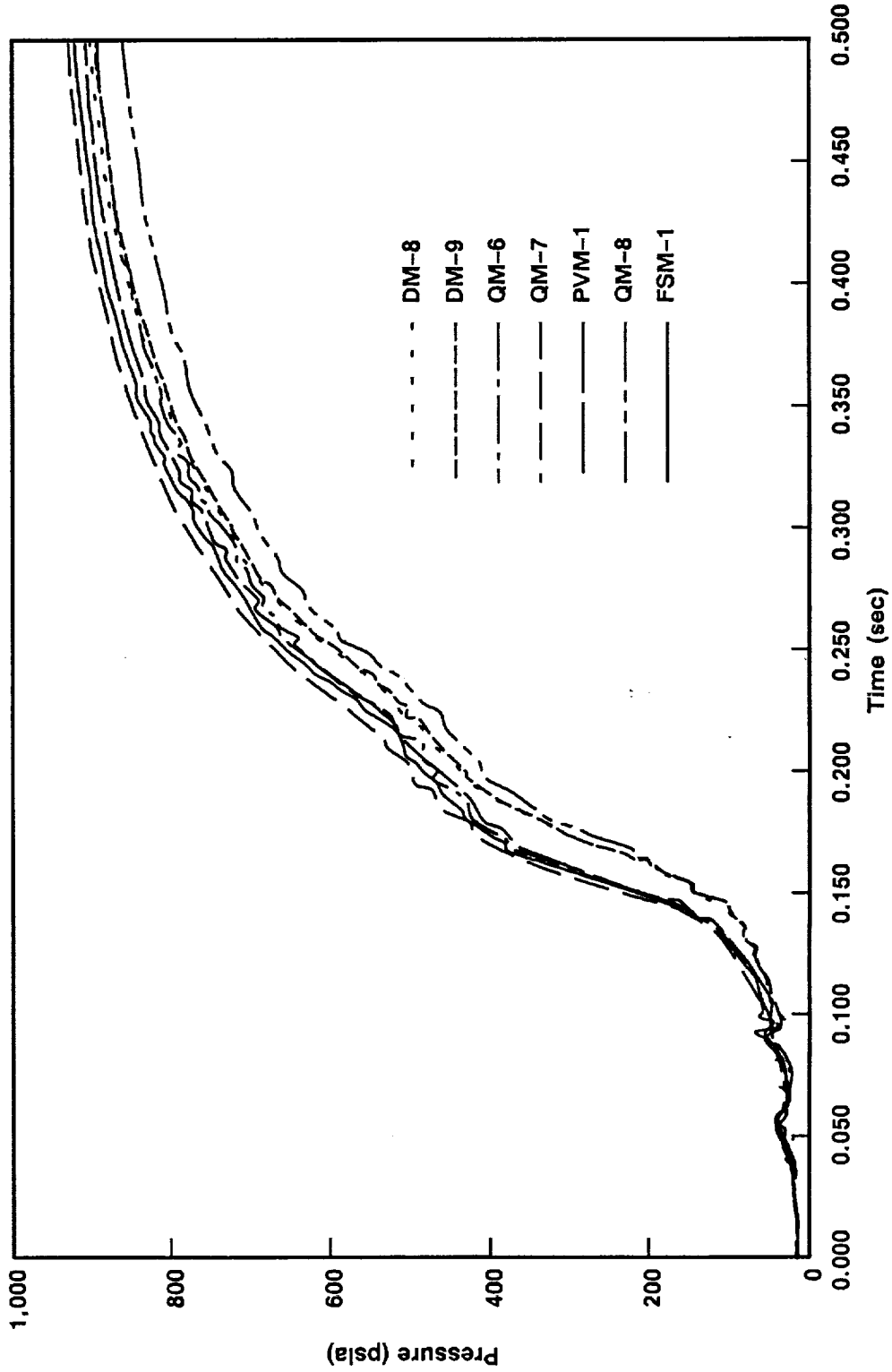


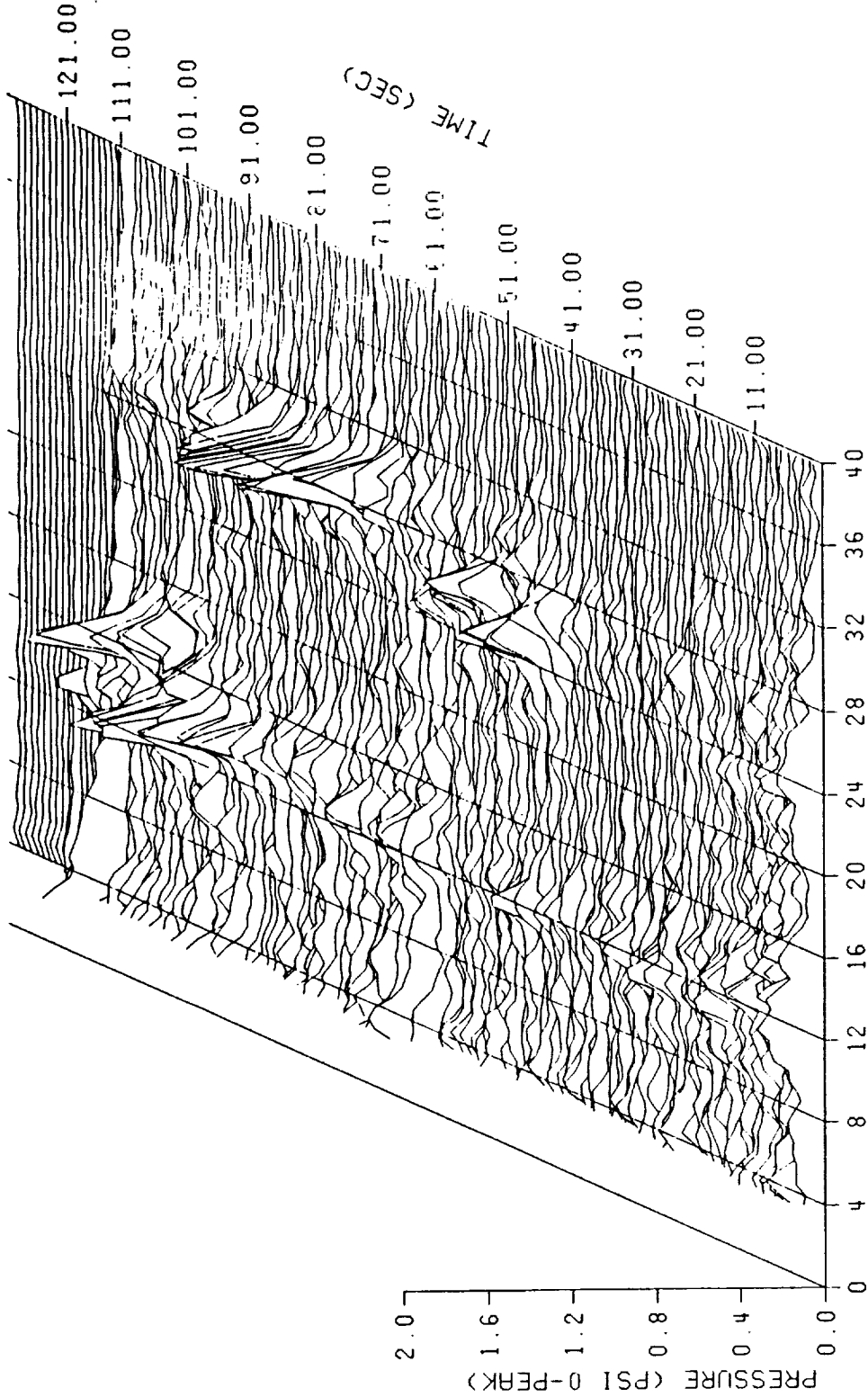
Figure 6-14. Ignition Transient

the FSM-1 igniter (80°F is the PMBT for the igniter specification limits, STW3-3176). The FSM-1 igniter performance characteristics were within the expected ranges. Comparison of the FSM-1 igniter performance at 80°F with the igniter limits at 80°F is shown in Table 3-4. The FSM-1 igniter is within the limits at 80°F.

FSM-1 was instrumented with three pressure transducers for headend pressure measurement (PNCAC001-PNCAC003) and one gage for igniter pressure measurement (PNCAC005). The signal from the headend OPT data channel (PNCAC001) was split to provide both ac-coupled data (for chamber pressure oscillation data) and mean pressure. In addition, the mean pressure data channels are used to calculate dynamic pressure and to verify the accuracy of the ac-coupled data.

Data acquired from gauge PNCAC001 are displayed in a waterfall plot format in Figure 6-15. The 1-L and second longitudinal (2-L) acoustic modes can be observed at about 15 and 30 Hz, respectively. This waterfall plot is fairly typical of RSRM designs. Figure 6-16 is a waterfall plot of the axial thrust gauge, FAPAX001. Figures 6-17 and 6-18 describe the running, instantaneous, peak-to-peak oscillation amplitudes of the 1-L and 2-L acoustic modes respectively for the FSM-1 motor headend pressure. This type of analysis is more representative of instantaneous oscillations than are the time averaged oscillations presented in a waterfall plot. Figure 6-19 is a waterfall plot of gage P000016 from a previously static tested RSRM, PVM-1, and is provided for comparison purposes and a number of observations can be made. Both motors have similar acoustic signatures. PVM-1 has stronger 1-L mode oscillation amplitudes than FSM-1, but both have magnitudes larger than HPM motors.

When using waterfall plots to compare static test motor oscillation amplitudes, it is important to remember that this format uses an averaging method of analysis. This presents no difficulty for steady state signals but has an attenuating



SHUTTLE FSM-1 PNCAC001 750 HZ 1-L, 2-L 2000 S/S
FREQUENCY-HERTZ

START TIME = 1.00000 SEC	TIME INCREMENT = 1.00000 SEC
END TIME = 129.000 SEC	X SKEW VALUE = 0.035000 IN.
TIME SLICE = 2.00000 SEC	Y SKEW VALUE = 0.075000 IN.
SAMPLE RATE = 2000. SPS	

Figure 6-15. Data From Gage PNCAC001

REVISION _____

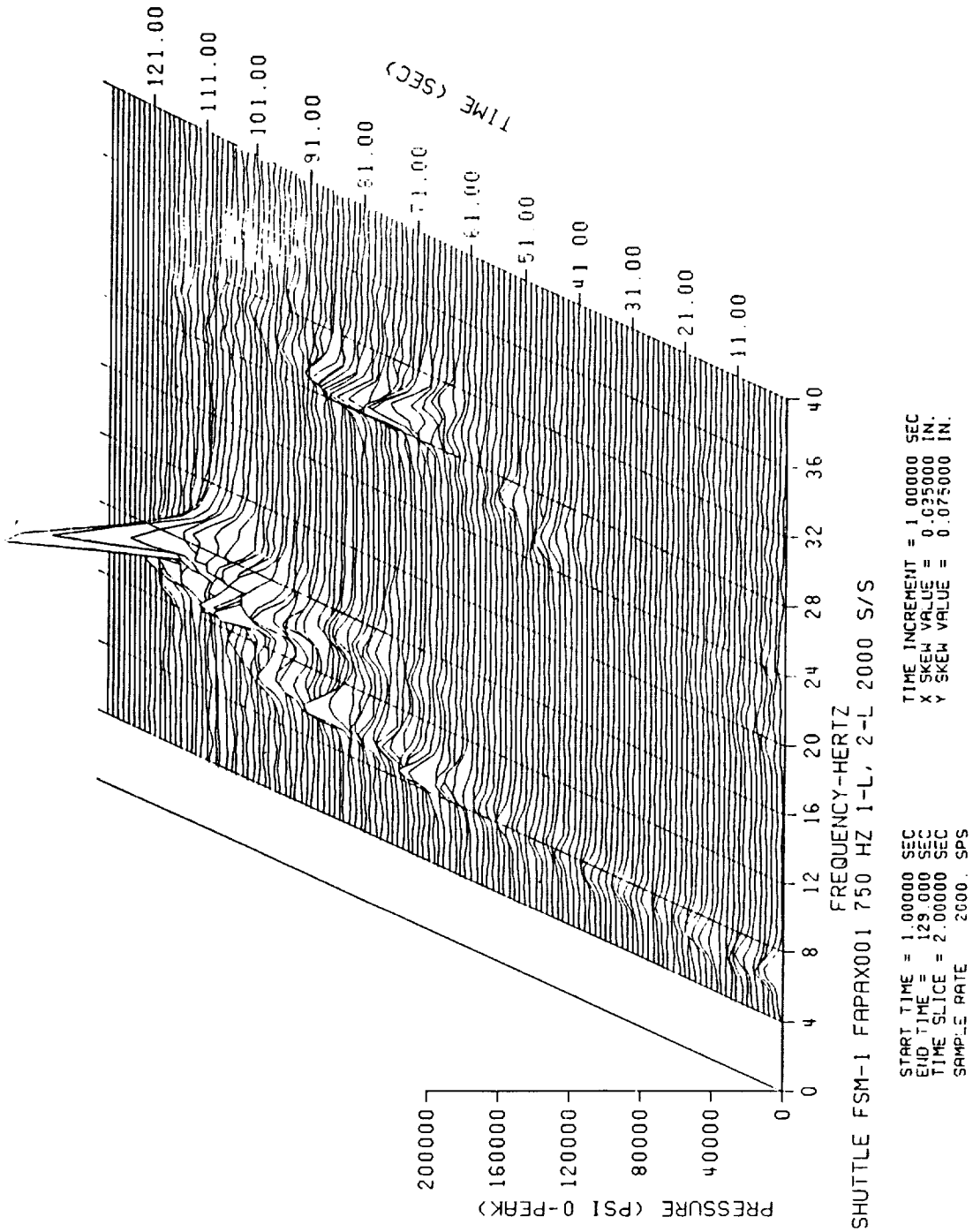
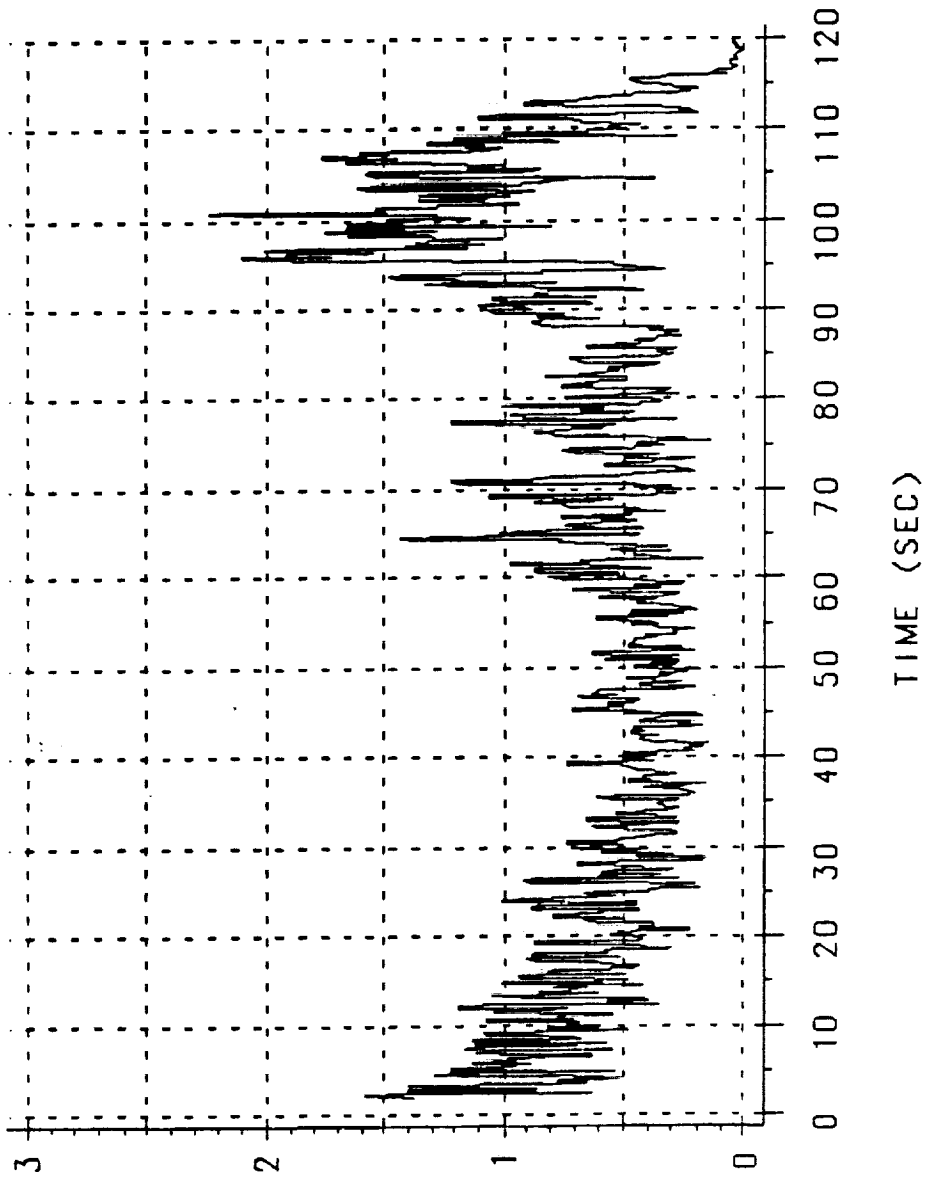


Figure 6-16. Axial Thrust Gage, FAPAX001



PRESSURE (PSI P-P)

TEST ——— FSM-1 500 PT

Figure 6-17. Maximum Oscillation Amplitudes—PNCAC001 1-L Acoustic Mode 2,000 sps

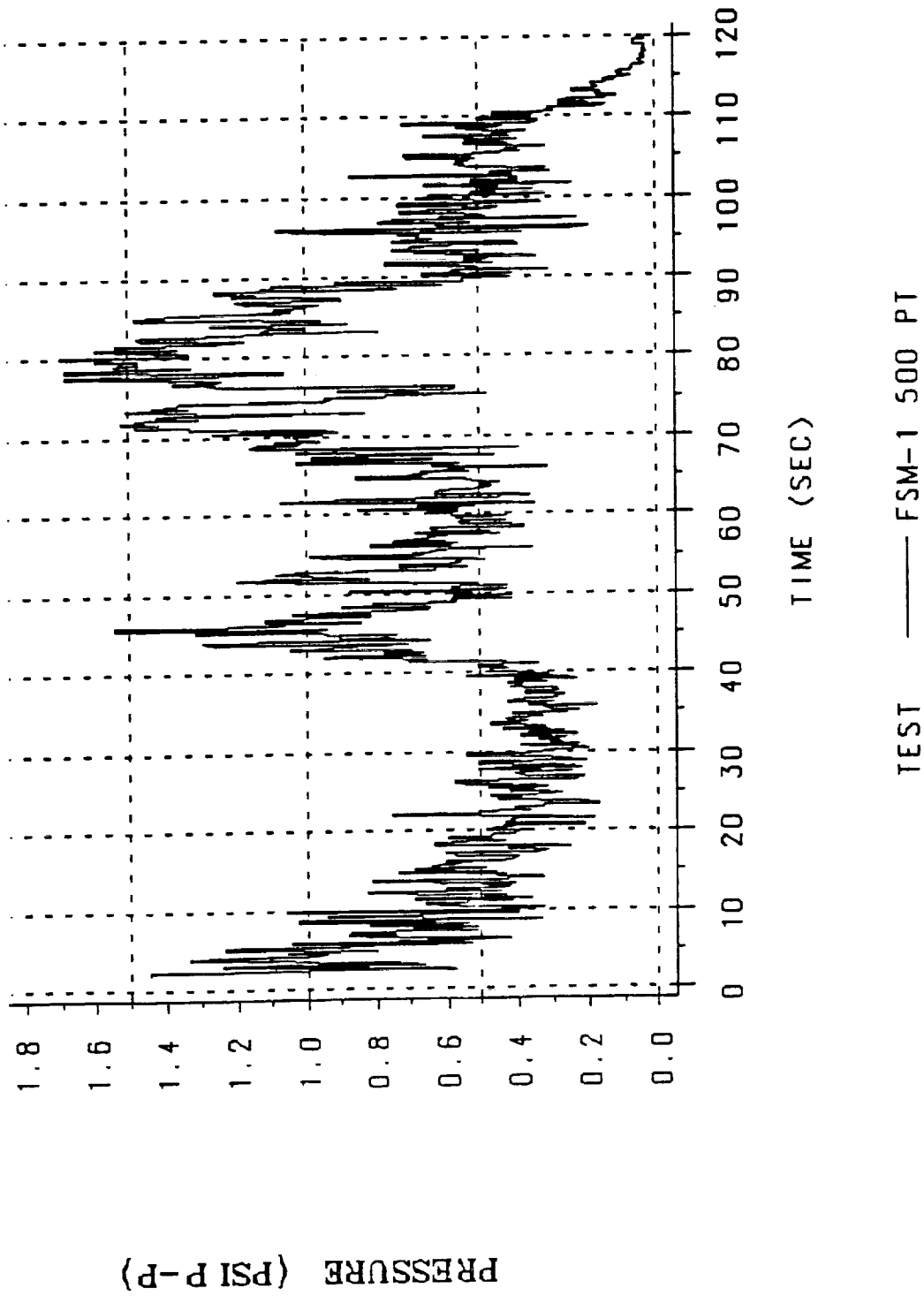


Figure 6-18. Maximum Oscillation Amplitudes--PNCAC001 2-L Acoustic Mode 2,000 sps

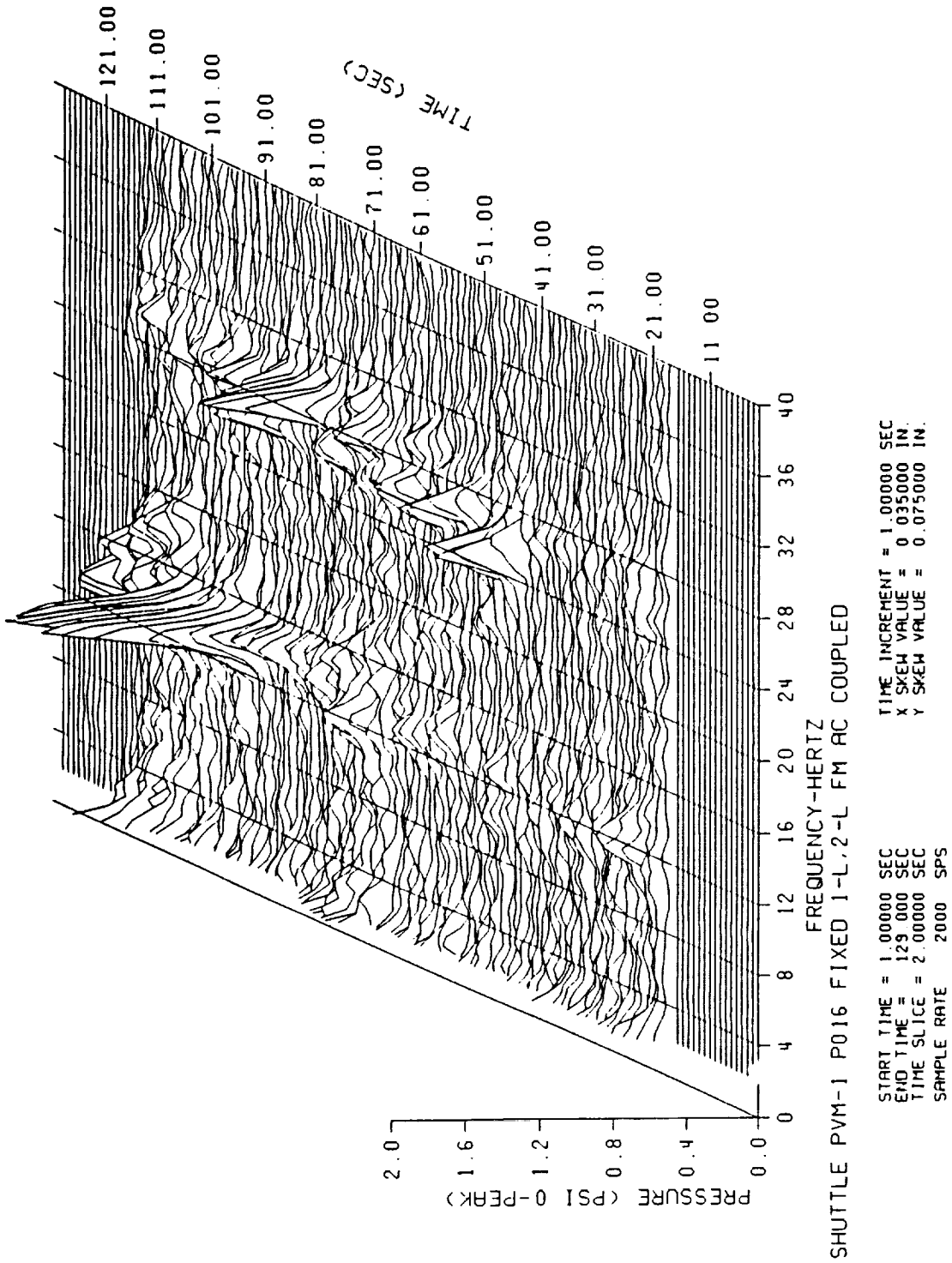


Figure 6-19. Data From Gage P000016

effect on transient signals. Since most of the data obtained from an SRM are transient, any oscillation magnitudes referred to as maxima are, in fact, not true but averaged values over a given time slice. These numbers are, nonetheless, very useful for comparison. Table 6-12 shows such a comparison for recent static test motors and the flight motors. This table contains the most recent data (errors found in previously measured data). DM-6 and DM-7 were filament wound case (FWC) motors.

Tables 6-13 and 6-14 provide the prefire and postfire weight and balance history for the total motor. The measured slag (466 lb) and the actual expended inert data (7,978 lb) have been incorporated into the postfire weight summary.

Table 6-13 shows that FSM-1 weight and cg values are within recommended CEI requirements. CEI requirements versus FSM-1 results are as follows:

	CEI Requirements	FSM-1
Maximum Inert Weight (lb)	148,960	147,785
Minimum Propellant Weight (lb)	1,104,140	1,106,109

	cg								
	Longitudinal			Lateral			Vertical		
	Max (in.)	Min (in.)	FSM-1 (in.)	Max (in.)	Min (in.)	FSM-1 (in.)	Max (in.)	Min (in.)	FSM-1 (in.)
Controlled Inerts	1,326	1,318	1,319	+0.3	-0.1	+0.03	+1.1	-0.9	+0.13
Loaded	1,178	1,165	1,171	+0.3	-0.3	+0.00	+0.3	-0.1	+0.02

Table 6-14 shows that FSM-1 burnout cg values are within recommended CEI requirements. CEI requirements versus PSM-1 results are as follows:

**Table 6-12. Maximum Pressure Oscillation
Amplitude Comparison**

<u>MOTOR</u>	<u>SOURCE OF MEASUREMENT</u>	<u>MODE</u>	<u>TIME OF MEASUREMENT</u>	<u>FREQUENCY (HZ)</u>	<u>MAX PRESSURE (PSI 0-TO-PEAK)</u>
FSM-1	Waterfall PNCAC001	1-L	100	14.0	0.64
		2-L	79	29.5	0.74
TEM-6	Waterfall PNCAC001	1-L	92	15.0	0.41
		2-L	98/99	29.5	0.67
TEM-6 (Aft)	Waterfall PNNAR005	1-L	92	15.0	0.31
		2-L	98/99	29.5	0.44
TEM-5	Waterfall PNCAC005	1-L	81	16.0	0.46
		2-L	100	29.5	0.57
TEM-4	Waterfall	1-L	115	14.5	0.37
		2-L	87	29.5	0.96
TEM-3	Waterfall	1-L	106	15.0	0.36
		2-L	102	30.0	0.58
TEM-2	Waterfall	1-L	78	16.0	0.43
		2-L	100	29.5	0.68
QM-8 *	Waterfall (P000002)	1-L	104	14.5	1.32
		2-L	55	27.5	0.47
TEM-1	Waterfall	1-L	79	15.5	0.37
		2-L	95	29.5	0.78
STS-27 (left)	Waterfall AC OPT	1-L	82	15.5	0.37
		2-L	82	29.5	0.60
STS-27 (right)	Waterfall AC OPT	1-L	82	15.5	0.57
		2-L	83	29.5	0.72
STS-26 (left)	Waterfall AC OPT	1-L	79	16.0	0.70
		2-L	95	29.5	0.87
STS-26 (right)	Waterfall AC OPT	1-L	83	15.0	0.54
		2-L	94	30.0	0.47
PVM-1 *	Waterfall	1-L	99	14.5	1.23
		2-L	79	29.5	0.77
QM-7 *	Waterfall P000001	1-L	93	14.5	1.40
		2-L	79	29.5	0.95
QM-6 *	Waterfall	1-L	107	14.5	1.05
		2-L	85	29.5	0.53
DM-9 *	Waterfall	1-L	107	14.5	0.81
		2-L	96	30.0	0.64
DM-8 *	Waterfall	1-L	78	16.0	0.58
		2-L	97	29.5	0.62
ETM-1A	Waterfall	1-L	84	15.5	0.45
		2-L	101	23.5	0.67
DM-7 **	Waterfall	1-L	77	15.5	0.90
		2-L	96	29.0	0.62
DM-6 **	Waterfall	1-L	76	15.5	0.51
		2-L	86	29.0	0.78
QM-4	Waterfall	1-L	81	15.5	0.31
		2-L	80	29.5	0.30

* RSRM static test motors.

** Filament wound case (FWC) HPM motors.

Table 6-13. Prefire Functional Summary

CODE	DESCRIPTION	WEIGHT (LBS)	CENTER OF GRAVITY			MOMENT OF INERTIA		
			LONG.	LAT.	VERT.	PITCH	ROLL	YAW
06.01.00.00.	CASE	98737.563	1188.740	0.015	-0.004	3651.854	110.414	3651.879
06.02.00.00.	INSULATION	20441.953	1366.953	0.000	0.000	939.552	21.612	939.552
06.03.00.00.	LINER	1342.540	1167.551	0.000	0.000	49.883	1.424	49.883
06.04.00.00.	INHIBITOR	1765.451	1120.180	0.000	0.000	27.634	1.134	27.634
06.05.00.00.	NOZZLE ASY	23505.740	1873.792	0.005	0.102	15.320	11.531	15.316
06.08.00.00.	IGNITER ASY	552.857	497.506	-0.024	-0.005	0.011	0.001	0.011
06.10.00.00.	INSTRUMENTATION	116.218	1246.229	0.452	0.630	5.519	0.152	5.562
06.13.00.00.	FIELD JOINT HEATERS	380.391	1191.001	8.085	17.028	7.706	0.453	7.610
06.14.00.00.	ASSY ATTACH PROV	372.772	1156.458	-0.000	20.069	14.659	0.364	14.574
06.15.00.00.	EXTERNAL INSULATION	569.544	1383.621	-0.766	5.201	23.741	0.394	23.495
06.00.00.00.	CONTROLLED INERTS	147785.029	1319.474	0.029	0.128	6775.629	147.542	6775.313
20.00.00.00.	UNCONTROLLED INERTS	276.949	1576.064	4.500	2.851	9.819	0.201	9.781
27.00.00.10.	TOTAL PROPELLANT	1106109.384	1151.267	0.000	0.000	34760.613	729.657	34760.613
27.27.00.10.	MOTOR PROPELLANT	1105975.524	1151.345	0.000	0.000	34746.110	728.179	34746.110
27.08.00.00.	IGNITER PROPELLANT	133.860	506.740	0.000	0.000	2.499	1.478	2.499
30.00.00.00.	SRM ASSEMBLY	1254171.362	1171.181	0.004	0.016	42352.002	877.401	42351.648

NOTES:

1 MOMENT OF INERTIA IS IN SLUG FEET SQUARED DIVIDED BY 1000 ABOUT AXES THRU PART OR ASSEMBLY CG

Table 6-14. Postfire Functional Summary

CODE	DESCRIPTION	WEIGHT (LBS)	CENTER OF GRAVITY		PITCH	MOMENT OF INERTIA	
			LONG.	LAT.		ROLL	YAW
06.01.00.09.	CASE	98737.563	1188.740	0.015	3651.854	110.414	3651.879
06.02.00.09.	INSULATION	17154.224	1328.069	0.000	817.346	21.612	817.346
06.03.00.09.	LINER	350.482	1086.678	0.000	8.005	1.418	8.005
06.04.00.09.	INHIBITOR	363.402	994.055	0.000	4.417	1.134	4.417
06.05.00.09.	NOZZLE ASY	21244.978	1871.627	-0.024	14.042	11.530	14.037
06.08.00.09.	IGNITER ASY	516.973	496.656	-0.005	0.010	0.001	0.010
06.10.00.09.	INSTRUMENTATION	116.218	1246.229	0.452	5.519	0.152	5.662
06.13.00.09.	FIELD JOINT HEATERS	380.391	1191.001	8.085	7.706	0.453	7.610
06.14.00.09.	ASSY ATTACH PROV	372.772	1156.458	-0.000	14.659	0.364	14.574
06.15.00.09.	EXTERNAL INSULATION	569.544	1383.621	-0.766	23.741	0.394	23.495
06.00.00.09.	CONTROLLED INERTS	139806.547	1307.048	0.026	6397.297	147.536	6396.981
20.00.00.09.	UNCONTROLLED INERTS	276.949	1576.064	4.500	9.819	0.201	9.781
27.00.00.29.	SLAG	466.000	1632.980	0.000	4.989	0.189	4.989
30.00.00.09.	TOTAL MOTOR	140549.496	1308.658	0.035	6427.037	147.927	6426.684

NOTES:

1 MOMENT OF INERTIA IS IN SLUG FEET SQUARED DIVIDED BY 1000 ABOUT AXES THRU PART OR ASSEMBLY CG

	cg								
	Longitudinal			Lateral			Vertical		
	Max (in.)	Min (in.)	FSM-1 (in.)	Max (in.)	Min (in.)	FSM-1 (in.)	Max (in.)	Min (in.)	FSM-1 (in.)
Burnout	1,325	1,305	1,309	+0.6	-0.4	+0.04	+1.6	-1.4	+0.14

Compliance with CEI measurement accuracy requirement is demonstrated by the Space Shuttle error analysis (TWR-11511).

6.8 STATIC TEST SUPPORT EQUIPMENT

6.8.1 Introduction

The deluge system and related instrumentation were similar to the configuration used on TEMs. The deluge system nozzle arrangement is shown in Figure 1-5.

6.8.2 Objectives

There were no specific objectives from Section 2 regarding static test support equipment.

6.8.3 Conclusions/Recommendations

All static test support equipment (TVC, deluge, and quench) performed satisfactorily with no anomalous conditions.

6.8.4 Results/Discussion

The deluge system performed adequately with no indication of excessive case heating. No anomalous temperature data was recorded by the deluge system instrumentation prior to, during or following its operation. The recorded initial and peak FSM-1 case temperatures were 81° and 100°F, respectively.

Figure 6-20 shows peak minus initial case temperature versus slag weight for static motor firings (only those motors fired since the redesign of the deluge system are included).

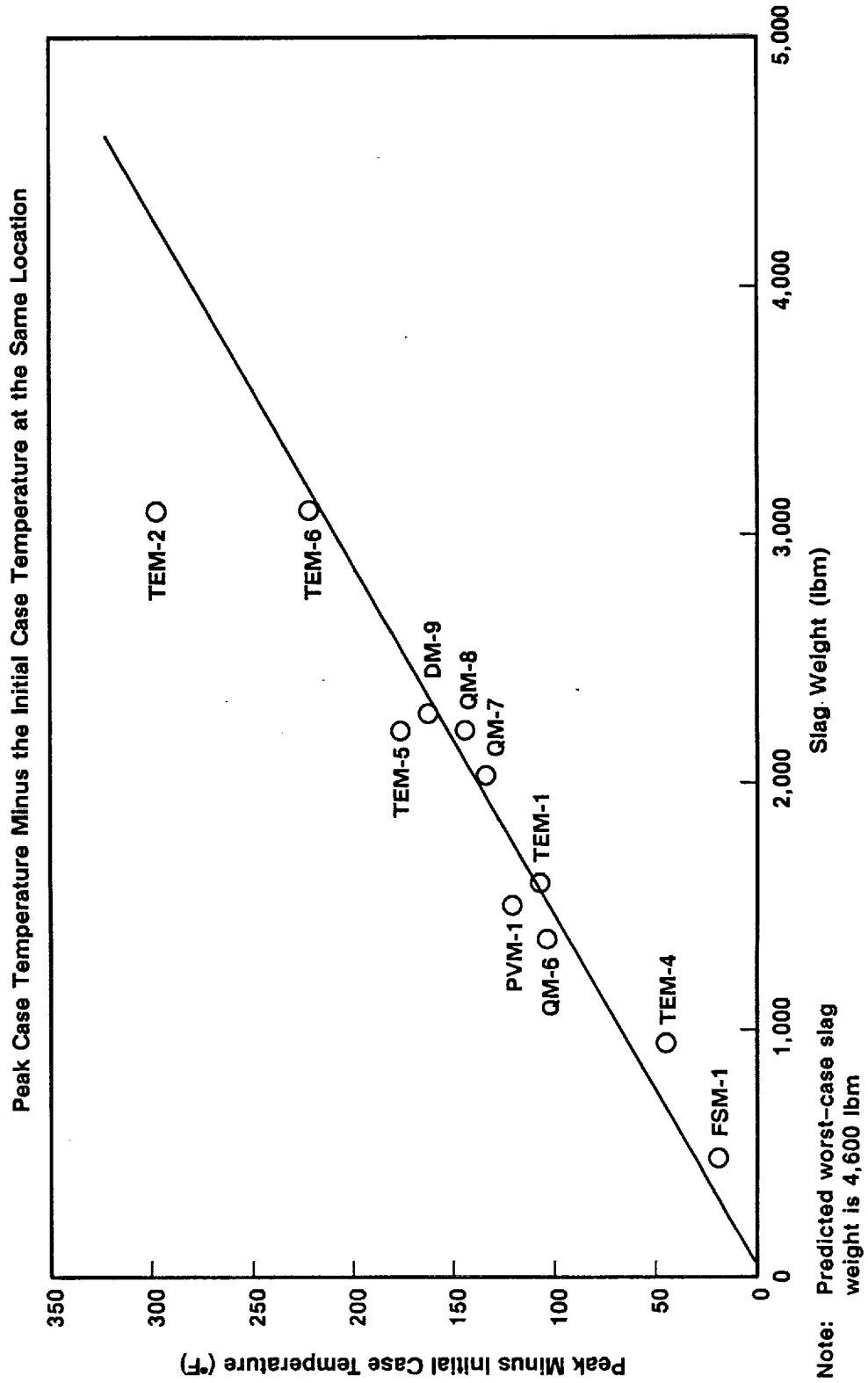


Figure 6-20. Maximum Static Test Motor Case Temperatures Versus Amount of Slag

A030422a

APPLICABLE DOCUMENTS

The latest revision of the following documents, unless otherwise specified, are applicable to the extent specified herein.

<u>Drawings</u>	<u>Title</u>
Unnumbered	FSM-1 Drawing Tree
1U50129	Case Segment, Aft
1U50131	Cylinder (Standard Weight)
1U50715	Case Segment, Stiffener--Lightweight
1U50716	Case Segment, Attach--Lightweight
1U50717	Case Segment, Cylinder--Lightweight
1U51063	Ring, Snubber Support
1U51369	Washer, Special
1U51473	Case Segment, Forward
1U51711	Plug, Protective, Nozzle
1U51899	Retainer, Pin--Field Joint, SRM
1U52295	Safety and Arming Device, Rocket Motor
1U52700	Ring Segment, Nozzle Severance
1U52840	Bearing Assy, Nozzle Flexible
1U52861	Nozzle Assembly, Final
1U52982	Case Segment--Capture Cylinder, Lightweight
1U52983	Case Segment--Capture Cylinder, Standard Weight
1U75150	Packing, Preformed Fluorocarbon
1U75166	Igniter, Rocket Motor--Test Configuration
1U76121	Exit Cone Sub Assy, Aft Insulated
1U76586	Nose--Throat--Bearing--Cowl--Housing Assembly, Nozzle
1U76676	Segment Assy--Loaded, Aft
1U76702	Cable Assembly, Power, Electrical-Heater, Forward Dome
1U76703	Cable Assembly, Power, Electrical, Branched-Heater, Forward Segment
1U76704	Cable Assembly, Power, Electrical, Branched-Heater, Forward Center Segment
1U76705	Cable Assembly, Power, Electrical, Branched-Heater, Aft Center Segment

REVISION _____

DOC NO. TWR-50068 | VOL
SEC | PAGE

7-1

1U76706	Cable Assembly, Power, Electrical-Heater, Aft Segment
1U77186	Segment, Assembly, Loaded, Forward, RSRM
1U77190	Segment Assembly Loaded, Center, FSM-1
1U77252	Heater--Field Joint
1U77253	Heater--Igniter to Case Joint
1U82840	Retainer Band Pin Assembly
2U65040	Assembly Fixture--Nozzle
2U65151	Static Test Arrangement
2U129410	Temperature Conditioning Unit, Aft Skirt
2U129749	Water Deluge System
2U129765	Forward Test Stand Sequence
2U132179	CO ₂ Quench System T-24
2U132180	Aft Test Stand Assembly Sequence--T-24
4U69505	Shield, Deluge System
7U76913	Instrumentation Assembly
7U76914	RSRM Test Assembly
7U77135	Joint Protection System Assembly, FSM

Specifications

CPW1-3600A	Prime Equipment Contract End Item Detail Specification (CEI)
ICD-3-44003	SRM/Aft Skirt and TVC Actuator
ICD-3-44005	SRM/SRB Electrical and Instrumentation
MC450-0018	Controller, Pyrotechnic Initiator
STW3-3176	Igniter, Solid Rocket Motor, Space Shuttle
STW4-2602	Ammonium Perchlorate with Conditioner
STW4-2621	Insulation, Acrylonitrile Butadiene Rubber (NBR), Asbestos and Silicon Dioxide-Filled
STW4-2868	Thermal Insulation, Ethylene Propylene Diene Monomer (EPDM)--Neoprene Rubber, Carbon Fiber-Filled
STW5-2833	TP-H1178 Propellant, Solid Rocket Motor, Igniter Space Shuttle Project
STW5-3223	Inhibitor, UF-3267, Solid Rocket Motor, Space Shuttle Projects
STW5-3224	Liner, Solid Rocket Motor, Space Shuttle Project
STW5-3343	Propellant, Solid Rocket Motor, TP-H1148

REVISION _____

DOC NO.	TWR-50068	VOL
SEC	PAGE	

STW7-2747 Leak Testing, Case Factory Joint, Space Shuttle
Redesigned Solid Rocket Motor

STW7-2853 Leak Test, Pressure Transducer Assemblies, Space Shuttle
Project SRM

STW7-2913 Procedure, Leak Test of Barrier-Booster Redundant Seals
STW7-2999 Calcium Grease, Field Joint, Factory Joint, Nozzle Joints
Assembly, Application of, and Component Installation Space
Shuttle SRM.

STW7-3320 Leak Testing, Aft End Ring-to-Fixed Housing Joint, Space
Shuttle Redesigned Solid Rocket Motor

STW7-3447 Leak Testing, Case Field Joint, Space Shuttle RSRM
STW7-3448 Leak Testing, Case-to-Nozzle Joint, Space Shuttle RSRM
STW7-3475 Leak Testing, Forward-to-Aft Exit Cone Joint, Space
Shuttle Redesigned Solid Rocket Motor

STW7-3476 Leak Testing, Forward End Ring-to-Nose Inlet Housing
Joint, Space Shuttle Redesigned Solid Rocket Motor

STW7-3477 Leak Testing, Nose Inlet-to-Throat Support Housing Joint,
Space Shuttle Redesigned Solid Rocket Motor

STW7-3478 Leak Testing, Throat Support Housing-to-Forward Exit
Cone Joint, Space Shuttle Redesigned Solid Rocket Motor

STW7-3632 Leak Test, Inner and Outer Igniter Joints, Space Shuttle
Project Solid Rocket Motor

STW7-3633 Leak Test, S&A

Documents

CTP-0112A Qualification Plan for Ammonium Perchlorate from
Western Electrochemical Corporation's New Utah Plant for
TP-H1148 and TP-H1178 Propellant

CTP-0125B Qualification Test Plan for the New Liner/Castable
Inhibitor Mixers

CTP-0171A Space Shuttle Flight Support Motor No. 1 (FSM-1) Static
Fire Test Plan

TWR-15111 Mass Properties Measurement Equipment and Net Weight
Error Analysis for Space Shuttle RSRM's

TWR-15723 Development and Verification Plan for the Redesigned
Solid Rocket Motor (D&V)

REVISION _____

DOC NO.	TWR-50068	VOL
SEC	PAGE	

7-3

TWR-16877	Redesigned Shuttle Rocket Motor Mass Properties Uncertainty Analysis
TWR-60094	Engineering Evaluation of the Usage of Clevis Pin Hole Bushings in the FSM-1 Static Firing
TWR-60250	Redesigned Solid Rocket Motor Static Test Postfire Engineering Evaluation Plan
TWR-60752	Single Size O-Ring Damage Tolerance Testing
TWR-60776	Postfire Hardware Special Issues FSM-1
TWR-61213	FSM-1 Forward Dome to Igniter Adapter Skip Analysis/Test Correlation
TWR-61407	RSRM Nose Inlet Assembly Structural Evaluation
DR No. 402566	Senior MRB, P/N 7U76909-01, Motor Subassembly, Test, FSM-1
MIL-STD-45662	Calibration Systems Requirements
SE-S-0073	Space Shuttle Fluid Procurement and Use Control
PRCBD S083831	Space Shuttle Fluid Procurement and Use Control (Waiver)
14A30649-02	SRB Aft Skirt

REVISION _____

DOC NO.	TWR-50068	VOL
SEC	PAGE	

7-4

DISTRIBUTION

<u>Recipient</u>	<u>No. of Copies</u>	<u>M/S</u>
T. Johnson	1	E62C
S. Vigil	1	E62C
G. Nielson	1	L52
T. Stratton	1	L61
T. Swauger	1	L61
G. Abawi	1	L61C
D. Joos	1	L62
R. George	1	L62A
R. Lange	1	L62A
D. South	1	L62A
J. Passman	1	L62B
C. Prokop	1	L62B
R. Buttars	1	L63
B. Hutchison	1	L63
N. Black	1	L71
P. Hughes	1	L71
J. Dykstra	1	L72
L. Frary	1	L72
H. Huppi	1	L72
N. Millsap	1	L72
J. Seiler	1	L72
F. Duersch	1	851
K. Sanofsky	1	851B
R. Papasian	45	E62A
Print Crib	5	Q51B1
Data Management	5	L72B